Dear readers,

The second law of thermodynamics results in the continuous flow of time. The increase of entropy in an isolated system brings about a lot of good things; it, for example, equalizes extremes, but, on the other hand, it can sometimes cause damages, which are quite often viewed as undoubted phenomena.

The last century dominant orientation for prevailing usage of fossil fuels, i. e. accumulated prehistoric solar energy, has to be abandoned, or energy has to be used ever more efficiently. Renewable sources of energy will have to be ready for use well enough before fossil fuels have been exhausted.

That is also the reason why the current volume of the Communications – Scientific Letters of the University of Żilina is devoted to some issues of energy from the point of view outlined above.

While some articles actually deal with non-conventional sources of energy, (as, for example, the following contributions: A solar timber-dryer equipped with an air collector; Energy evaluation of the municipal solid waste pyrolysis; Unsteady flow simulation and combustion of ethanol in diesel engines), the authors of other contributions pay attention to more efficient use of primary energetic sources (as in the Non-conventional principle of conversion of heat into cold in an internal combustion engines; Characteristics of a diesel engine with a ceramic coated piston head; Cooling the working rolls of the finishing section of wide-strip hot rolling mill; or The influence of vehicle maintenance conditions on chosen electric parameters of the starter during the combustion engine start-up).

Finally, there are articles that apparently do not show any relation to the mentioned problems (Breakdown of the impeller wheel of a TG2 Kaplan turbine, or The usage of arcs radii profile variation for the synthesis of railway wheel and rail head profiles), but in their substance, they solve technical problems very closely related with use of energy.

Vladimír Hlavňa

Jozef Výglaský – Naďa Langová – Peter Horbaj *

A SOLAR TIMBER-DRYER EQUIPPED WITH AN AIR COLLECTOR

A generally well-known high energy requirement for technological processes of timber drying and the fact that the world's supply of the conventional energy sources has considerably decreased are the decisive factors forcing us to look for some new, if possible, renewable energy sources for this process emphasising their environmental reliability.

One of the possibilities of how to replace, at least partly, the conventional energy sources – heat in a drying process is solar energy.

Air-drying of timber usually has a series of disadvantages such as time expenditure, drying defects in the wood and inadequate final moisture content. To avoid these drawbacks, kiln drying is used in many cases to dry the timber, but this involves higher investments for equipment and greater operating costs. The energy used to dry timber is approximately 60 to 70 % of the total energy used to manufacture timber.

A method that obviates or reduces the disadvantages of air-drying and, at the same time, reduces the costs of kiln drying, is drying with solar heat. For the most part, fossil fuels are currently used to dry timber products. Solar energy can replace a large part of this depletable energy since solar energy can supply heat at the temperatures most often used to dry wood (i.e. from 40 to 100 °C). Solar timber-dryers offer an attractive solution.

Key words: solar timber-dryer, energy savings, solar air collector, drying defects, drying quality

1. Introduction

The Slovak Republic (the SR) similarly as other countries with the well-developed industry including wood processing industry can easily spend five or more per cent of its national energy consumption on drying processes. Wood drying, as with other goods drying, requires a large quantity of energy.

2. Wood-processing industry

The tree-covered area of the Slovakian forestland represents 19,258 km^2. Primary forest resources for timber production represent a substantial wood potential. It is considered that woodcutting for industrial use is at the level of 5 mil. m^3 p.a. Their processing to timber is about 70 to 75 %, which represents more than 3.5 mil. m^3 of timber with high moisture content. It is recommended that all timber should be dried to a level of moisture content, at least 20 % or less depending on its final use.

Artificial drying of timber is one of the major components of heat consumption in the wood-processing industry. It is generally known as a high energy ratio, i.e. up to 60 – 70 % of the total energy used for the production of timber is consumed mainly for timber drying. Therefore, in order to be able to indicate and determine ways on how to improve operation efficiency, decrease overall costs of drying, achieve satisfactory quality of dried timber, and at the same time implement the above technology in an environmental-friendly way, it is necessary to specify both in a complex way and in detail the currently highly topical process of timber-drying. One of the possibilities of saving fossil fuels used for timber drying is also the use of solar energy, as an alternative energy source for solar-based timber-drying kilns. In economical and energy/policy sense, the sun energy due to its availability and flexibility in terms of usage of new technology seems to be very important and at the same time in our environment one of the most promising renewable energy sources. Energy gained from sun radiation increases neither the concentration of the carbon dioxide nor other "dangerous" gases in the air, hence it does not worsen the "greenhouse effect".

3. Climate conditions

The SR is a mountainous country. All the Slovak mountains belong to the Carpathian system. According to the global climatological classification, the SR belongs to the mild climate zone. Regular rotations of four seasons and variable weather throughout the year are typical for this country. Compared to the Czech Republic and Austria which lie more to the west, the climate in the SR has more continental features. The average January temperature ranges from –1°C in the Danube lowlands to –12 °C on the top of the Tatra Mountains. Average temperatures in July exceed 20 °C in the Slovak lowlands, while at the elevations of 1000 m a.s.l. they reach about 14 °C. The southern SR receives about 2,000 hours of bright sunshine each year, while the north-west of the country receives only 1,600 hours. Average annual precipitation for the whole territory of the SR is 743 mm. Snow cover is not stable, and

* **Jozef Výglaský[1], Naďa Langová[1], Peter Horbaj[2]**
[1]Faculty of Environmental and Manufacturing Technology, Technical University in Zvolen, T. G. Masaryka 2117/24, 960 53 Zvolen, Slovak Republic, E-mail: viglasky@vsld.tuzvo.sk, langova@vsld.tuzvo.sk
[2]Mechanical Engineering Faculty, Technical University in Košice, Vysokoškolská 4, 04200 Košice, Slovak Republic, E-mail: peter.horbaj@tuke.sk

winters in the lower altitudes are usually without permanent snow covering.

4. Objectives

In the various studies on solar heat drying published during the last decades (e.g. Steinmann-Vermaas 1990, Steinmann 1992), it has been shown that the operating conditions are influenced by numerous factors, such as location, climate, wood species, dimensions and type of kiln used. Therefore it is not possible to generalise, and each situation, location and particular application must be studied in detail.

The research was focused basically on the design of the kilns, and the aspects of regulation and control have been studied with regard to the fact that the period of solar radiation is determined by natural laws, i.e. its range varies greatly during the day and even season, therefore it is necessary to provide, apart from the solar energy, the heat supply from another energy source in a continual drying kiln to optimise the co-operation of two heat energy sources.

5. The Solar Timber Drying Kiln

The prototype solar kiln placed in the furniture factory is shown schematically of its solar air collector in Figure 1. The test runs described in this contribution were carried out in the town of Skalica, 48° 51′ Northern latitude, 17° 14′ Eastern meridian, 178 m a.s.l. and with approximately 2,100 hours of sunshine per year. The collector is external to the drying chamber so that the collector area and orientation are not limited by the geometry of the kiln.

6. Construction details of the kiln

Structure of the kiln

We used a commercial drier type KWB 111 that was slightly accommodated to be joined to a solar air collector. The single-row low-capacity kiln has a 7 m^3 sawn timber volume. The timber stack measures are as follows: the width of 1500 mm, the height of 1750 mm, and the length of 6000 mm. The kiln is designed to dry coniferous and broad-leaved sawn timber or bulks at 100 °C max. drying temperature.

Solar air collector

As specific conditions occur during the drying process of sawn timber using solar energy by means of solar air collectors, the first part of our investigation was aimed at a comprehensive theoretical analysis followed by an experimental analysis of the solar air collector work from the viewpoint of optimising its parameters for application in the chamber kiln heating system. An experimental solar system was designed at the Technical University in Zvolen to test and investigate representative characteristics of solar air collectors [1].

The heat for the kiln is supplied by 20 m^2 external air heating, solar collector facing south and inclined at 45° to the horizontal (latitude of the solar kiln site 17° 14′) for optimum year round performance. One centrifugal blower sucks heated air from the collector into the drying chamber, through an insulated duct. Heat output of the solar air collector (see Figure 2).

Air was circulated over the collector and through the load at 3 $m.s^{-1}$. Vents and a spray system were used to control the relative humidity in the kiln.

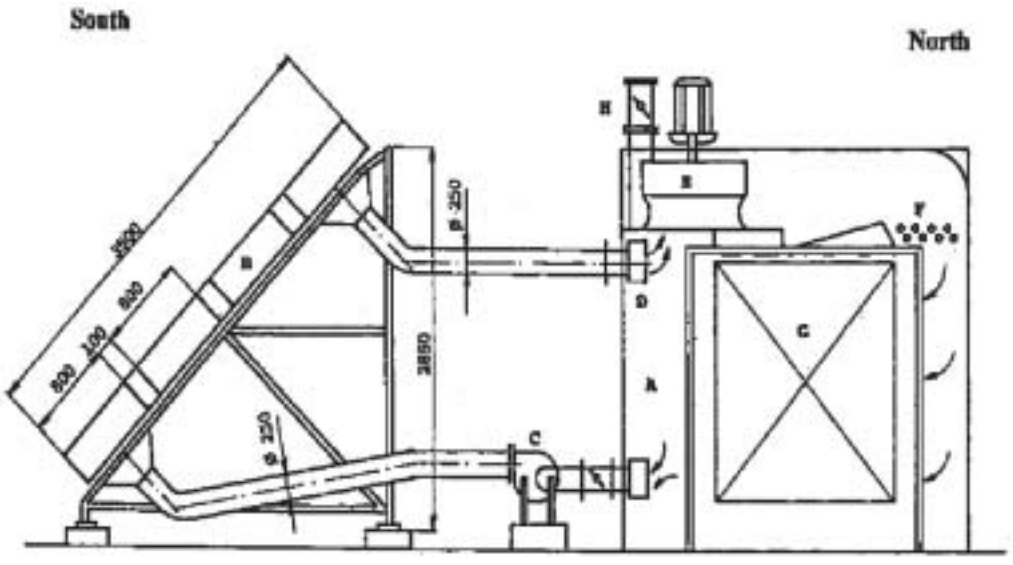

Fig. 1 The Solar Timber Drying Kiln
The Solar Kiln Scheme. (A) Drying chamber; (B) Solar collector; (C) External blower to induce air flow through the collector; (D) Hot air discharge to internal fans; (E) Internal fans; (F) Heaters; (G) Wood stack; (H) Aeration stacks.

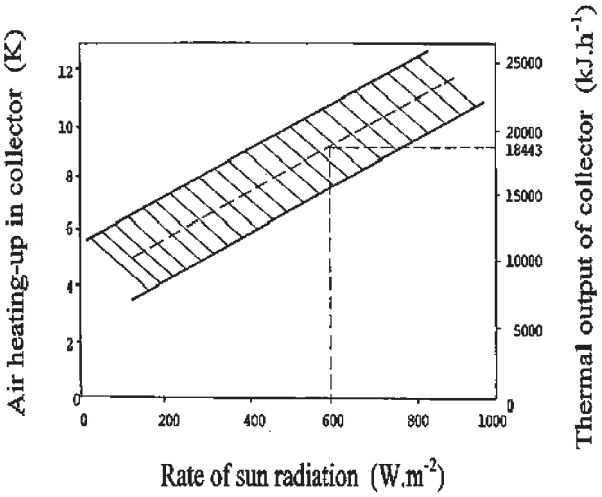

Fig. 2 Heat Output of Solar Air Collector used for the Solar Timber Drying Kiln

The solar kiln was controlled up to now by a semi-automatic control system consisting of: a differential temperature controller, a maximum relative humidity controller, a minimum relative humidity controller, a humidistat, a thermostat, and a timer. The whole control system can be manually checked by switches, but a sensitive and effective equilibrium moisture content (EMC) control system based on control logic is required for performance in the solar kiln to protect wood quality as well as to maintain optimum drying rate and also to prevent energy loss through useless venting.

The temperature and relative humidity of the air inside and outside the kiln, the mass of the kiln load, the status of the venting system (open/closed), the moisture content of the kiln load, the time of the day, and the solar radiation were recorded at 15 min. intervals.

The ratio of collector area to loading capacity is 2.86 $m^2.m^{-3}$, which agree with recommendation – the optimum collector ratio in respect to drying rate lies in the range between 2 and 7 $m^2.m^{-3}$ run [5].

7. Experimental Part

Solar drying

Test drying runs were carried out using wood species – Pine Monterey [Pinus radiata D. Den.], thickness dimension of 24 mm to assess the kiln by the following criteria:

- Drying time.
- Final wood moisture content.
- Drying quality.
- Supplemental energy.
- Temperature and relative humidity conditions in- and outside the kiln.
- Efficiency of the drying process.

Solar radiation.

The solar radiation recorded during runs was done by the radiation pyrometer HEMI (Solar Sensor 118 SN-8580, Swiss Instrument – HEMI-Messgeräte, 100 V = 1 000 $W.m^{-2}$).

Furthermore, the average initial moisture content of the sawn timber to be solar dried was 60 % in the evaluated run. The species dried was Pine radiata, sawn in planks measuring 3,000 mm in length, 100 mm in width and 24 mm in thickness. In the evaluated run the 7.0 m^3 kiln load was piled using 18 mm square piling sticks and placing the boards edge to edge in each layer. Six kiln samples (3 quarter-sawn, and 3 flat-sawn) were built into the stack in order to study/double check the progress of drying.

During runs, the kiln was operated and supervised for 8 hours per day by a skilled operator. The operator's main task was to maintain the drying gradient as near as possible to the target-drying gradient through the adjustment of the humidistat and the maximum and minimum relative humidity controllers. The rest of the job was done by the semi-automatic kiln control system mentioned above. The drying process during the evaluated run was carried out under the control of the automatic system, without any intervention.

A test for the existence and intensity of casehardening stresses was made immediately prior to the conclusion of both runs. Six prongs were cut 200 mm from one end of sample boards from each pile. The prongs were made by cutting out the centre portion to within 25 mm of one end of 13 mm thick cross-sections. The intensity of casehardening was assessed after allowing the prongs to dry indoors for 8 hours.

After 80-hours or 5-day solar drying period the average moisture content of sawn timber found to be 20 % in representative evaluated run.

During the run the drying chamber temperature was varying in range of 30–40 °C, but the drying condition expressed by the equilibrium moisture content (EMC) was constant, in the mean average of 10 %.

8. Air-drying

Simultaneously with the solar drying and using the same species and sizes, air-drying test runs were carried out. The drying quality was evaluated, and both drying time and final wood MC were recorded. It was then possible to calculate the drying rates of both methods and compare them.

9. Results and discussion

The variables were selected according to a preliminary plan, which would allow conclusions about the two different drying methods, by comparing the results. The variables considered were:

- Species of wood.

- Thickness.
- Time of year.
- Initial and final moisture content.

Comparing drying time of runs (same thickness – e.g. 24 mm, same species – e.g. Pine, solar kiln and air drying), the conclusion is that solar drying is 6 times faster (80 hours) than air-drying (480–510 hours).

With regard to the species, comparing the runs (same thickness, different species) leads to the conclusion that although solar drying of hardwood is slower and more expensive than air drying, it is more profitable than for softwoods (conifers).

Comparing the results of runs (same species, different thickness), the conclusion is that solar drying is more profitable for thicker samples.

Since solar drying is only faster than air-drying below 70 to 80 % wood MC, the initial moisture content is of importance. The influence of the final moisture content is particularly marked below 20 %, as the solar method becomes more profitable the lower the desired final wood moisture is.

With regard to cracks, splits, honeycombing and final moisture content, the quality of solar dried timber is better than for air-dried stock. The quality is comparable or even superior to that obtained by the conventional kiln drying method [8, 9, 10, 11, 12, 13].

As expected, the efficiency of solar drying improves with an increase of the average external temperature and is more effective during the first stage of the drying process than in the second stage when the wood MC is already below 40 %.

With regard to economics it must be pointed out that the supplemental energy consumed (kWh) per kg of evaporated water is only approx. one-tenth to the amount used in a conventional kiln.

As the efficiency of the tested solar timber-drying kiln depends strongly on the environmental conditions and mainly on the intensity of the solar radiation collected, the results are only transferable directly to locations of similar latitude.

10. Solar timber drying kiln control

In a solar kiln, the maximum temperatures are approximately 50 °C, which lasts only for a very short period of time each day, and is only achieved when the wood is partially dry and can endure these temperatures. Temperature control is not necessary in solar wood drying kilns and, therefore, only the relative humidity of the kiln air has to be controlled according to the given drying schedule.

The relative humidity inside the solar kiln should be computer controlled in such a way that venting will take place if it rose above the target value as given by the drying schedule and if, at the same time, the absolute humidity of the outside air is less than the absolute humidity of the air inside the kiln. Unless both conditions are not satisfied simultaneously, venting will not occur. This will be to prevent air with too high moisture content from entering the kiln. With this control, venting will be optimised, preventing loss of energy [6, 7].

An efficient solar kiln control system giving the best possible quantitative and qualitative results for the final product should ensure that the drying operation is always modulated to match a current timber condition at any moment of a drying period. Such a system should guarantee the maximisation of energy input to the drying chamber and the minimisation of energy losses through ventilation and useless air circulation.

11. Additional heating system

An idea of additional heating system to speed up drying and to support the drying process during periods of low solar radiation as well as to increase the average night temperature is recommended to be take into account [2].

With regard to the fact that the period of solar radiation is determined by natural laws, i.e. its range varies greatly during the day and even season it is necessary to provide, apart from the solar energy, the heat supply from another energy source in a continual drying kiln.

The problem of an additional heating system used in the solar kiln to improve its efficiency was successfully solved at the Technical University in Zvolen. Several control aspects were investigated [2, 3, 4].

This problem has been solved in an original way of regulating the heating system with a binary source of heat. The above regulation makes it possible to optimise the co-operation of two heat energy sources in the kiln in such a way that it maximises utilisation of solar energy and minimises the heat consumption from conventional energy source, e.g. steam or hot water.

A systematic approach is required in this field to generate results which would serve as guidelines in the design, control and use of a solar kiln of a new generation.

12. Conclusions

Many rural and small urban localities are strongly economically dependent on wood processing plants. These small processing plants (as well as the large ones) are beginning to experience difficulties in energy supplies and costs. Because of high economics, not all mills are able to burn mill residues for energy (i.e. excessive capital costs), and must rely on fossil fuels for energy.

The application of solar energy to wood processing holds exciting promise of energy savings. To illustrate this, consider timber

drying – one of the major energy users in wood processing. Most of this energy is fossil fuel based.

Why is solar energy utilisation so potentially exciting?

First, wood processing requires temperatures between 30 °C and 80 °C and requires energy at a fairly even demand. Therefore, extra large solar collecting surfaces are not required.

Second, a great deal of experimentation has been done in solar energy technology.

A few experimental, small-scale, solar timber-drying kilns have been built in the Slovak Republic as well as in other parts of Europe and the World. Therefore, although designs will continue to improve, workable designs are available today.

This task Application of solar air collector for sawn timber drying and other tasks were researched as part of the main task Utilisation of non-conventional and secondary energy sources for sawn timber drying and kiln which was carried out at SDVU in Bratislava and other co-operating institutions – Vzduchotechnika Nove Mesto nad Vahom, THERMO-SOLAR ZIAR as well as the Technical University in Zvolen.

Acknowledgements

This research was partly sponsored with grants from the Scientific Grant Agency of Ministry of Education of the Slovak Republic and Slovak Academy of Sciences, under the contract No. 1/2382/05 VEGA; EC Projects: PN 116441-CP-1-2004-1-FR-MINERVA-M, title: BIO-eTRAIN "The Implementation of an e-Learning University for Bioenergy"; Project No: 012429 – BIOPROS "Solutions for the safe application of wastewater and sludge for high efficient biomass production in Short-Rotation-Plantations"; Leonardo da Vinci Project: EnTraCoP - Enhancing the Teaching of Collaborative Planning in Natural Resource Management, the Agreement No.: 2005 FI- 05-B-F-PP-160633. Project "FET-EEU" full title: Future Energy Technologies for Enlarged European Union; Proposal/Contract No.: 510417. The authors are indebted to the mentioned institutions for helping to sponsor this research work.

References

[1] VÍGLASKÝ, J.: *Proposal for an experimental way and installing of an experimental system for testing solar air collectors.* (TU in Zvolen, Report no. A02-522-804/1, 1987), 26 p. (in Slovak).

[2] VÍGLASKÝ, J.: *R&D of a highly efficient solar air collector for its application at a low capacity sawn timber kiln.* (TU in Zvolen, Report no. A 02-522-804/2, 1988), 66 p. (in Slovak).

[3] VÍGLASKÝ, J.: *Technical-economic evaluations of a solar air collector application at a sawn timber kiln.* (TU in Zvolen, Report no. 02-522-804/3, 1989), 53 p. (in Slovak).

[4] VÍGLASKÝ, J.: *A new energy model of a solar kiln, in Proceedings of the Scientific Seminar on "Zvolen – town of wood science and practice".* TU Zvolen, (1993): pp. 365-374 (in Slovak).

[5] STEINMANN, D. E.: *The effect of collector area and solar tracking on the performance of a solar lumber drying kiln.* In: Proceedings of 3rd IUFRO International Wood Drying Conference. Vienna, Austria. pp. 283–291 (1992).

[6] FRUHAUFOVÁ, I.: *Actualization of environmental regionalization SR – work for ArcView. Enviromagazín,* 4/2003, ISSN 1335-1877 (In Slovak).

[7] HORBAJ, P., KUŠNÍR, M.: *Experience of production of biogas and wood gas for use in a cogeneration unit.* In: „Production and purification of fuels from waste and biomass Technical, Environmental and Social Considerations", European Commission Directorate General Joint Research Centre, Institute for Energy, CLEANWEB Technical Workshop in collaboration with the Technical University of in Košice and BIOMASA Association, Slovakia, 11.–12.10.2004, Košice http://ie.jrc.cec.eu.int/prewin.

[8] MARKOVÁ, I., KLEMENT, I.: *Thermal analysis (TG, DTG and DSC) of hornbeam wood after drying.* In: Wood Research, Vol. 48, No. 1/2, 2003, pp. 53–61.

[9] MARKOVÁ, I.: *Investigation of the drying process of hornbeam wood using thermal analysis methods (TG, DTG and DSC).* In: The Proceedings of International Conference "Issues of Hardwood Research and Utilisation in Europe". University of West Hungary, Sopron, September 25 – 26, 2003, 8p.

[10] RAJČAN, E., DANIHELOVÁ, A., RUŽINSKÁ, E.: *The Influence of Adhesive on Physical and Acustical Characteristics of Wood.* In: The Proceedings of the 12th International Symposium „Progresses in production and application of Adhesive in Wood Industry". TU in Zvolen, 1995, pp. 293–297.

[11] RAJČAN, E., DANIHELOVÁ, A., RUŽINSKÁ, E.: *The Influence of Adhesive on Physical and Acustical Characteristic of Wood.* WOOD, Vol. 50, No. 12, 1995, pp. 236–265.

[12] DANIHELOVÁ, A.: *Experimental verification of validity of the funcionality of the modulus of elasticity on moisture content.* In: The Proceedings of International Conference ACOUSTICS '96, Zvolen, 1996, pp. 36–40.

[13] DANIHELOVÁ, A.: *Influence of some gaseous and liquid substances on physico-acoustical characteristics of spruce wood.* Wood Research, Vol. 43, No. 2, 1998, pp. 29–39.

Vladimír Hlavňa – Dušan Sojčák – Rastislav Isteník *

NONCONVENTIONAL PRINCIPLE OF CONVERSION OF HEAT INTO COLD IN AN INTERNAL COMBUSTION ENGINE

The paper presents results achieved by a team of 12 researchers from the Faculty of Mechanical Engineering of the University of Žilina who participated in the solution of the project of the above-mentioned title within the period of the years 2002 – 2005. The basic research project focuses on the cooling internal combustion engine as an element of qualitatively new equipment designed for more effective utilization of fuel energy by a nonconventional progressive principle of heat conversion cooled by thermocompression. The issue of permanently sustainable life is approached from three hierarchical levels: a first level is a cooling internal combustion engine; a second level is a combined cogeneration complex power source; and a third level is a permanently sustainable power system. The cooling internal combustion engine is actually the basic element of the subsystem in the three-level complex of permanently sustainable life. It is still necessary to verify expected advantages of this unconventional combustion engine, potential savings of primary energy and foresee possible problems arisen during the simulation of the engine.

1. The project objective

The project objective is to carry out basic research into the fundamentals of a cooling combustion engine designed for more effective utilization of fuel primary energy by means of a nonconventional progressive principle of conversion of heat into cold through thermocompression. The subject of basic research is a nonconventional cooling combustion engine reciprocal movement of the piston and discontinuous combustion examined from the point of view of:

a) theoretical analysis,
b) consecutive mathematical modelling of thermodynamic and energetic states of the cooling combustion engine (taking into consideration the fact that it is the "cooling" engine),
c) selection of components and media focusing on the increase of cooling output generated by the cooling combustion engine and on decrease of thermal losses.

All the above mentioned activities require a flow simulation of the coolant in the engine cooling system as a component of the absorptive cooling circuit with its analysis and consequent synthesis with the objective of designing a suitable configuration of the absorptive cooling circuit and suitable choice of coolant. To determine the data necessary for a mathematical modelling and subsequent verification of calculations and selection of components and coolants it is required:

a) to design a testing model of the cooling combustion engine and for this purpose to accommodate the existing testing stand of the combustion engine,
b) to carry out some experiments.

Expected social benefits are as follows:

- extension of existing knowledge, dissemination of new knowledge – internationally oriented,
- application of new knowledge into teaching materials of institutions of higher learning – professionally oriented,
- transfer of knowledge into solutions of other applied reasearch tasks – specifically oriented,
- enrichment of scientific and technical know how – specifically oriented aspect of solution.

2. Results of solution

The assessment is carried out chronologically in relation to the given objectives.

The year 2002

The following activities were carried out:

1. theoretical analysis and mathematical modelling
2. testing stand – reconstruction.

To determine thermal flows from the individual chambers of inserted cylinders it is necessary to know mass flows around the cylinders and temperatures in the corresponding places. This can be solved by a method of composition of the cooling system hydrodynamic elements characteristics. The dependence of specific energy on the mass flow in the cooling circuit can be described by the following set of equations:

$$Y_a = k_{1a} \cdot m_{wa}, \tag{1}$$

$$Y_b = Y_{ab} + k_{1b} m_{wb}, \tag{2}$$

$$Y_c = k_{1c} \cdot m_{wc}, \tag{3}$$

* **Vladimír Hlavňa, Dušan Sojčák, Rastislav Isteník**
Faculty of Mechanical Engineering, University of Žilina, Univerzitná 1, 010 26 Žilina, Slovakia,
E-mail: Vladimir.Hlavna@fstroj.utc.sk, Dusan.Sojcak@fstroj.utc.sk; Rasto.Istenik@fstroj.utc.sk

$$Y_d = k_{1d} \cdot m_{wd}, \quad (4)$$

$$Y_e = Y_{cd} + k_{1e} \cdot m_{we}, \quad (5)$$

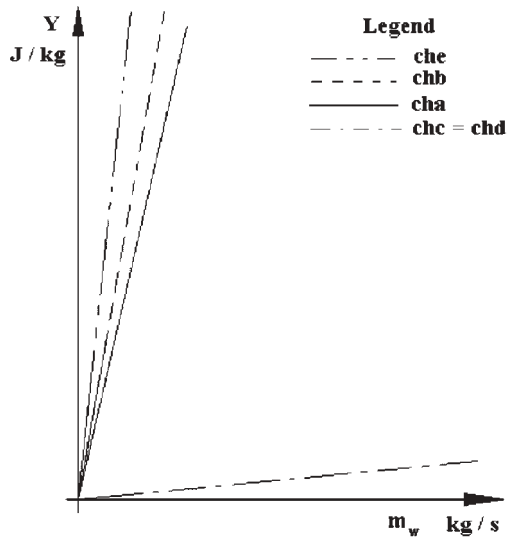

Fig. 1(left) Characteristics of the cooling system: ***che*** *– characteristics of collector pipe, thermostat and radiator,* ***chb*** *– characteristic of cylinders and cavities around the cylinders,* ***cha*** *– entry of cylinder blocks,* ***chc*** *– characteristics of partitions around cylinders,* ***chd*** *– exit from cylinder heads.*

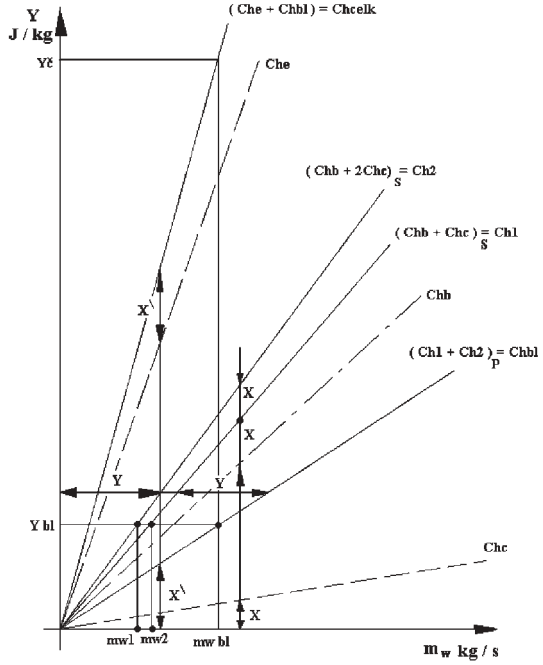

Fig. 2(right) ***Chbl*** *– characteristic of the block,* ***Ch1*** *and* ***Ch2*** *characteristics of cylinders,* ***Chcelk*** *– overall characteristic,* ***Yč*** *– pump specific energy,* ***mw bl*** *– flow in the block,* ***mw2*** *– flow around the second cylinder,* ***Ybl*** *– specific energy of the block,* ***Che*** *– characteristics of the collector pipe, thermostat and radiator.*

The resultant characteristic of the systems is given by the composition of individual characteristics of elements from Fig. 1, where the series connected elements are summed at a constant mass flow, the parallel connected elements are summed at a constant specific energy, Fig. 2.

Thermal flows from the individual chambers of inserted cylinders can be defined by means of the following equations:

$$Q_{ich} = Q_{ih} + Q_{iw} \quad (6)$$

$$Q_{ih} = m_{ih} \cdot c_{iw} \cdot (t_{ih} - t_{i+1,w}) \quad (7)$$

$$Q_{iw} = m_{iw} \cdot c_{iw} \cdot (t_{iw} - t_{i+1,w}) \quad (8)$$

$$m_{i-1,w} = m_{ih} + m_{iw} \quad (9)$$

The year 2003

The following activities were carried out:

1. theoretical analysis and mathematical modelling:
   - A theoretical diagram of cycle was completed and physical and chemical properties LiBr-H_2O were found out.
   - Modelling and calculation of the inserted cylinder deformation.
   - The issue of bubble formation on the surface of the inserted cylinder was solved.
   - Modelling and simulation of flows of coolant and energetic flows.
   - The project – updating of programme of experiment automation – completed.
   - Specification of measurement places.
   - Design of measurement chain – sensors, transmitters, ...

2. testing stand
   - Methodology of measurement was prepared.
   - Cooling circuit – design of arrangement, constructional design of an expansion container and engine adjustment, external pump, sent to a manufacturer, purchases.
   - Provision of the external pump and purchase of fuels.
   - Constructional design of the expansion container.
   - Reconstruction of the testing stand, arrangement of the original measurement chain for measurement with the help of LiBr.

3. experiments
   - Measurement of the engine surface temperatures – evaluation.
   - Tests of the original engine – measurements of coolant flows.
   - Mapping of the engine: characteristics, surface temperatures for two coolants (water, LiBr), assessment.

There was no agressive harm or damage of sample material, i.e. neither etching nor dissolving observed.

The following activities were carried out:

- Modelling and computation of the inserted cylinder deformation.

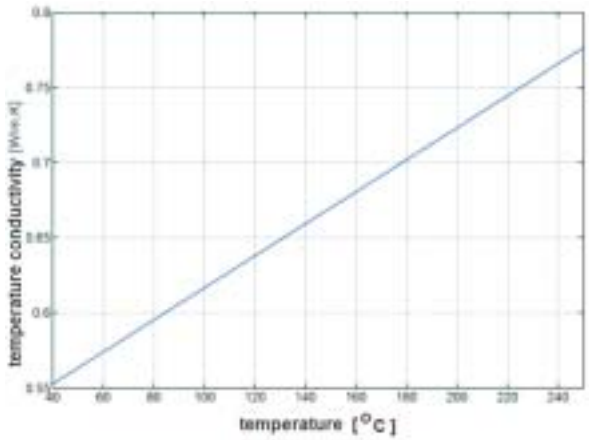

Graph 1 Thermal conductivity of coolant

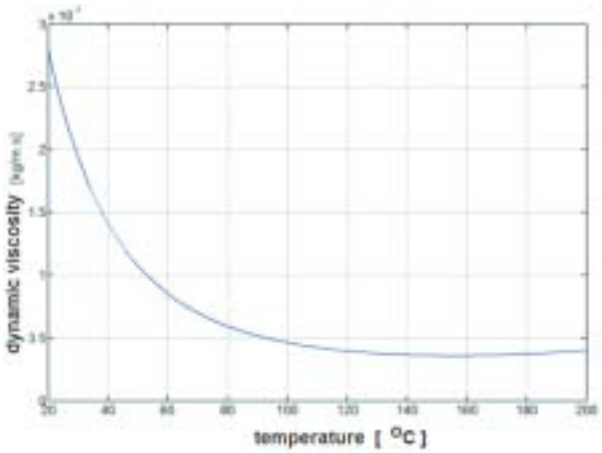

Graph 2. Dynamic viscosity

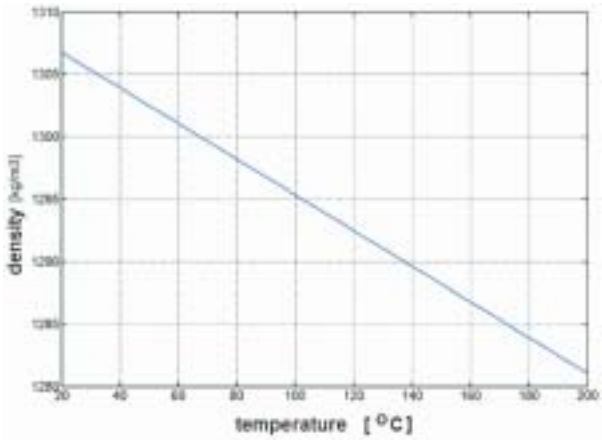

Graph 3 Density of coolant

- Geometry of the combustion engine cylinder generated in the ANSYS software.

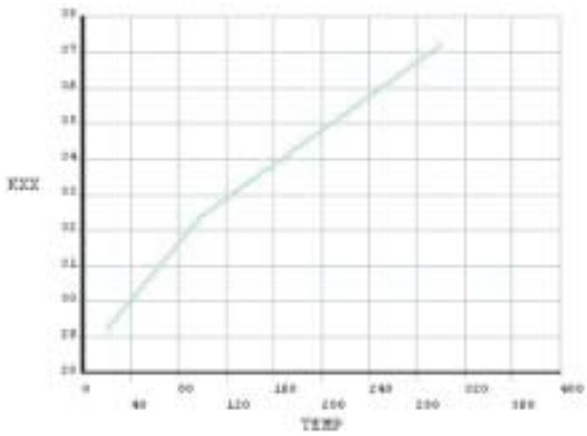

Fig. 3 Dependence of thermal conductivity coefficient λ on temperature

- Boundary conditions.
- Coordinates of geometric keypoints.
- Material characteristics.
- Thermal analysis of the cylinder.
- The final elements network.

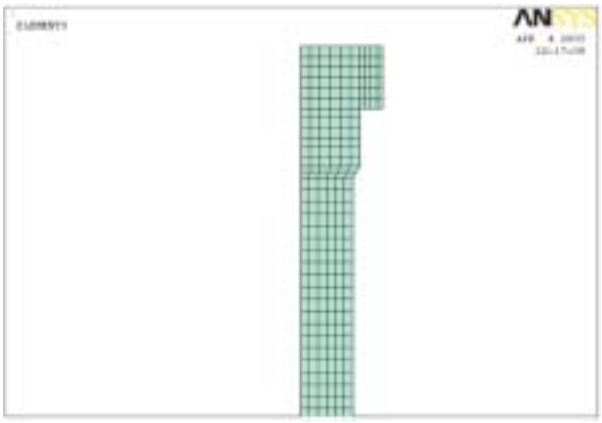

Fig. 4 Mesh of the model in ANSYS.

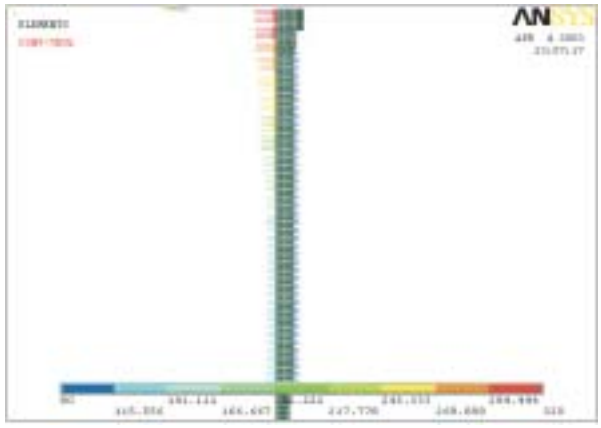

Fig. 5 Applied thermal loading in C°.

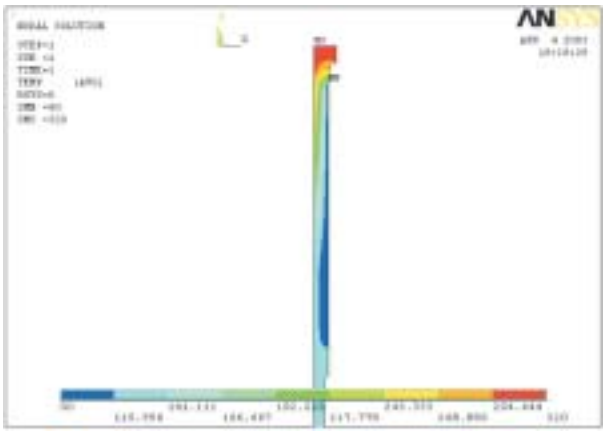

Fig. 6 Results of heat transfer in C°

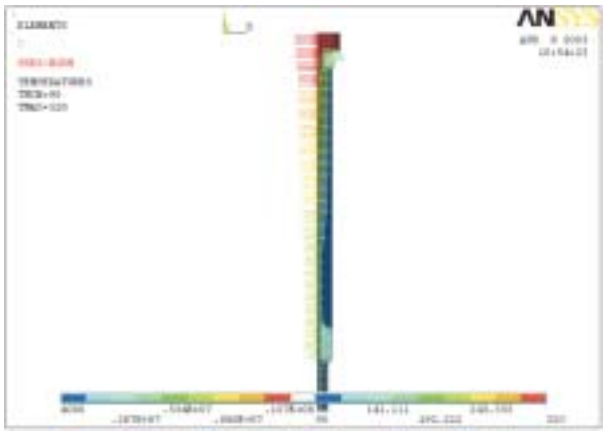

Fig.7 Graph of pressure loading (from either side).

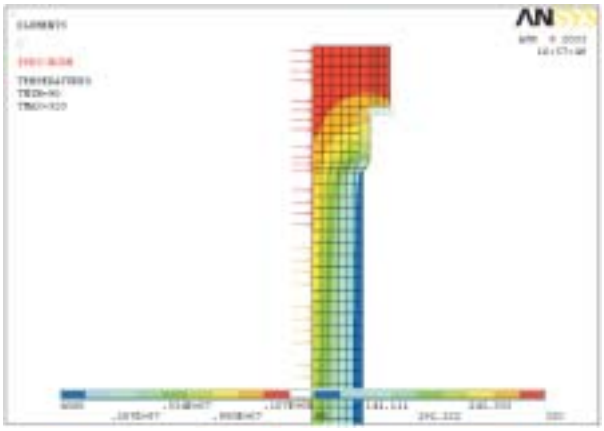

Fig. 8 Graph of pressure

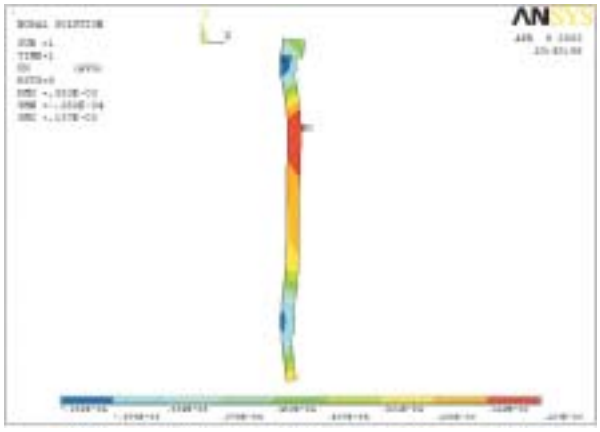

Fig. 9 Graph of displacements in the axis direction (displacements in metres) and temperatureloadings

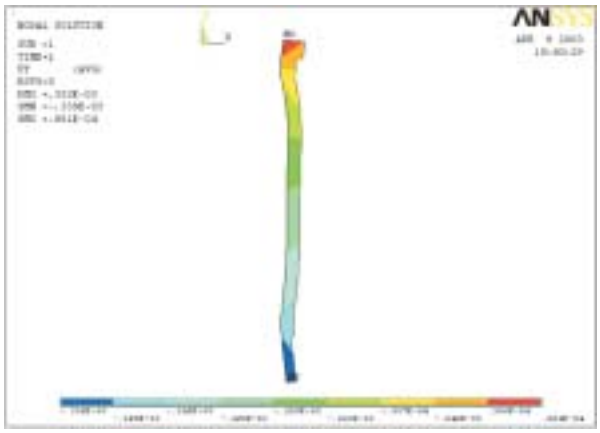

Fig. 10 Graph of displacements in direction (displacements are in metres)

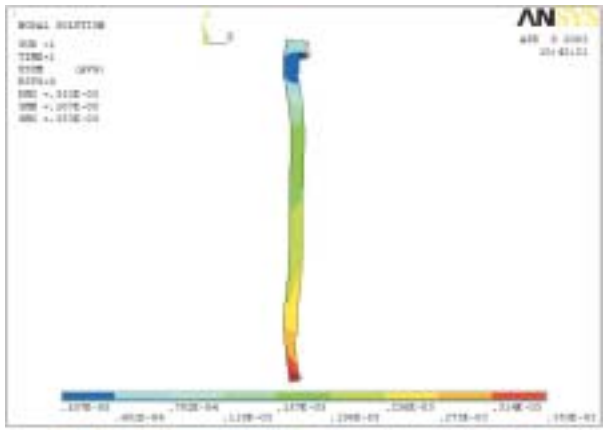

Fig. 11 Graph of full displacement of y-axis (displacements are in meters)

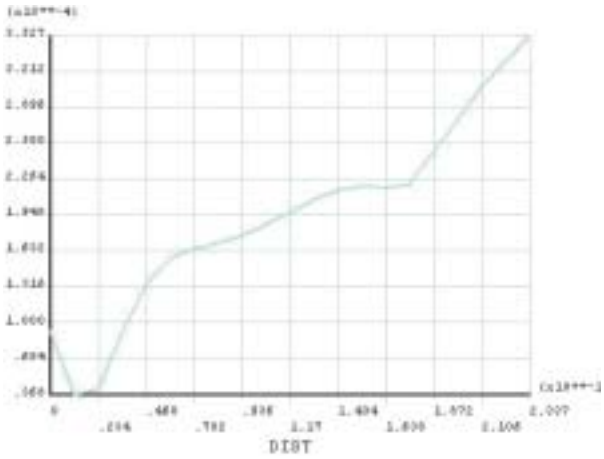

Fig. 12 Graph of full displacement dependences [m]
(horizontal axis – cylinder length, vertical axis – full displacement)

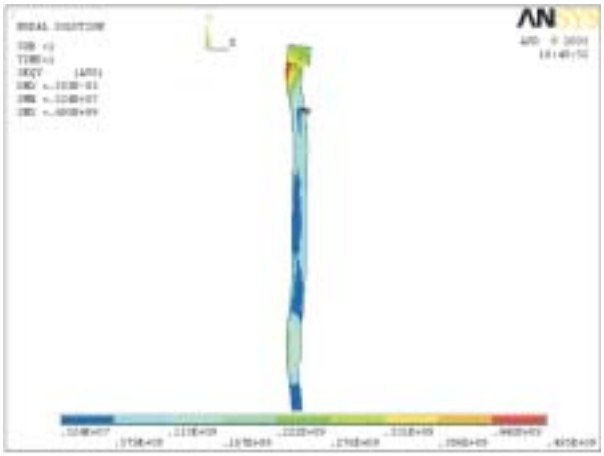

Figs. 13 Graph of stress distribution (Pa)

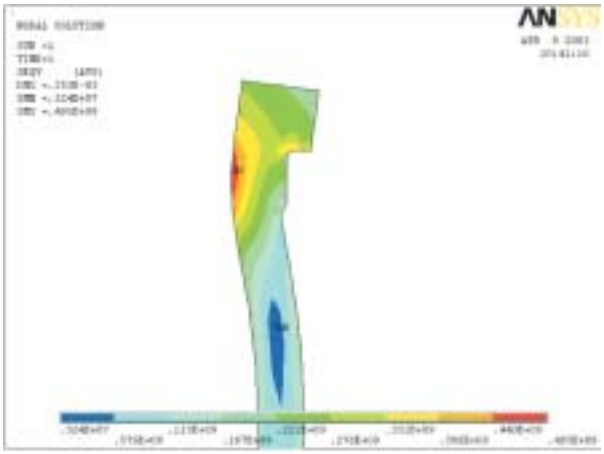

Fig. 14 Graph of stress distribution (Pa)

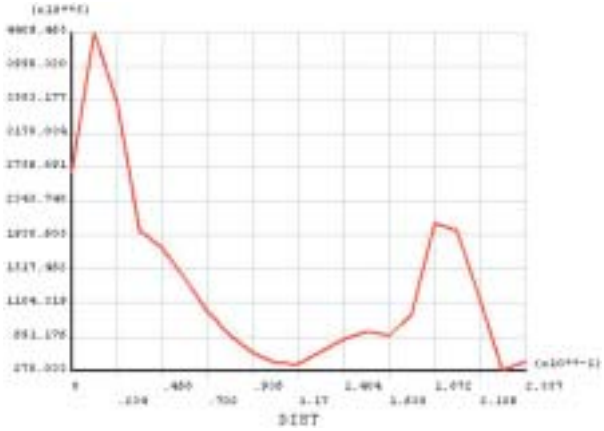

Fig. 15 Graph of stress dependence on the length
(horizontal axis – cylinder length [m], vertical axis – stress [Pa])

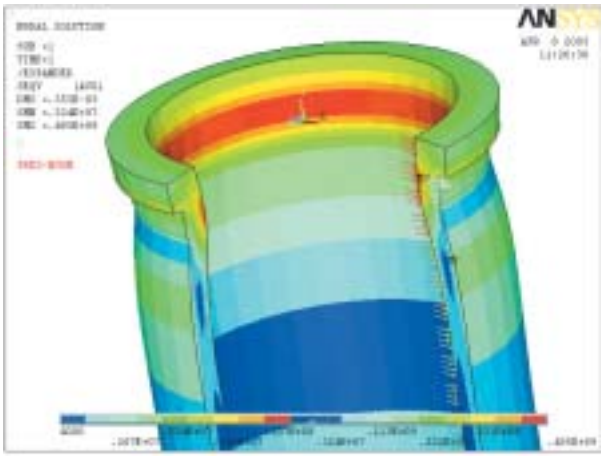

Fig. 16 Stress distribution (Pa)

From the results of the computation it was found out the the liner was loaded mainly in the upper part some 22 mm from the head by a relatively high stress of 445 MPa. The displacements can be considered insignificant mainly due to their position (in the y–axis direction in the liner top and in the x–axis direction in the upper quarter of the liner.

Modelling and simulation of coolant flow and energetic flows.

A mathematical model for flow analysis

The analysis is based on a mathematical model for turbulent flow of "renormalized groups type – RNG $k - \varepsilon$ – turbulent model". A renormalized procedure applied in turbulence lies in a gradual elimination of small turbulences. Simultaneously, equations of motion (Navier – Stokes equations) are transformed in such a way that turbulent viscosity, forces and nonlinear members are modified. Supposing that the turbulences are related to dissipation ε, then,

Mass flow rate and temperatures. Tab. 1

Mass flow rate from outlet [kg.s^{-1}]	Mass flow rate round cylinders [kg.s^{-1}]	temperature on outlet from cylinders [K]
outletV1a = 0.096	$m_{w1} = 0.233$	$T_{vch1} = 370.97$
outletV1b = 0.137		
outletV2a = 0.098	$m_{w2} = 0.237$	$T_{vch2} = 369.12$
outletV2b = 0.139		
outletV3a = 0.105	$m_{w3} = 0.260$	$T_{vch3} = 368.21$
outletV3b = 0.155		
outletV4a = 0.0984	$m_{w4} = 0.279$	$T_{vch4} = 361.41$
outletV4b = 0.181		

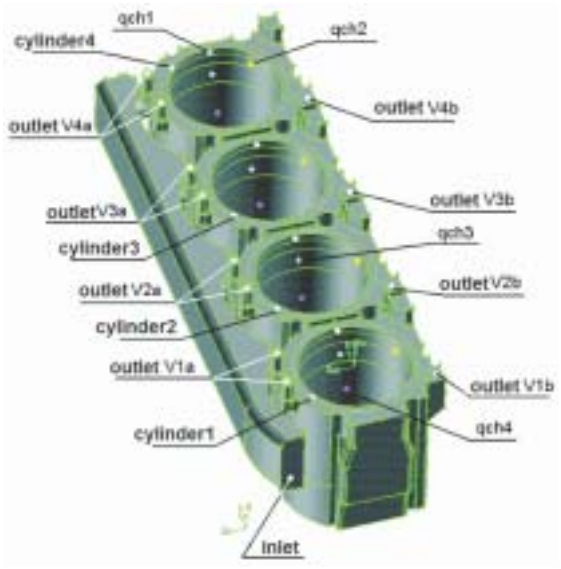

Fig. 17 Specification of boundary conditions

the turbulent viscosity μ_i depends on a degree of turbulences and the RNG method constructs this viscosity with the help of iterative elimination of narrow bands of wave numbers. The following equation is used for the iterative process:

$$\frac{d\mu_{eff}}{dl} = \frac{A_l \varepsilon l^3}{\mu(l)^2}. \tag{10}$$

The averaged RNG model derived by a statistical method has formally the same shape as the classical $k - \varepsilon$ model. The equation for transfer of momentum has the form:

$$\frac{\partial}{\partial t}(\rho\bar{u}_i) + \frac{\partial}{\partial x_j}(\rho\bar{u}_i\bar{u}_j) = \frac{\partial}{\partial x_j}\left[\mu_{eff}\left(\frac{\partial\bar{u}_i}{\partial x_j} + \frac{\partial\bar{u}_j}{\partial x_i}\right) - \right.$$

$$\left. - \left(\frac{2}{3}\mu_{eff}\frac{\partial\bar{u}_i}{\partial x_i}\right)\right] - \frac{\partial\bar{p}}{\partial x_i} + \rho g_i + F_i, \tag{11}$$

and, consequently, transport equations are used:

$$\frac{\partial}{\partial t}(\rho k) + \frac{\partial}{\partial x_j}(\rho\pi_j k) = \frac{\partial}{\partial x_j}\left(\alpha k \mu_{eff}\frac{\partial k}{\partial x_j}\right) + \mu_t S^2 - \rho\varepsilon$$

$$\frac{\partial}{\partial t}(\rho\varepsilon) + \frac{\partial}{\partial x_j}(\rho\mu_j\varepsilon) = \frac{\partial}{\partial x_j}\left(\alpha_\varepsilon\mu_{eff}\frac{\partial\varepsilon}{\partial x_j}\right) +$$

$$+ C_{1\varepsilon}\frac{\varepsilon}{k}\mu_t S^2 - C_{2\varepsilon}\rho\frac{\varepsilon^2}{k} - R \tag{12}$$

For more details see [4].

Computed and measured data Tab. 2

	Data computed by model	Data measured experimentally
Mass flow through block [kg.s^{-1}]	$m_w = \sum_{i=1}^{4} m_{wi} = 1.01$	$m_w = 1.01$
Average mising temperature leaving block [K]	$T_{vch} = \frac{\sum_{i=1}^{4} T_{vchi}}{4} = 367.17$	$T_{vch} = 367.24$
Total thermal flow to the cooling system [W]	$Q_{ch} = M_{ch} \cdot c \cdot \cdot (T_{vch} - T_{vých}) = = 41274.66$	$Q_{ch} = M_{ch} \cdot c \cdot \cdot (T_{vch} - T_{vých}) = = 41571.6$

Thermal flow from inserted cylinder. Tab. 3

Thermal flow from inserted cylinder Q_{chi} [W]	
Q_{ch1}	13 240.5
Q_{ch2}	11 626.3
Q_{ch3}	11 760.8
Q_{ch4}	4 652.0
Total thermal flow into coolant $Q_{ch} = \sum_{i=1}^{4} Q_{chi}$	41 279.6

Specification of places for measurement. Design of measure chain - sensors, transmitters.

The quality of the actual evaporation process is influenced by a constructional arrangement of the non-conventional cooling circuit of the combustion engine, pressure and temperature conditions under which the evaporation is assessed and concentration of alternative coolant. The cooling potential of atmospheric circuit is examined. Temperature conditions are defined by the boiling point of non-conventional coolant.

When compared with the former cooling system designed for tractor or automobile engines, for the non-conventional cooling system the following items can be defined:

Mass equation of the non-conventional system:

$$M_{ch} = m_{chl} + m_{chd} \tag{13}$$

Energetic equation of the non-conventional system (disredarding other thermal losses):

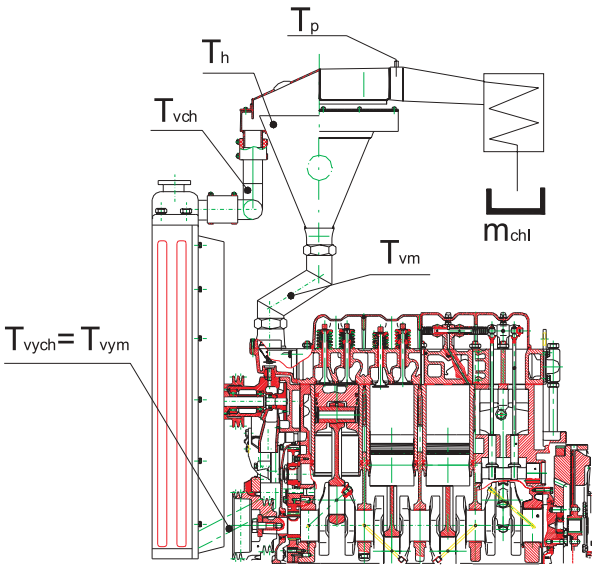

Fig. 18a m_{chl} - coolant mass flow, T_{vm} - temperature on engine outlet, T_p - vapour temperature, T_h - surface temperature in evaporator, T_{vch} - temperature of lean solution leaving the evaporator and entering the radiator, T_{vych} and T_{vym} - temperature entering the combustion engine.

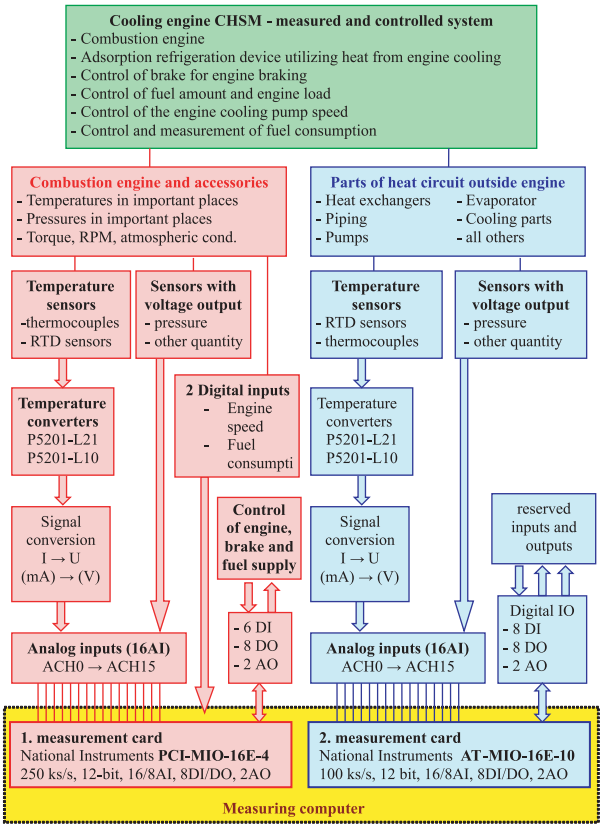

Fig. 18b Scheme of the measurement system of CHSM cooling engine

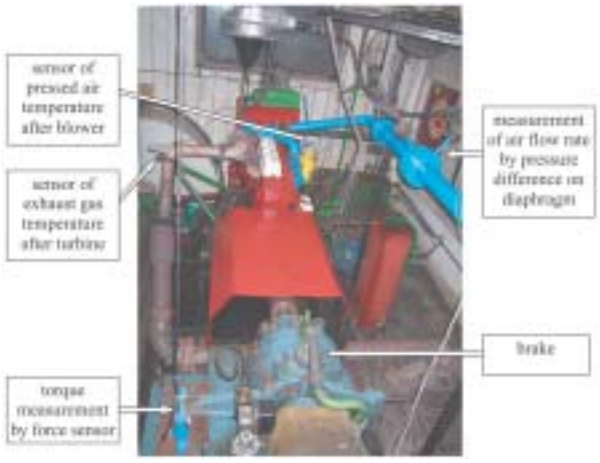

Fig. 18c Placement of selected measurement sensors

$$Q_{ch} = Q_{výp} + Q_{och} \tag{14}$$

Evaporation efficiency:

$$U_{tk} = \frac{Q_{výp}}{Q_{ch}} = 1 - \frac{Q_{och}}{Q_{ch}} = 1 - \frac{m_{chd} \cdot c \cdot (T_{vch} - T_{vych})}{M_{ch} \cdot c_r (T_{vm} - T_{vym})} =$$

$$= 1 - \frac{m_{chd} \cdot c \cdot \Delta T_{ch}}{M_w \cdot c_r \cdot \Delta T_M} \tag{15}$$

$$U_{tk} = 1 - \frac{Q_{och}}{Q_{ch}} = 1 - \frac{(T_{vch} - T_{vych})}{(T_{vm} - T_{vym})} = 1 - \frac{\Delta T_{ch}}{\Delta T_M}. \tag{16}$$

Within further reconstruction (reconstruction – adjustment of temperature sensors, insulation of the evaporation container) the $Q_{och} < Q_{ch}$ states are modelled at the atmospheric pressure. When defining this state it is necessary to follow trends of chosen parameters (oil temperature, exhaust gases temperature, flow through the block, temperature of the liquid at entering or leaving the engine, temperatures in the evaporation container, torque, consumption), which might clarify the transport of heat from the combustion space to the surface in the evaporation container.

Consequently, it is possible to define the value of a reduced output number as:

$$COP_{RED} = \frac{Q_e \cdot \eta_{el} + Q_{ch} \cdot U_{tk}}{Q_p}. \tag{17}$$

If we are able - when realizing the complex cooling system in the required conditions – to define the state $\Delta T_{ch} = 0$ under suitable temperature and heat conditions on the combustion engine, then $U_{tk} = 1$. Then, it follows that we are able to maximally utilize after-expansion exergy in the cooling system and that we are also able to transform it into evaporation heat required for defining the cooling output of the absorptive unit.

Points for temperature measurement.

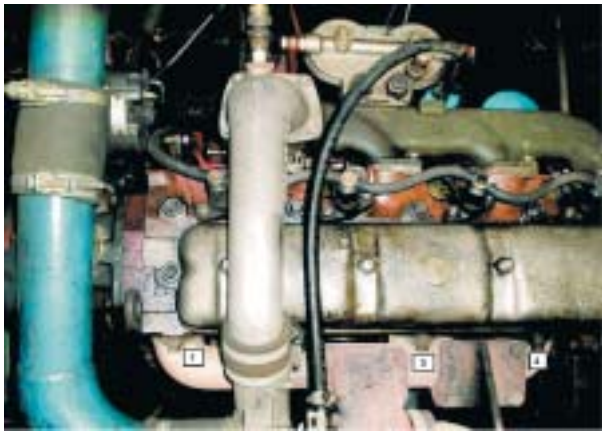

Fig. 19 Top view

Fig. 20 View of the turbocharger side

Fig. 21 View of the engine back

Fig. 22 View 1, the injection pump

Fig. 23 View 2, view of the injection pump.

Graphs of measured values (graph 4 and graph 5).

The year 2004

The following activities were carried out:

1. theoretical analysis and mathematical modelling
   - Drawing documentation for forced adjustments of the engine and test stand.
   - Checking and connecting the sensors for new tests, i.e. observation of the evaporation process, temperature states at intensification of evaporation under atmospheric pressure and consequently at underpressure.
   - Detailed topography of cavities of the engine cooling jacket, designed simplified virtual model of the engine cooling jacket, realistic meshing.
   - Modelling – meshing of the cavities of the engine cooling jacket – for calculation.
   - Solution of boundary tasks and conditions for the modelling of heat flows in the block.
   - Checking calculations and simulation of influence of changes in the boundary conditions.
   - Preliminary calculation (thermal balance) of quantities characterizing the state of coolant in particular places of the energetic circuit with the cooling combustion engine.

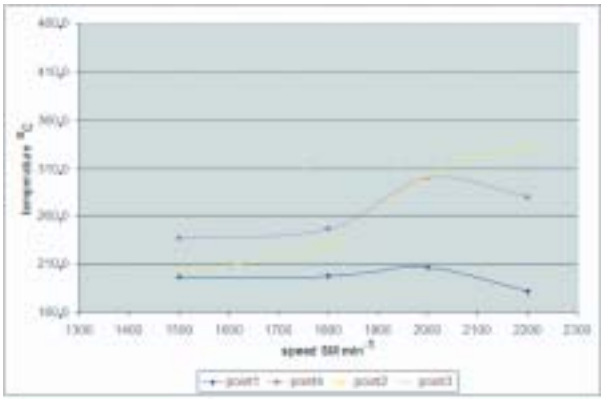

Graph 4(left) Change of temperature for revolutions in defined points.

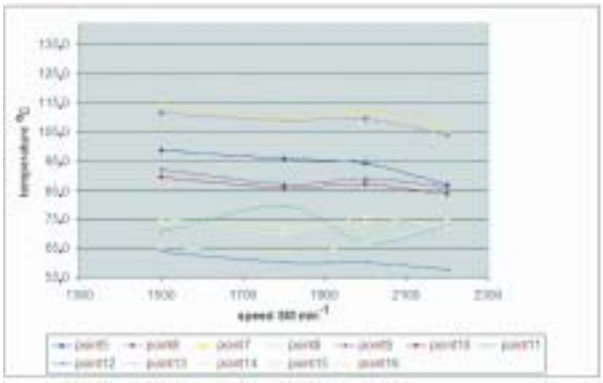

Graph 5(right) Change of temperaturefor revolutions in defined points.

2. experiments
   - Measurements of surface temperatures of the engine – assessment.
   - Dismantling and assembly of the engine for the purpose of topography of the cooling jacket (of real cavities).
   - Tests of the original engine – with an alternative coolant (LiBr).
   - Tests of the engine with an adjusted cooling system with the evaporator to define the output reduced number.
   - The arrangement of the test stand and its control with the focus on automation of tests of the engine with a modified cooling circuit with an external pump in order to verify the results from the virtual modelling.

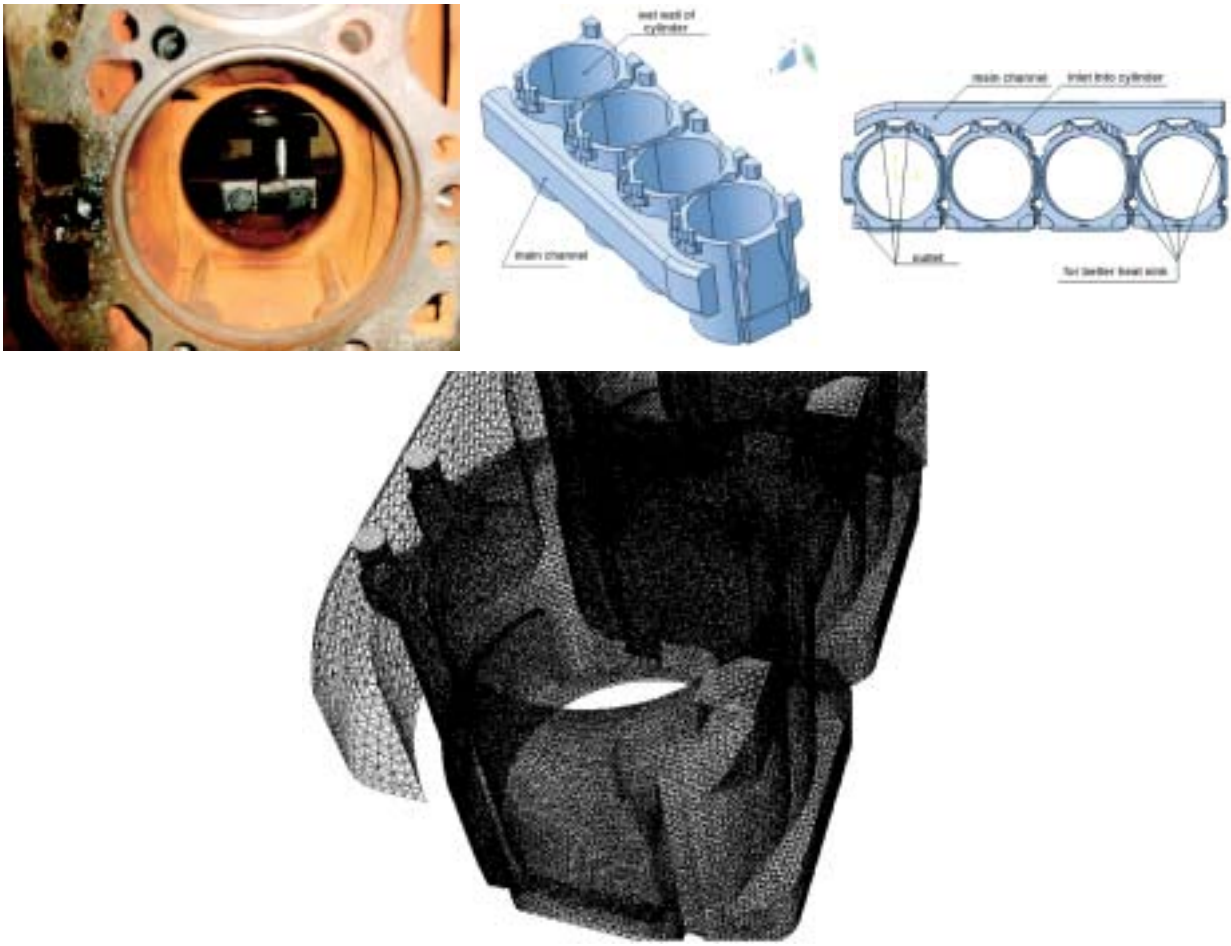

Fig. 24 Cavities of cooling jacket – real, virtual model, mesh

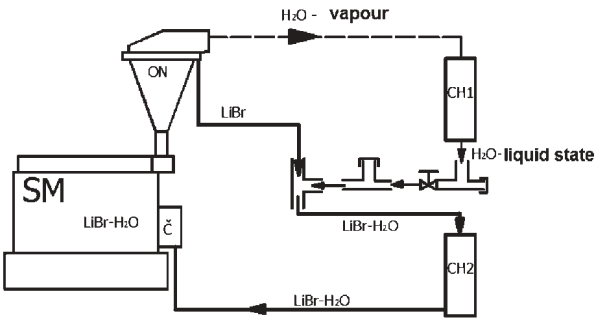

Fig. 25 (left) Assembly of atmospheric test stand.

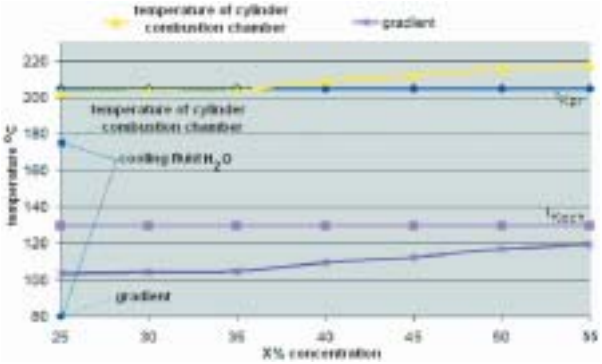

Graph 6 (right) t_{Kpr} - criterion of critical average temperature of overheating, t_{Koch} - criterion of critical average temperature of cooling.

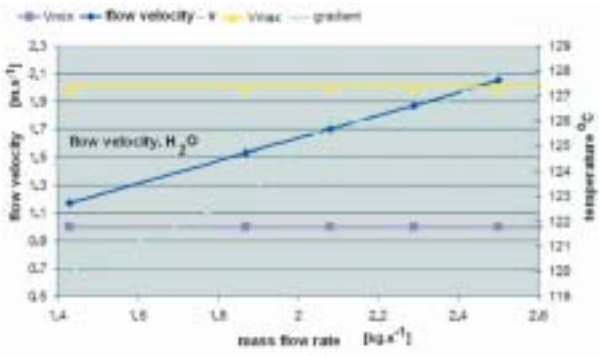

Graph 7(left) v_{min} - min. value of interval recommended for velocity of flow in the engine block, v_{max} - max. value of interval recommended for velocity of flow in the engine block.

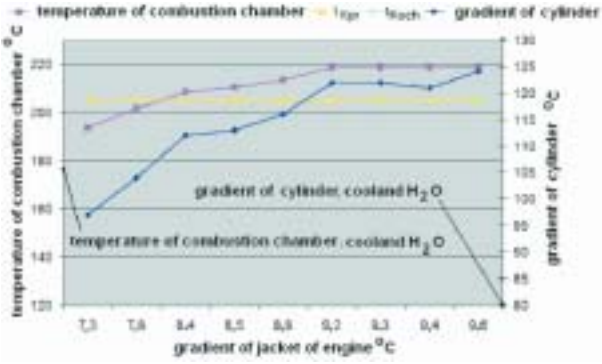

Graph 8 (right) Course of observed temperatures on gradient under the constant condition of output temperature from the ICE block.

The resultant point of the cooperation of the ICE with the absorptive cooling system.

All the investigated parameters were recorded and assessed with a computer programme.

Alternatives of the cooling system arrangement

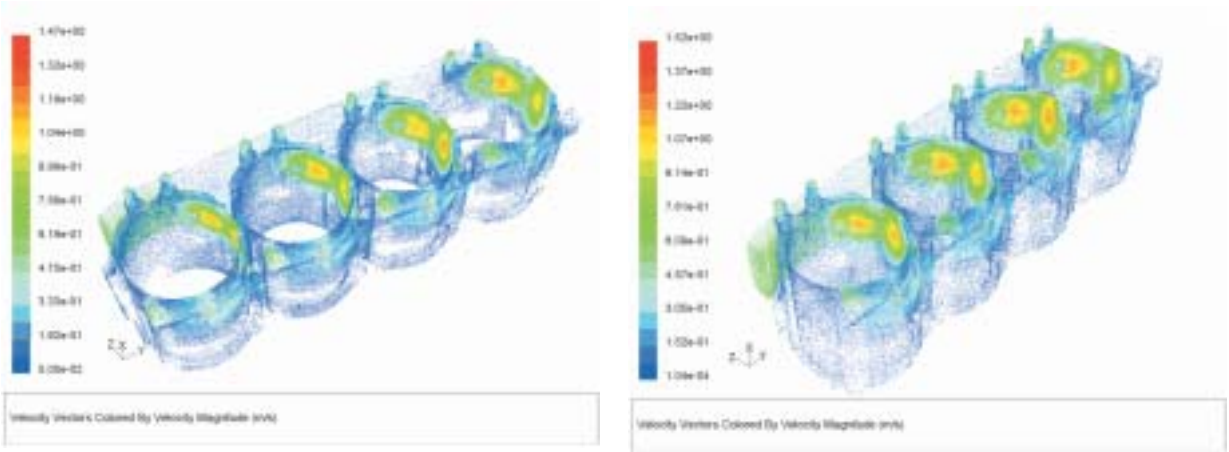

Fig. 26 Velocity field of flow (original coolant on the left, alternative coolant on the right)

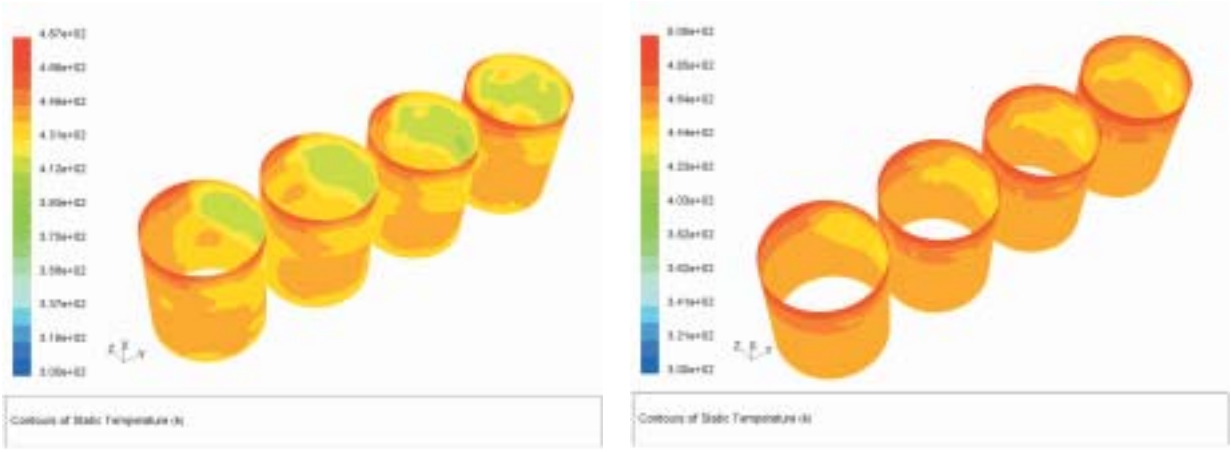

Fig. 27 Temperature fields (original coolant on the left, alternative coolant on the right)

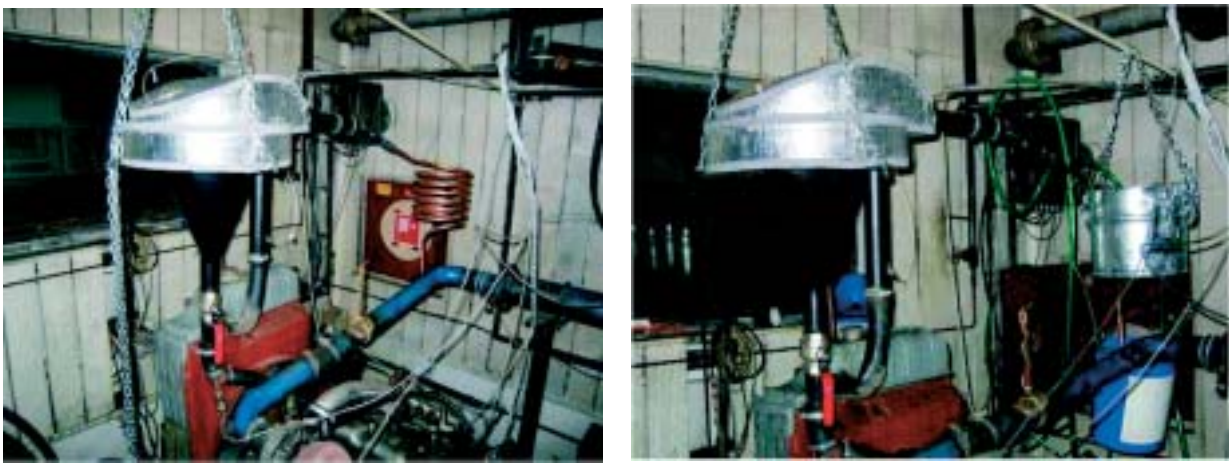

Fig. 28 A alternative – left: view of non-cooled copper spiral, right: view of cooled copper spiral

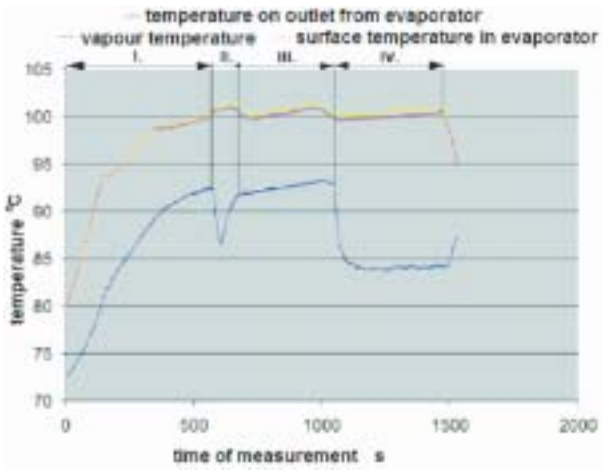

Graph 9 Measurements for A alternative

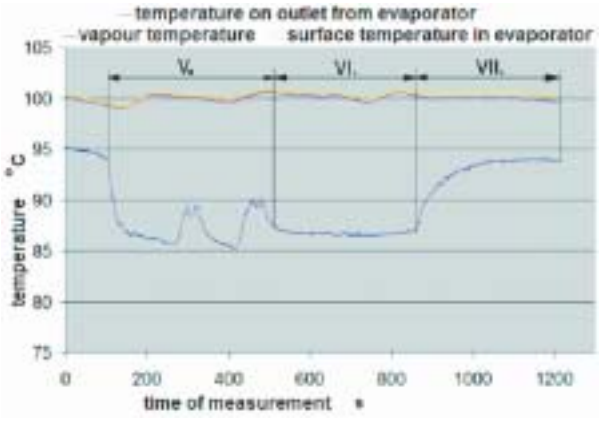

Graph 10 Measurements for B alternative

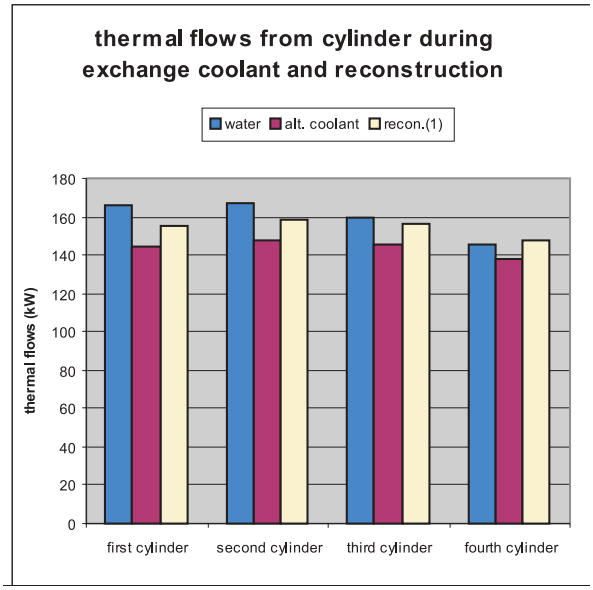

Graph 11. Results of modelling of exergy flow

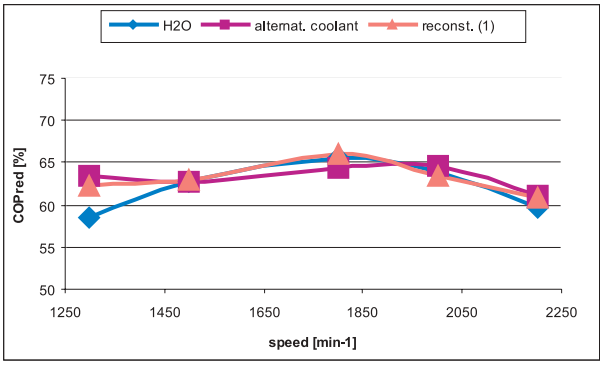

Graph 12 Performance coefficient

The year 2005

The following activities were carried out:

1. experiments
   - Measurements taken on the engine with the adjusted cooling circuit with the external circulation pump with the aim of assessing real flows of coolant for further virtual modelling.

2. alternatives of solution, assessment and final reviewing procedure.
   - Heat and energetic losses for different flows of coolant and constant revolutions of the engine.
   - Evaluation of the project main objective.
   - Final opinions of reviewers.

Quantitative assessment of publications written during the project solution:

Publications in foreign and domestic journals	Number: 10

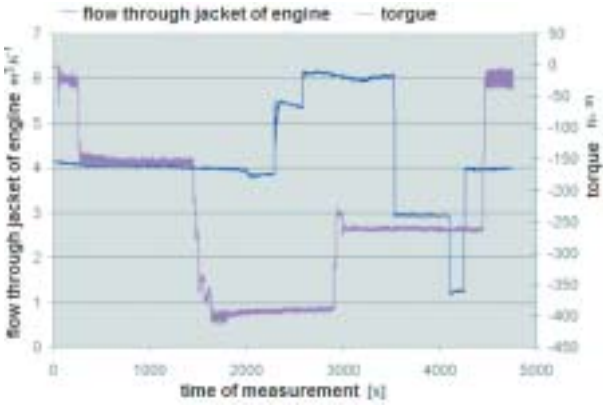

Graph 13(left) Changes in flow through the ICE block and engine loading (that is why the values are negative)

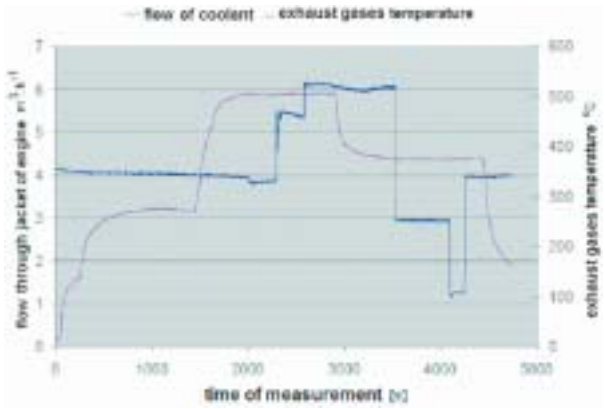

Graph 14(right) Changes in exhaust gases temperature and flow of coolant through the block

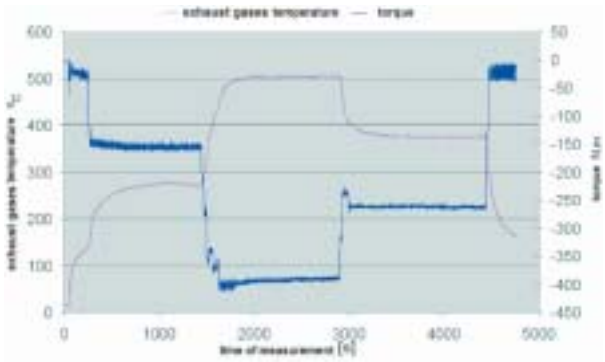

Graph 15(left) Changes in torque and and exhaust gases temperature

Scientific monographs (also individual chapters) abroad	Number: 1
Scientific conferences (presentations, posters)	Number: 17
Doctoral dissertations and diploma theses	Number: 7

Graph16(right) Temperature changes in relation to the change of coolant flow

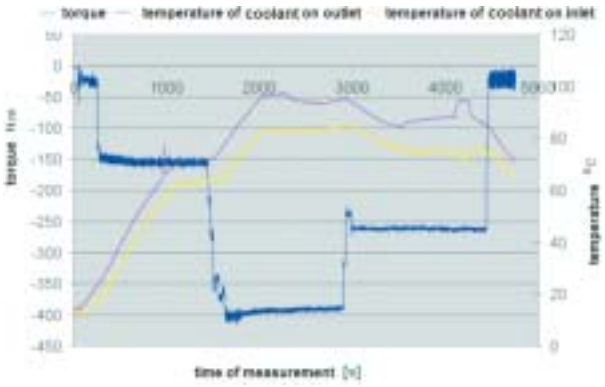

Graph 17(left) Temperature changes in relation to torque change

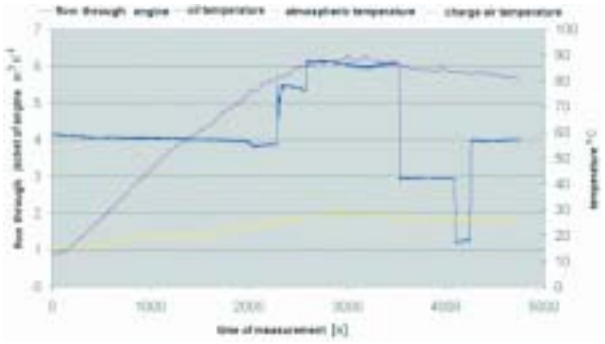

Graph 18(right) Changes in temperatures of oil and charge air

3. Social benefits

Extension of existing knowledge

The results of both theoretical solution and experiment were continuously published in journals and presented at conferences not only in the Slovak Republic but also abroad.

Aplication of new knowledge in educational materials of institutions of higher learning

Within the framework of the pedagogical process students of engineering and doctoral forms of study get acquainted with the results of theoretical solution and during laboratory practical activities and individual students activities (e.g. theses and dissertations) directly participate in the project solution.

Transfer of knowledge for consequent task solutions

On the basis of the results achieved within this project solution we submitted an application for another project "Non-conventional energetic unit with a cooling combustion engine". The project was approved by the Agency for Support of Science and Technology as APVT-20-018404. The project makes use of the results gathered from basic research, i. e. more effective utilization of fuel primary energy (in this specific case it is oil) by means of nonconventional principle of transfer of heat into cold by thermocompressions in the piston combustion engine (cooling combustion engine).

Extension of scientific and technical know how

The project solution confirmed the possibility of utilization of thermocompression in the classical piston combustion engine and thus contributed to the extension of the contemporary scientific and technical knowledge.

The paper is based on the final report on the project.

The contribution was created within the framework of the project Nr. APVT - 20 - 010302, which is supported by the Agency for Support of Science and Technology of the Slovak Republic.

Emília Wagnerová – David Uríček *

ENERGY EVALUATION OF THE MUNICIPAL SOLID WASTE PYROLYSIS

This contribution deals with possibilities of using pyrolysis as a method for municipal solid waste (MSW) disposal. Taking into account the possibilities of MSW separation, specific sorts of wastes were selected and subjected to laboratory experiments. The main aim of experimental measurements was to determine the distribution of the caloric value of an original sample in the products of pyrolysis. The aim of this research was to determine the energy content of selected MSW sorts and to recommend the method of their thermal disposal.

Key words: pyrolysis, municipal solid waste, caloric value, human environment

1. Introduction

Worsening environmental situation in the whole world is caused mainly by the excessive and continually rising amount of waste. The European Union program of waste management includes also a strategic plan aimed at solving this problem, with possible use of waste for energy production. When there is no possibility to prevent the production of waste or to recycle waste, the waste should be disposed of using technology with the least possible impact on the environment [1]. Thus, different sorts of wastes should be disposed of using different methods.

The problem of waste includes the whole cycle: production – use – disposal. When the waste material cannot be recycled, primary effort is to reduce its volume and then, considering its composition and technical properties, to technologically use it. The reduction of the waste volume may be more or less successfully performed by thermal treatment of waste. This technology exploits also the combustibility of waste, i.e. its energy content. Most of solid combustible waste has higher calorific value than quality brown coal. Thermal processes of waste disposal include combustion, gasification and pyrolysis. While combustion and gasification are exothermic processes that need oxygen supply, pyrolysis is an endothermic process requiring no oxygen. However, none of these technologies is totally harmless to the environment, since being thermal technologies they all are, directly or indirectly, loaded with the negatives of the combustion process [2].

The aim of the research whose results are presented also in this contribution was to determine the energy potential (content) of selected MSW sorts and, using the obtained data, to advance a recommendation as to the method of their thermal treatment. To do so we have chosen selected waste samples for experimental measurements using laboratory pyrolysis apparatus.

2. Selection of waste for experimental test

The selection of samples was based on frequently present MSW components suitable for disposal using thermal technology. The possibility of their separation was also taken into account. Following components were chosen for experimental tests: packaging paper – TP, newsprint – NP, cotton – BA, synthetic textile – PA, polypropylene – PP, polyethylene – PE, polyethylene-terephthalate – PET. Samples of selected waste components were subjected to the pyrolysis process and the energy content of the pyrolysis products was then evaluated. Due to insufficient analysis of plastic components their energy evaluation could not be made in full. Proximate and ultimate analysis of investigated samples prior to pyrolysis, determined by laboratory measurements, is given in Table 1.

Proximate and ultimate analysis of samples (* calculated) Table 1

Sample	Water	Ash	Combustible*	C^d	H^d	N^d	O^{d*}	S^d	Q_s	Q_n
	[% wt.]								[MJ.kg^{-1}]	
TP	5.55	15.25	79.2	36.84	5.19	< 0.1	39.23	0.02	13.21	11.93
NP	5.89	26.42	67.69	37	4	< 0.1	30.77	0.06	12.02	11.05
PA	0.40	0.31	99.29	51.5	4.1	0.4	43.64	0.05	15.81	14.90
BA	5.11	0.96	93.93	45.3	6.9	<0.1	46.58	0.11	15.87	14.31

* **Emília Wagnerová, David Uríček**
Department of Power Engineering, Technical University of Košice, Faculty of Mechanical Engineering, Vysokoškolská 4, 042 00 Košice, Slovakia

3. Apparatus for experimental measurements

The design of the apparatus was based on a basic requirement of the pyrolysis method, which is an oxygen-free environment. In our apparatus the working space was filled with an inert gas – nitrogen. The material was heated by an electrical resistance furnace. In laboratory conditions, using laboratory apparatus, no continual operation was envisaged. When designing the apparatus the rate of pyrolysis, temperature in the working zone as well as the method of capturing the produced residues were also taken into account. The scheme of the apparatus is shown in Fig.1.

In order to prevent the penetration of air into the working space the pressure above atmospheric (100 mm of technological liquid) realized by liquid seal is maintained in the oven. Gas produced by pyrolysis is captured in the gas collecting vessel after bubbling through the technological liquid of the seal. It was necessary to choose such a liquid, which would not absorb the traced components since such an absorption would distort the results. We used a solution of vinegar and water with the acidity of at least 4.5 pH [3]. The principle of our laboratory apparatus fully suits the requirements for a future technological solution of a pilot plant [4].

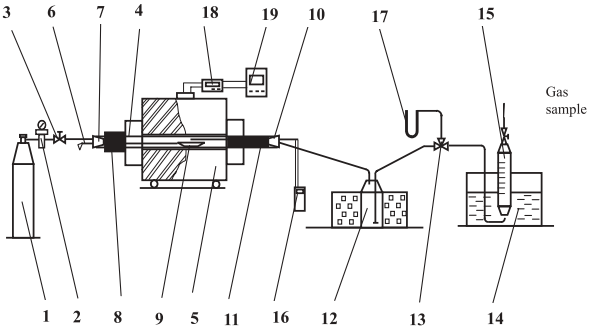

Fig. 1 Scheme of the laboratory pyrolysis apparatus
1 - cylinder of N2, 2 - pressure control valve, 3 - closing valve, 4 - furnace body (quartz tube), 5 - electrical resistance furnace, 6 - adjustable bar, 7 - input tube closing, 8 - feed-in chamber, 9 - combustion boat, 10 - output tube closing, 11 - output chamber, 12 - gas cooler, 13 - 3 - way valve, 14 - technological liquid, 15 - gas collecting vessel, 16 - Pt-RhPt thermocouple with thermometer Testo 945, 17 - U manometer, 18 - thermoregulator TC-31, 19 - electric supply meter

4. Evaluation of experimental measurements

Our aim was not to investigate pyrolysis as a technological process and thus verify what is already known [5–9]. The aim of our measurements was to determine the quantitative and qualitative energy content of the pyrolysis products and to compare them with the energy content of the original waste. The measurements were performed at three different temperatures (600, 800 and 600/800 °C). All the samples, each with a mass of 0.5 g, were subjected to pyrolysis under the same conditions and the decrease of the sample mass, the volume of the produced gas and its composition were observed during the pyrolysis process. The amount of the produced condensate could not be measured and so it was determined by computation based on the preservation of mass. The results of measurements are presented in the form of histogram. Fig. 2 shows the relative amount of pyrolysis residues.

It may be concluded from these graphs that the highest conversion of solid material into liquid and gas products is shown by plastic, while paper shows the lowest conversion degree. This may be connected with the ash content in the original sample. With increasing temperature the amount of the gas product increases while that of the solid product decreases.

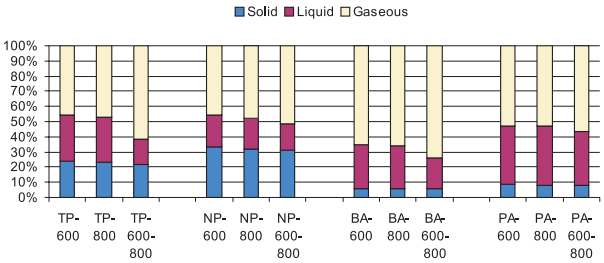

Fig. 2 Relative masses of individual pyrolysis products

We determined the calorific value of produced residues – pyrolysis gas and solid rest. To the calorific value of gas products contribute combustibles CH_4, H_2, CO and higher hydrocarbons. From their quantitative participation, at given temperature of pyrolysis, we determine the influence of particular components on the total calorific value. The relative content of particular combustible components at various temperatures for the gas product is shown in Fig. 3.

These graphs show that at higher temperature (i.e. 800 °C) the yield of hydrogen increases in comparison to methane. At lower temperature the situation is reverse and the yield of methane is higher. CO content only slightly increases with the temperature, but, except for PE and PP, its content is generally high. From the energy point of view the pyrolysis seems quantitative richer in the gas product.

The energy balance of the products of waste pyrolysis depends not only on the calorific value of a product but also on the amount of these products. To be able to compare the energy potential of selected waste sorts before and after pyrolysis, for the final evaluation we transform all energy values into the thermal energy [kJ] of products and we compare them as such. Energy evaluation of the products produced by the pyrolysis of selected components of waste was performed for their solid and gas product. Liquid product of pyrolysis had insufficient volume for performing elemental analysis and so it was not accounted for in the energy evaluation. Thermal energies of selected sorts of waste before and after pyrolysis are given in Fig. 4.

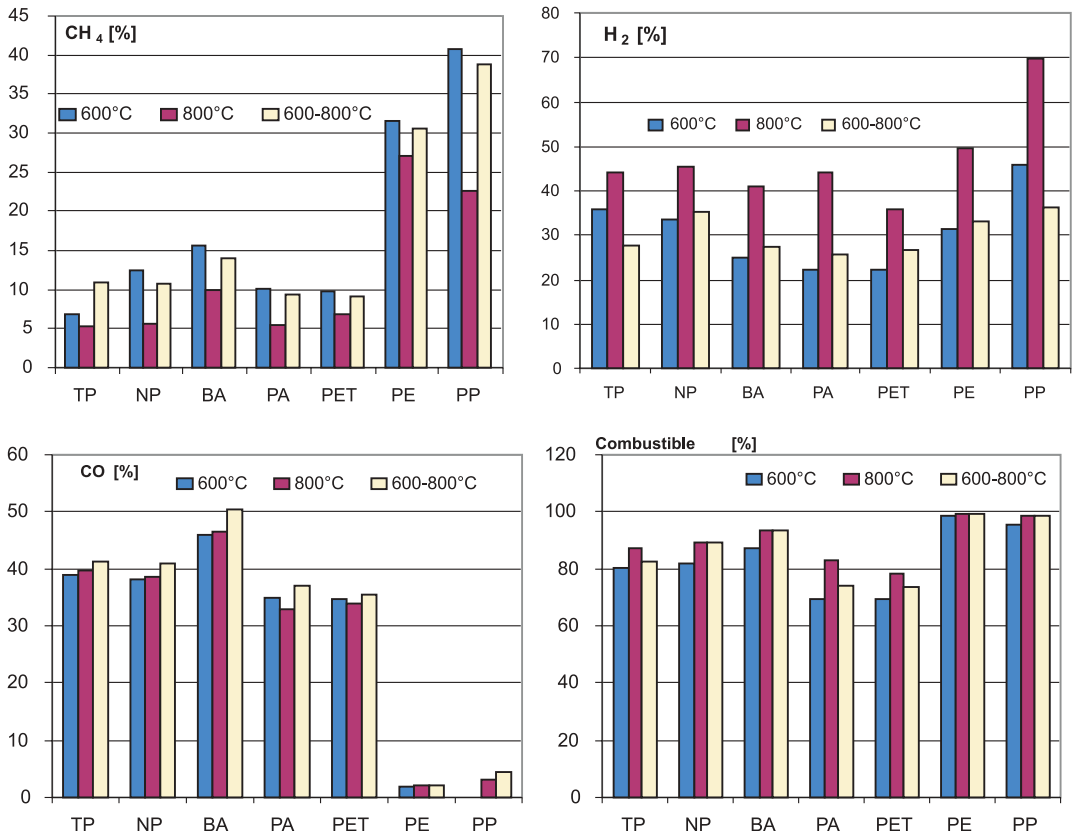

Fig. 3 Influence of temperature on CH_4, H_2, CO and combustible yield

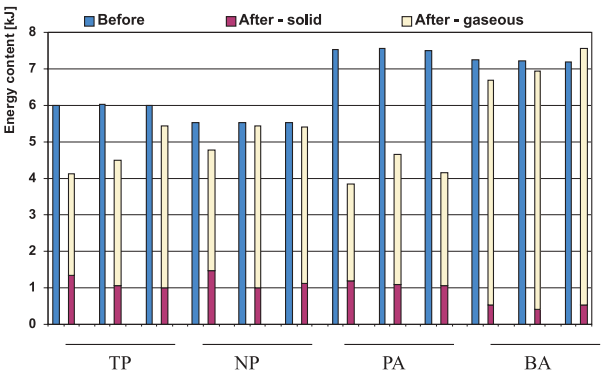

Fig. 4 Energy content of waste before and after pyrolysis

5. Conclusion

We can conclude that pyrolysis leads to the substantial reduction of the volume and mass of waste and that with the increasing temperature the volume of the produced gas increases. Considering the energy potential the pyrolysis seems to be quantitative richer in the gas product:

- H_2 content is higher at the temperature of 800 °C,
- CH_4 content is higher at the temperature of 600 °C,
- Pyrolysis gas contains a relatively high amount of CO (except for PP and PE).

On the basis of the obtained results we can recommend that for the disposal of PE, PP (plastics) and cotton (BA) it is suitable to use pyrolysis, for TP and NP (paper) incineration and for PA and PET gasification. When deciding on the use of a particular thermal treatment for the waste disposal it should be taken into account that pyrolysis is a method with endothermic reaction [10, 11] and, therefore, it is necessary to consider well if the use of this method is justified.

Acknowledgements

This work has been supported in part by the Scientific Grant Agency of Ministry of Education of the Slovak Republic and Slovak Academy of Sciences under the Grant No.1/9398/02 and 1/2918/05. The authors would like to thank for support that made this work possible.

References

[1] EC Waste Framework Directive, EU, 1991.
[2] MOLČAN, P., KLENOVČANOVÁ, A., IMRIŠ, I.: *Characteristic of harmful compounds incipient by the waste incineration* [in Slovak]. – Acta Mechanica Slovaca, 3/2003 RAVYPaSE, SjF TU Košice, Košice, 2003, pp. 319–322.
[3] WAGNEROVÁ, E. URÍČEK, D: *Pyrolysis of selected parts of MSW in laboratory conditions*. – Systems, Vol. 9, Special Issue 2/2, Polish Systems Society, 2004. pp. 637–642.
[4] URÍČEK, D., BEŽOVSKÝ, M., VARGOVČÍK, V.: *Laboratory apparatus for energy evaluation of MSW pyrolysis* [in Slovak]. – Acta Mechanica Slovaca, 3-A/2004, SjF TU Košice, Košice, 2004, pp. 519–522.
[5] BRIDGWATER, A. V., GRASSI, G.: *Biomass pyrolysis liquids upgrading and utilisation.* – Elsevier, London – New York, 1991.
[6] KLASS, D. L.: *Biomass for Renewable Energy, Fuels, and Chemicals.* – Academic Press, London, 1998.
[7] LIN, K-S. et al.: *Pyrolysis kinetics of refuse-derived fuel.* – Fuel Processing Technology, No. 60, 1999, pp. 103–110.
[8] GARCIA, A. N. – MARCILLA, A. – FONT, R.: *Thermogravimetric kinetic study of the pyrolysis of municipal solid waste.* – Thermochimica Acta, 254 (1995), pp. 277–304.
[9] WU, CH.-H. et al.: *Thermal treatment of coated printing and writing paper in MSW: Pyrolysis kinetics.* – Fuel, No. 12, 1997, pp. 1151–1157.
[10] OBROUČKA, K.: *Thermal waste disposal* [in Czech]. – FMaMI VŠB – TU Ostrava, Ostrava, 1997.
[11] TÖLGYESSY, J., PIATRIK, M.: *Water, Air and Solid Waste Technology* [in Slovak]. – Chtf STU Bratislava, Bratislava, 1994.

Ján Lábaj – Dalibor Barta *

UNSTEADY FLOW SIMULATION AND COMBUSTION OF ETHANOL IN DIESEL ENGINES

The paper presents the survey of ethanol application as the fuel for diesel engines which is added to diesel fuel or injected to the inlet manifold. The paper describes unsteady flow simulation in the inlet manifold of a 4 cylinder diesel engine with injected ethanol (Martin Diesel UR IV). The calculation of mixing rates is based on transient spray-plume-growth with concentration and temperature profile applying the CFD code (software of Fluent Inc. USA). The calculation of combustion was performed using a RNG $k-\varepsilon$ (renormalization group) turbulent model, standard wall function and a PDF model for chemical equilibrium of gas composition and kinetics in the combustion chamber.

Key words: diesel engines, combustion, ethanol, equilibrium and kinetic of gas composition

1. Introduction

The simulation of the processes concerning the combustion mixture creation has been for a long time period only at the level of an experimental matter. By means of the computer technology development and by application of differential methods the problems of the very consistent computational grids in the area of nozzle drills and in the locality where the combustion mixture is created at the fuel beam as well as the problems with enormous gradients of pressures, concentrations or velocities have been partly overcome. The aim of this work was to compare the exhaust emissions created at the combustion of ethanol mixed in diesel and ethanol injected in the intake manifold with the emissions originated by the combustion of pure diesel fuel. The simulation was done for the ethanol injection into the intake channel of the engine head of the Martin Diesel UR IV engine and at the combustion process specified for a compression ignition engine at the consideration of the equilibrium composition of emissions and kinetics of combustion of ethanol. For simulated calculation the equations of continuity, Navier – Stokes equations, equations for energy balance and Arrhenius rate equation were applied.

2. Applied numerical method

For formation of the combustion mixture the following basic balance equations can be applied.

The continuity equation for the component α:

$$\frac{\partial \theta \rho_\alpha}{\partial t} + \nabla \cdot (\theta \rho_\alpha \vec{u}) = \nabla \cdot \theta \rho D \nabla \frac{\rho_\alpha}{\rho} + (\dot{\rho}_\alpha)_p \qquad (1)$$

where: θ represents the volume portion taken by gas,
$(\rho_\alpha)_p$ describes the velocity of density change of the α component caused by evaporation.

For individual particles

$$(\dot{\rho}_\alpha)_p = 0, \quad \alpha \neq v \qquad (\dot{\rho}_v)_p = -\frac{1}{V} \sum_k \frac{dm_k}{dt}, \qquad (2)$$

where the element v represents evaporated fuel, V is volume throughout all the particles and m_k stands for the mass of k-particle.

Then the equation for the momentum compliance can be written in the form:

$$\frac{\partial \theta \rho \vec{u}}{\partial t} + \nabla \cdot (\theta \rho \vec{u} \vec{u}) = -\theta \nabla p + \nabla \cdot$$

$$\cdot \theta(\mu \overleftrightarrow{e} + \lambda \overleftrightarrow{I} \nabla \cdot \vec{u}) - \frac{1}{V} \sum_k D_k (\vec{u} - \vec{u}_{pk}) \qquad (3)$$

where: u_{pk} represents the velocity of k-particle, D_k is the function of the particle carrying, e is tensor of viscosity tension and $\bar{I}$ stand for the unit tensor.

For Stokes' streaming round the drop

$$D_k = 6\pi\mu\, r_k + \frac{1}{2} \pi r_k^2 \rho C_D \left| \vec{u} - \vec{u}_{pk} \right| \qquad (4)$$

where r_k is the particle semi-diameter and C_D coefficient of particle drag.

The equation of the inner energy I:

* **Ján Lábaj, Dalibor Barta**
University of Zilina, Univerzitná 1, 01026 Žilina, Slovak Republic,
E-mail: jan.labaj@fstroj.utc.sk, dalibor.barta@fstroj.utc.sk

$$\theta\rho\left[\frac{\partial I}{\partial t}+\vec{u}\cdot\nabla I\right]=\frac{\theta p}{\rho}\left[\frac{\partial\rho}{\partial t}+\vec{u}\cdot\nabla\rho\right]+\nabla\cdot\theta\left[K\nabla\mathrm{T}+\rho D\sum_{\alpha}h_{\alpha}\nabla\frac{\rho_{\alpha}}{\rho}\right]+\theta\left[\frac{\mu}{2}\vec{\vec{e}}:\vec{\vec{e}}+\lambda(\nabla\cdot\vec{u})^{2}\right]+$$
$$+\frac{1}{V}\sum_{k}\left[\left(D_{k}-\frac{1}{2}\frac{dm_{k}}{dt}\right)|\vec{u}-u_{pk}|-q_{k}+(h-h_{v})\frac{dm_{k}}{dt}\right] \quad (5)$$

where. q_k represents the intensity of thermal transfer from gas into the k-particle,
h_α is specific enthalpy of α component,
h – total enthalpy,
μ, λ – first and second viscosity coefficients.

The equations are solved by means of the finite volume method as follows:

$$\frac{d}{dt}\int_{V}\rho_{\alpha}\,dV-\int_{S}\rho_{\alpha}(\vec{u}_{g}-\vec{u})\cdot\vec{n}dS=\int_{S}(\rho D\nabla\frac{\rho_{\alpha}}{\rho})\cdot$$
$$\cdot\,\vec{n}\,dS+\int_{V}(\dot{\rho}_{\alpha})_{c}\,dV \quad (6)$$

$$\frac{d}{dt}\int_{V}\rho\vec{u}dV-\int_{S}\rho\vec{u}(\vec{u}_{g}-\vec{u})\cdot\vec{n}dS=-\int_{S}\rho\vec{n}dS+$$
$$+\int_{S}(\mu\,\vec{\vec{e}}+\lambda\,\vec{\vec{I}}\,\nabla\cdot\vec{u})\cdot\vec{n}dS \quad (7)$$

$$\frac{d}{dt}\rho IdV-\int_{S}\rho I(\vec{u}_{g}-\vec{u})\cdot\vec{n}dS+\int_{V}\rho\nabla\cdot\vec{u}dV=$$
$$\int_{S}(K\nabla T)\cdot\vec{n}dS+\int_{V}(\frac{\mu}{2}\vec{\vec{e}}:\vec{\vec{e}}+\lambda(\nabla\cdot\vec{u})2+\dot{Q}_{c})dV \quad (8)$$

where: V is volume, S surface and n – normal line.

3. PDF model

The composition of exhaust gas was calculated as equilibrium by searching the minimum of the system free enthalpy. To proceed from the assumption of high temperatures where the diffusion and mixture formation represent slower processes compared to chemical kinetics and, therefore, play the predominant role for exhaust gas formation. On the basis of this idea the calculation was done for diffusion flame in a high turbulent regime respecting the probability density function PDF. This function written as $p(f)$ describes a time interval of the fluctuation variable f, which is in the interval $f + \Delta f$. Then, the values within the time interval are calculated as Δf.p(f). The mathematical formula can be written as follows:

$$p(f)\,\Delta f=\lim_{T\to\infty}\frac{1}{T}\sum_{i}\tau_{i}\,, \quad (9)$$

where: τ_i represents the time interval when the function f is in the extent of Δf. The form of the function $p(f)$ depends on the natural turbulence fluctuations within f., $p(f)$ is expressed as a mathematical function PDF whose form is derived from the experiment.

The probability density function $p(f)$ describes the transient fluctuations of the turbulent stream and for its definition the time depended average values are used. In such a way the time depended

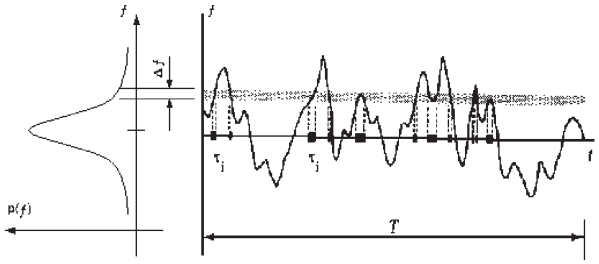

Fig. 1 Graphical illustration of the probability density function p(f)

average value for exhaust component concentration and temperature can be formulated in the form

$$\bar{\Phi}_{i}=\int_{0}^{1}p(f)\Phi_{i}(f)df \quad (10)$$

for one individual fraction of the system. Concerning also the secondary stream the average value can be calculated using the following equation:

$$\bar{\Phi}_{i}=\int_{0}^{1}\!\!\int_{0}^{1}p_{1}(f_{fuel})p_{2}(p_{secondary})\Phi_{i}(f_{fuel},p_{secondary})df_{fuel}dp_{secondary} \quad (11)$$

where: p_1 is PDF for f_{fuel} and p_2 PDF for $p_{secondary}$

Similarly, also the time related average value of liquid density can be calculated only for one mixture

$$\frac{1}{\bar{\rho}}=\int_{0}^{1}\frac{p(f)}{\rho(f)}\,df \quad (12)$$

when two different streams come into the system, then:

$$\frac{1}{\bar{\rho}}=\int_{0}^{1}\!\!\int_{0}^{1}\frac{p_{1}(f_{fuel})p_{2}(p_{secondary})}{\rho(f_{fuel}),(p_{secondary})}\,df_{fuel}dp_{secondary} \quad (13)$$

when for the secondary stream $\rho(f)$ or $\rho(f_{fuel}, p_{secondary.})$ exists.

The selection of the function (e.g. Gauss function) can be provided on the basis of experimental measurements of fluctuations.

The double delta function can be written in the form:

$$p(f)=\begin{cases}0.5, & f=\bar{f}-\sqrt{\bar{f}'^{2}}\\ 0.5, & f=\bar{f}+\sqrt{\bar{f}'^{2}}\\ 0, & elsewhere\end{cases} \quad (14)$$

Then the calculation of the double delta function is not complicated and can be made more precise than the alternative β PDF function.

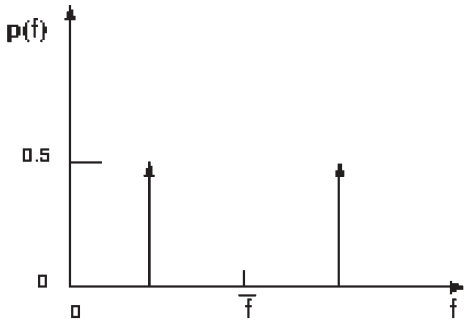

Fig. 2 Double delta function in the PDF form

The β function in PDF form can be expressed in the following version:

$$p(f) = \frac{f^{\alpha-1}(1-f)^{\beta-1}}{\int f^{\alpha-1}(1-f)^{\beta-1}\,\alpha f}\ ,$$

where $$\alpha = \bar{f}\left[\frac{\bar{f}(1-\bar{f})}{\bar{f}'^2} - 1\right] \qquad (15)$$

and also $$\beta = (1-\bar{f})\left[\frac{\bar{f}(1-\bar{f})}{\bar{f}'^2} - 1\right].$$

From the created tables the program at the calculation will read the values of temperatures and concentrations for multi-stream turbulent streaming and at mixing of streams which chemically react.

A non-adiabatic PDF model of combustion calculates the total enthalpy from the energy equilibrium equation:

$$\frac{\partial}{\partial t}(\rho H) + \frac{\partial}{\partial x_i}(\rho u_i H) = \frac{\partial}{\partial x_i}\left(\frac{k_t}{c_p}\frac{\partial H}{\partial x_i}\right) + \tau_{ik}\frac{\partial u_i}{\partial x_k} + Sh\,. \qquad (16)$$

The solution is possible when the Lewis number = 1. The total enthalpy

$$H = \sum_j m_j H_j$$

where m_j is a mass portion of j component and H_j

$$H_j = \int_{T_{ref,j}}^{T} c_{p,j}\,dT + h_j^0(T_{ref,j}),$$

where h_j^0 is a compound enthalpy of j-component at the temperature of T_{ref}.

4. A virtual model of the intake channel and combustion chamber

The task of a model creation for the mixture formation represents one of the complicated problems in the field of gas dynamics, and from this point of view it is necessary to make some simplifications and to select and apply the existing sub-models for turbulent streaming, drop distribution or boundary layer. The task was solved in two stages. Separately the ethanol injection in the intake channel for the engine Martin Diesel URIV (4 cylinders in line, turbo-charged) and separately the combustion of ethanol mixed in a diesel as the combustion of air / ethanol mixture ignited by injection of pure diesel. At the task solving the method CFD (Computational Fluid Dynamic) was applied. For the calculation of drop evaporation the professional programs offer the distribution curve by software. The calculation of the combustion mixture formation can be provided on the basis of the published empirical relations or by detailed mathematical models, but in this case the most sophisticated computer technology is required.

5. Initial and boundary conditions for calculation

The fuel injection was realised by one-point injection in the intake channel. The surface grid of the intake channel and valve (in an open position) is illustrated in Fig. 3. The apparent intake pressure by a turbo-blower is 0.08 MPa, the intake air temperature 120 °C. For the ethanol injection the piston movement was simulated by a boundary condition as the velocity of gas movement out from the cylinder or in the opposite way which was adequate for a suction stroke at 2200 rpm. in the range of TDC up to 40° CA after BDC when the intake valve closes. The task was solved as not-stationary. The temperature of the intake channel was 80°C, the calculation interval 10 deg. CA. The fuel injection was realised during the whole suction stroke. For drop evaporation the stochastic model was applied, for streaming the model for turbulence RNG $k-\varepsilon$, standard grid function. At the calculation in the FLUENT 5 programme the Rosin-Rammler distribution function was applied, which is in this programme pre-defined.

For the combustion process simulation the back-pressure was simulated with the values of real measured combustion pressure at the combustion of pure diesel. The surface grid of combustion chamber without the engine head grid is presented in Fig. 4, the grid of the part of injection nozzle which reached the combustion chamber in Fig. 5, the grid of injection nozzle drills in Fig. 6. The fuel injection began at 10° BTDC and in the case of pure diesel the injection ended at 11° ATDC. The calculation was made with the interval of 2° CA for all the three cases. At the combustion simulation of the ethanol / air mixture the injection timing was reduced to 1/4 with the identical injection beginning. With the purpose of a model simplification the diesel fuel was substituted by a fictive hydrocarbon $C_{16}H_{29}$. The injector drill diameter $d = 0.27$mm. The temperature of injected fuel $T_p = 423$ K. The fuel rate of flow through one injection drill $Q_p = 11.10^{-6}$ kg.s^{-1}. The interval of injection timing 21° CA. The wall temperature in the combustion chamber $T_s = 700$ K. The velocity of fuel flow through the injection drill $v_p = 180$ m.s^{-1}.

For more precise calculation it was convenient to apply a kinetic model with the detailed description of ethanol transformation through the intermediate products in CO and subsequently in CO_2. Through this model it would be possible to simulate the formation of aldehydes and unburned hydrocarbons at the diesel fuel combustion. Such a model was prepared but due to the insufficient computer parameters only the simulation of the mixture formation in

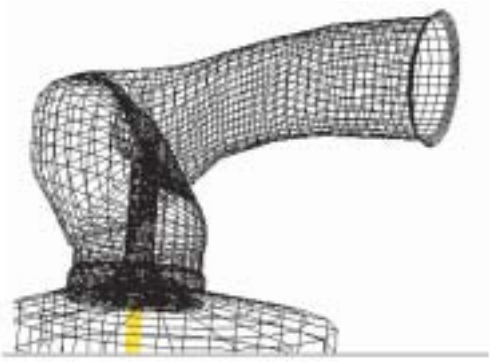

Fig. 3 Surface grid of intake channel

Fig. 4 Surface grid of combustion chamber without the engine head grid

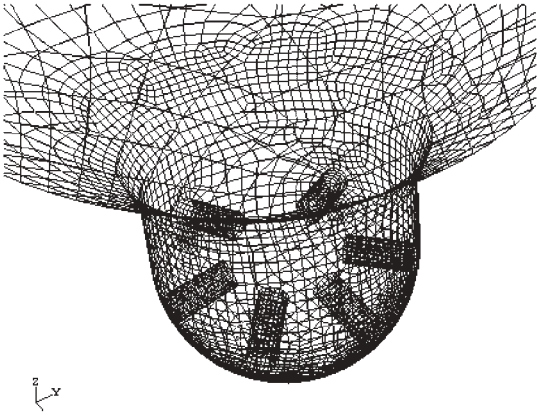

Fig. 5 Surface grid of injection nozzle

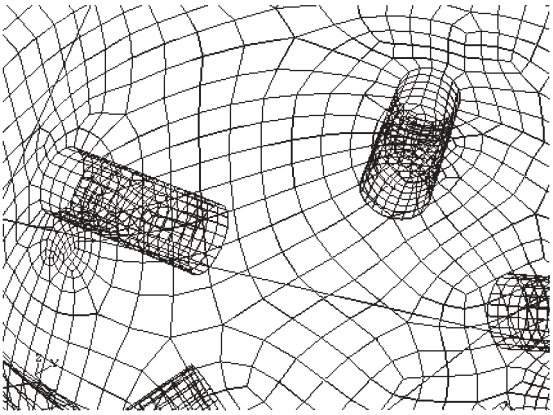

Fig. 6 Surface grid of injection nozzle drills

the combustion chamber was realised. The figures illustrate the exhaust emission concentration at 10° CA ATDC (in the point of the maximal combustion pressure).

6. Figures of the simulated velocity and temperature fields

Figs. 7 – 9 illustrate the ethanol concentration in the boundary layer in the intake channel vs. the angle of crankshaft. Figs. 10 – 13 present the cooling effect of injected ethanol. At the end of the suction stroke the temperature increase can be observed. It is caused by heating-up from the walls and by dynamics of the suctioned mixture.

Due to different specific caloric values (pure diesel vs. diesel / ethanol mixture) also the difference in the combustion chamber can be observed (illustrated in Figs. 13 and 14).

At the application of ethanol in diesel the increased temperature in the location of nozzle drill can be observed which can cause a higher temperature of the injection nozzle. The higher cylinder loading caused by cooling of the suctioned mixture results in the increase of temperature in the combustion chamber. The ignition portion represented 1/4 from the total fuel portion at the maximal engine power, e.g. 1/4 from the injection timing at the identical injection pressure. Fig. 15 illustrates static temperature, this figure must be assessed together with the Fig. 27 in which the curves of the constant velocity (iso-tacheo-curves) of combustion mixture streaming are presented. From this reason in Fig. 15 no change of temperature at the injection nozzle drill is evident, the fuel injection was finished before the timing point of 10° after TDC. Figs. 16 and 17 document the decrease of CO concentration comparing to the operation with pure diesel. Ethanol has a lower theoretical air consumption than diesel and at the identical fuel portion the engine operating with ethanol shows a higher air surplus. At the combustion of ethanol ignited by diesel (25%) the higher concentration of CO at the combustion chamber walls and also in average occurs (Fig. 18). The identical effect could be observed as for the unburned hydrocarbons concentration due to the extinguish effect at the combustion chamber walls.

The similar behaviour can be observed also for nitrogen oxide concentration. When the engine operates at lean combustion mixture, through the addition of ethanol into the fuel the NO concentration in combustion chamber will be decreased (Figs. 19 and 20).

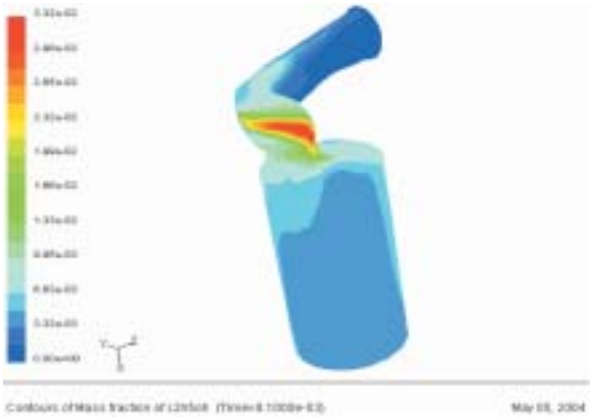

Fig. 7 Mass fraction number of ethanol 72° CA after TDC

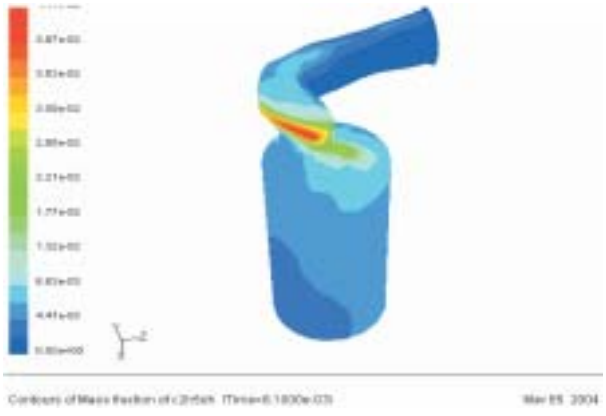

Fig. 8 Mass fraction number of ethanol 108° CA after TDC

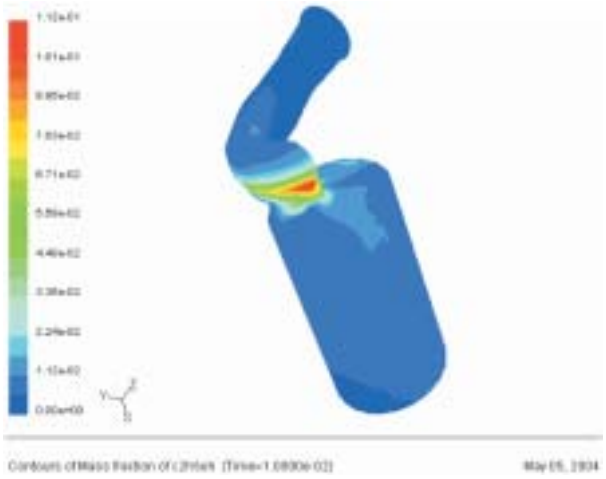

Fig. 9 Mass fraction number of ethanol 144° CA after TDC

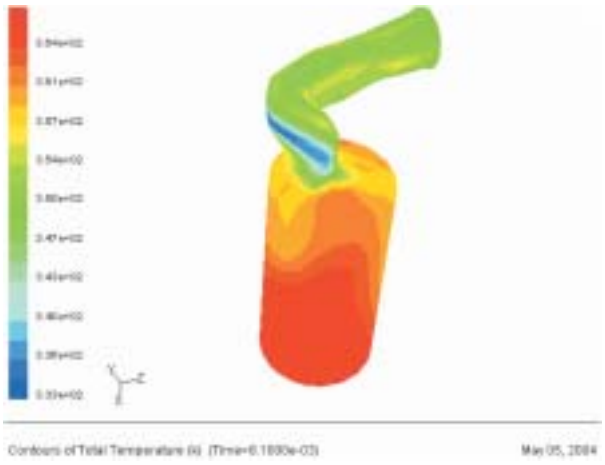

Fig. 10 Temperature (K) 72°CA after TDC

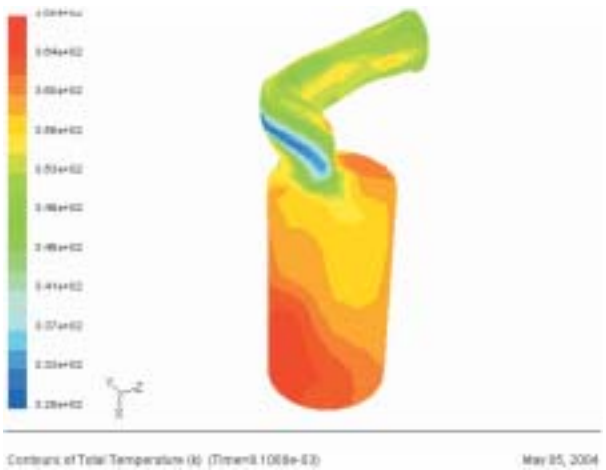

Fig. 11 Temperature (K) 108° CA after TDC

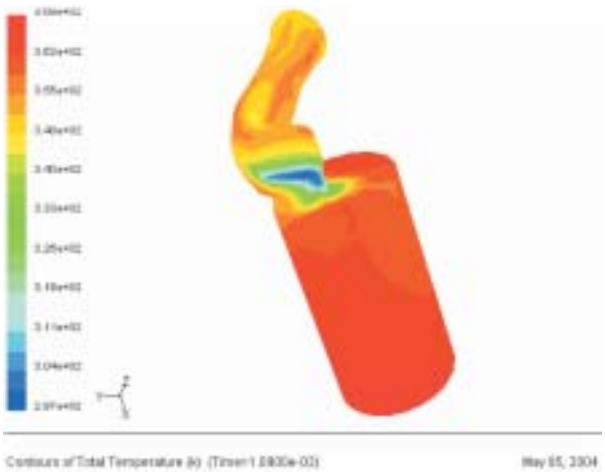

Fig. 12 Temperature (K) 144° CA after TDC

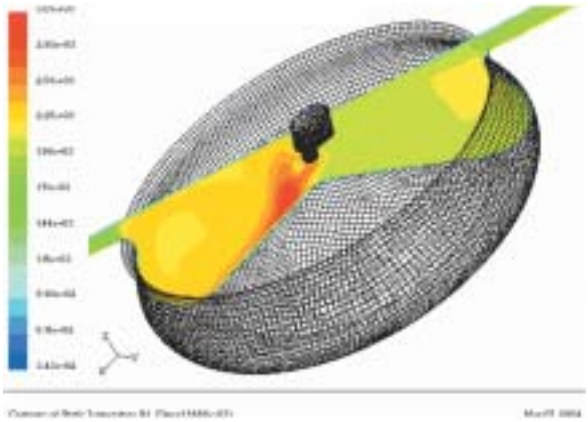

Fig. 13 Static temperature (K) 10° CA after TDC, fuel: $C_{16}H_{29}$. Average temperature in combustion chamber = 2100 K

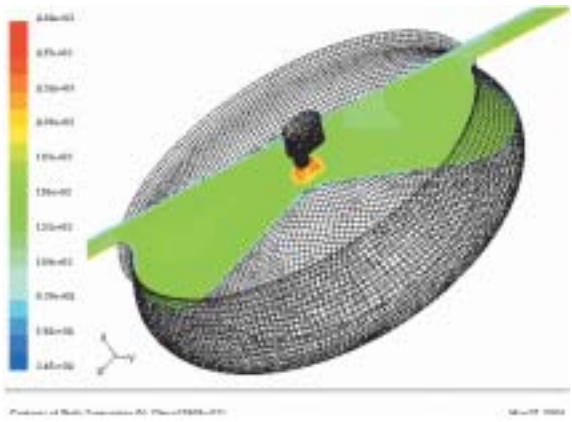

Fig. 14 Static temperature (K) 10° CA after TDC, identical fuel mass injection comparing to pure diesel fuel: 20 % ethanol in $C_{16}H_{29}$. Average temperature in combustion chamber = 1500 K

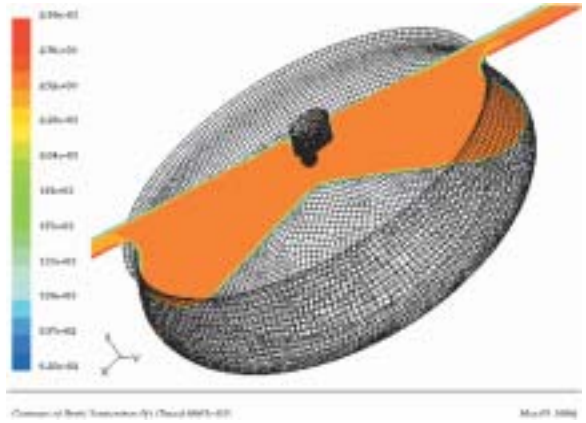

Fig. 15 Static temperature (K) 10° CA after TDC, fuel: ethanol / air mixture, ignition portion 25 % of the total energy content, identical heat input as at pure diesel T = 2550 K

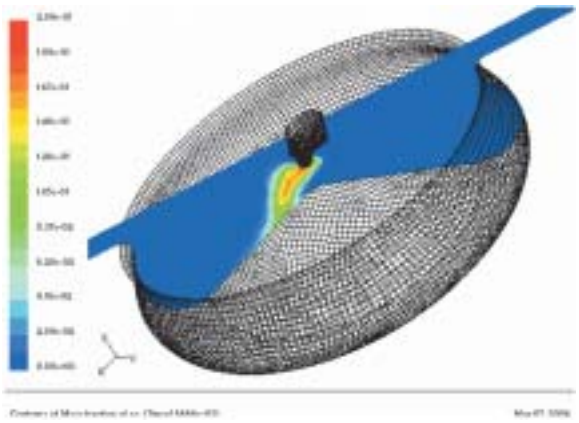

Fig. 16 Mass fraction number of CO 10° CA after TDC, fuel: $C_{16}H_{29}$, Average concentration of CO (mass fraction number) in combustion chamber = 0.002936

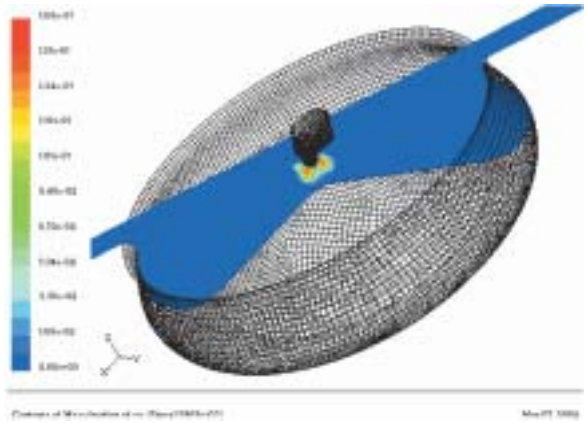

Fig. 17 Mass fraction number of CO 0°CA after TDC, identical fuel portion as at diesel operation, fuel: 20 % ethanol in $C_{16}H_{29}$. Average concentration of CO (mass fraction number) in combustion chamber = 0.001433

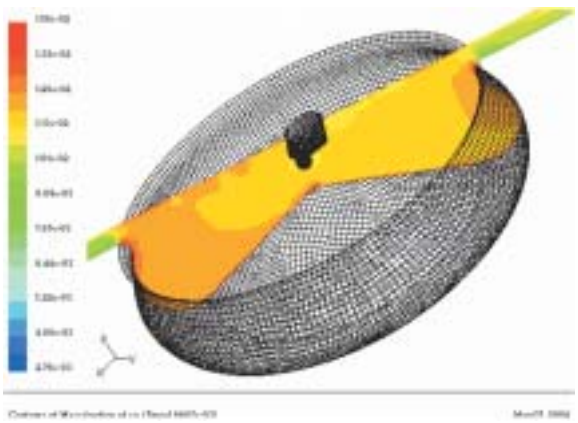

Fig. 18 Mass fraction number of CO 10° CA after TDC, fuel: ethanol with air ignition portion 25 % of total energy content, identical heat input as at diesel operation. Average concentration of CO (mass fraction number) in combustion chamber = 0.01176

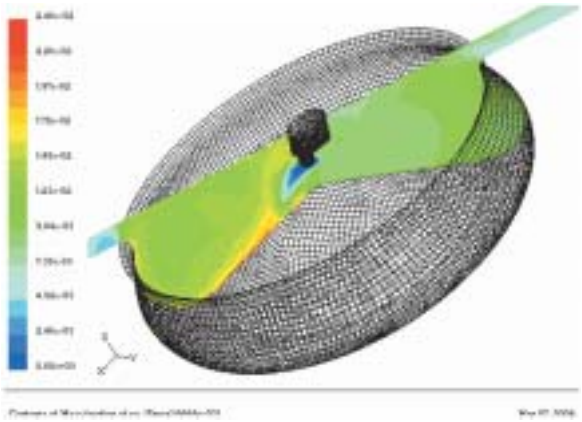

Fig. 19 Mass fraction number of NO 10° CA after TDC, fuel: $C_{16}H_{29}$, Average NO concentration (mass fraction number) in combustion chamber = 0.01046

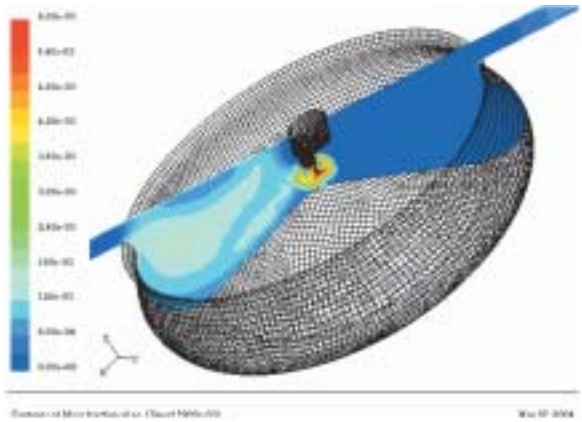

Fig. 20 Mass fraction number of NO 10° CA after TDC, fuel: 20 % ethanol in $C_{16}H_{29}$ identical fuel portion as at diesel operation. Average NO concentration (mass fraction number) in combustion chamber = 0.01033

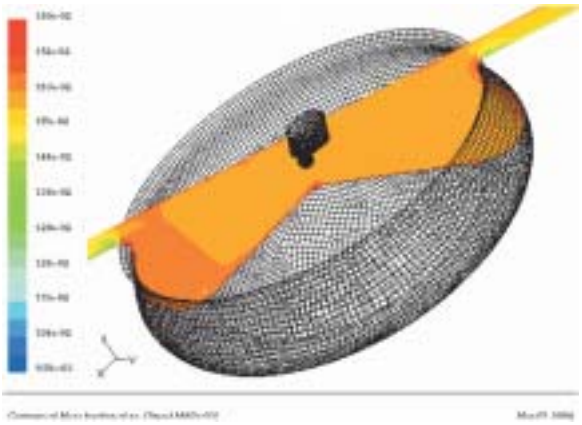

Fig. 21 Mass fraction number of NO 10° CA after TDC, fuel: ethanol with air, ignition portion 25 % of total energy content, identical heat input as at diesel operation. Average NO concentration (mass fraction number) in combustion chamber = 0.01615

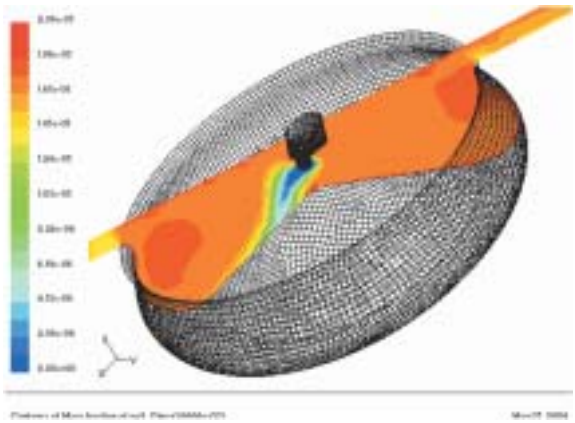

Fig. 22 Mass fraction number of NO2 10° CA after TDC, fuel: $C_{16}H_{29}$. Average NO_2 concentration (mass fraction number) in combustion chamber = 1.6848e−5

In the case that the engine operates at the same power output with the ethanol injection in the suction channel through the higher charging by combustion mixture the NO concentration will be increased (Fig. 21). The NO concentration is kinetically retarded during the power stroke at its maximal value.

Equilibrium concentrations of NO_2 in the combustion chamber are very low, the concentration of NO is predominant, while the transformation of NO into NO_2 takes place in the exhaust system and then in the atmosphere. The NO_2 concentration depends on the temperature and oxygen content in the beam of injected fuel.

Figs. 25 – 27 illustrate the iso-tacheo-curves in the combustion chamber which document the change in combustion process when ethanol is applied in diesel fuel or injected in the suction manifold. The figures presented not only the changes of local velocity but also the modification of the whole velocity field. The high average velocity shown in Fig. 27 can be considered as the result of fictive combustion process in the whole combustion chamber at the calculating model based on the equilibrium state of exhaust gas composition.

7. Combustion simulation of ethanol in a diesel engine – kinetic model

The final part of paper shows kinetic combustion of ethanol with CFD method in combustion chamber of diesel engine. The coefficients for a kinetic model are from Fluent. Inc. database (Tab 1).

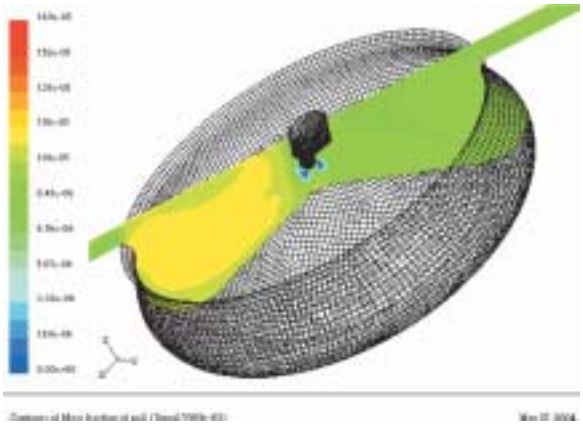

Fig. 23 Mass fraction number of NO2 10° CA after TDC, fuel: 20 % ethanol in $C_{16}H_{29}$ identical fuel portion as at diesel operation. Average NO_2 concentration (mass fraction number) in combustion chamber = 1.0078e-5

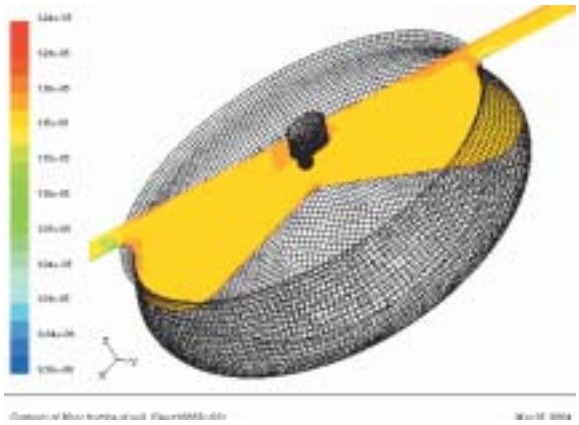

Fig. 24 Mass fraction number of NO2 10° CA after TDC, fuel: ethanol with air ignition portion 25 % of total energy content. Identical heat input as at diesel operation. Average NO_2 concentration (mass fraction number) in combustion chamber = 1.1652e-5

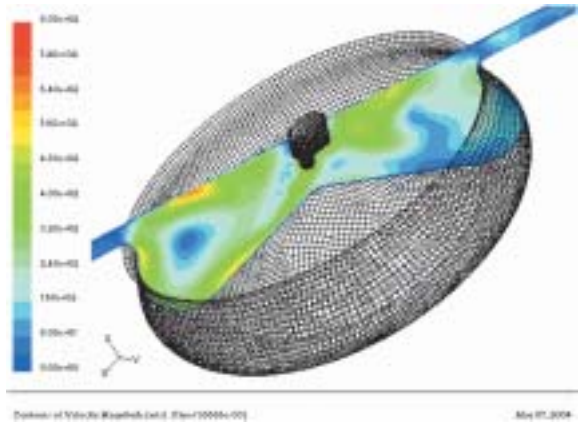

Fig. 25 Iso-tacheo-curves 10° CA after TDC, fuel: $C_{16}H_{29}$. Average velocity of burned mixture in combustion chamber = 231 m/s

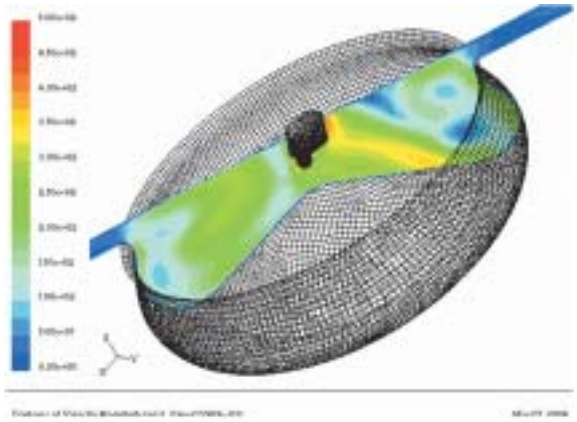

Fig. 26 Iso-tacheo-curves 10° CA after TDC, fuel: 20 % ethanol in $C_{16}H_{29}$ identical fuel portion as at diesel operation. Average velocity of burned mixture in combustion chamber = 163 m/s

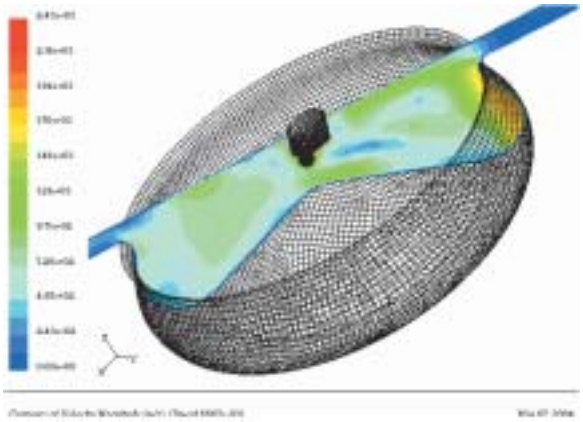

Fig. 27 Iso-tacheo-curves 10° CA after TDC, fuel: ethanol with air ignition portion 25 % of total energy content identical heat input as at diesel operation. Average velocity of burned mixture in combustion chamber = 675 m/s

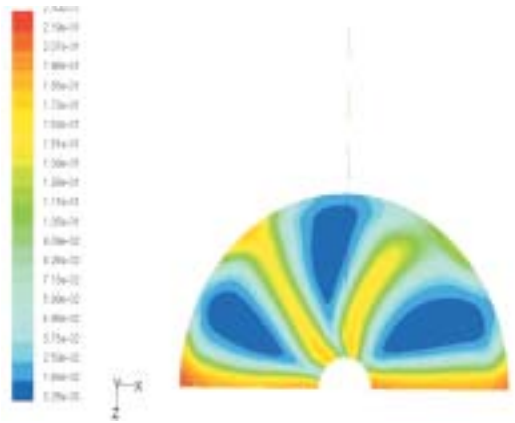

Fig. 28 Tangential flow at top dead center to plane of injection orifice (mass fraction of oxygen for kinetic model)

Coefficients for kinetics of combustion of ethanol Tab. 1

Species	Stechiometric. coef. υ	Rate exponent η
C_2H_5OH	1	0,15
O_2	3	1,6
CO_2	2	0
H_2O	3	0

8. Initial and boundary conditions for kinetic calculation

Fuel injection began at −15° BTDC and the injection ended 6° ATDC. The calculation was made with the interval of 0.0038 s. With the purpose of the model simplification the diesel fuel was substituted by ethanol. The injector drill diameter $d = 0.27$mm. The interval of injection timing was 21° CA. The wall temperature in combustion chamber $T_s = 700$ K. The velocity of ethanol flow through the injection drill $v_p = 229$ m.s^{-1}. For more precise calculation it was convenient to apply a kinetic model with the detailed description of ethanol transformation through the intermediate products in CO and subsequently in CO_2. For simple chemical reaction $C_2H_5OH + 3O_2 = 2CO + 3CO_2$ for volumetric reaction is pre-exponential factor $A = 8.435 \cdot 10^9$, activation energy $E = 1.256.10^8$ J.kg^{-1}.mol^{-1}, - termless backward reaction, - thermal conductivity = 0.0454 W.m^{-1}.K^{-1}, - dynamic viscosity $\mu = 1.72.10^{-5}$ kg.m^{-1}.s^{-1}, - mass diffusivity $D = 2.88.10^{-5}$ m^2.s^{-1}, - $c_p = 1000$ J.kg^{-1}.K^{-1}, - Sauter mean diameter $SMD = 40$ μm, the tempera-

Fig. 29 Droplets of ethanol (kg/s) -10 °CA before TDC, kinetic model

Fig. 30 Droplets of ethanol -5 °CA before TDC, kinetic model

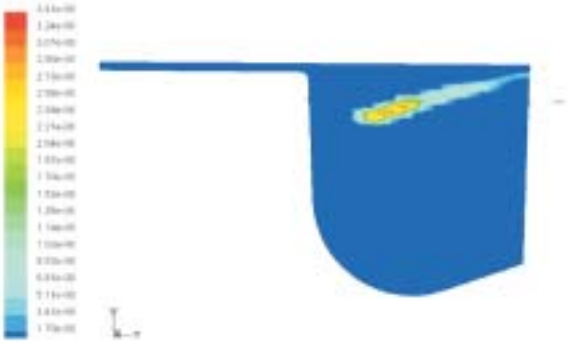

Fig. 31 Droplets of ethanol 0 °CA before TDC, kinetic model

Fig. 32 Droplets of ethanol 5 °CA after TDC, kinetic model

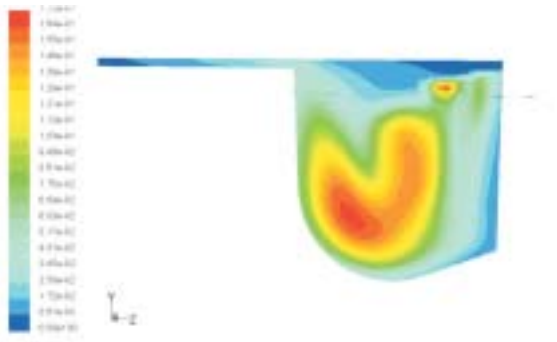

Fig. 33 Mass fraction of CO_2, -10 ° CA before TDC, kinetic model

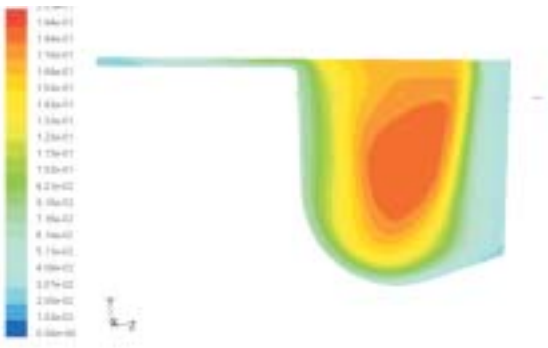

Fig. 34 Mass fraction of CO_2, -5 ° CA before TDC, kinetic model

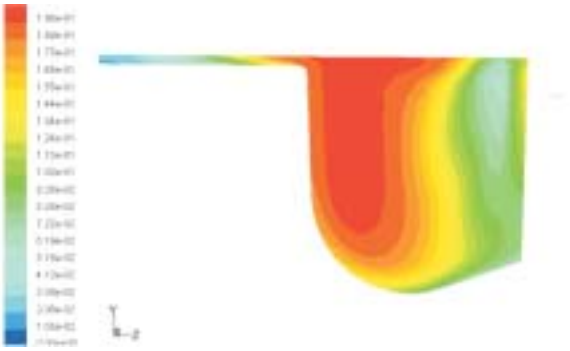

Fig. 35 Mass fraction of CO_2, 0 ° CA after TDC, kinetic model

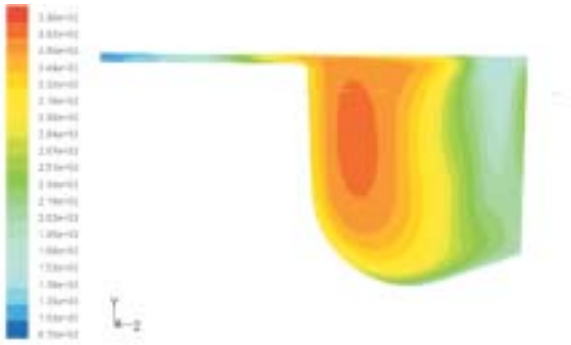

Fig. 36 Temperature K, 0° CA after TDC, kinetic model

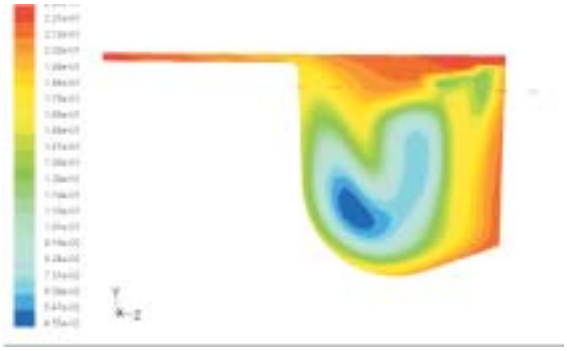

Fig. 37 Mass fraction of O_2, -10 ° CA before TDC, kinetic model

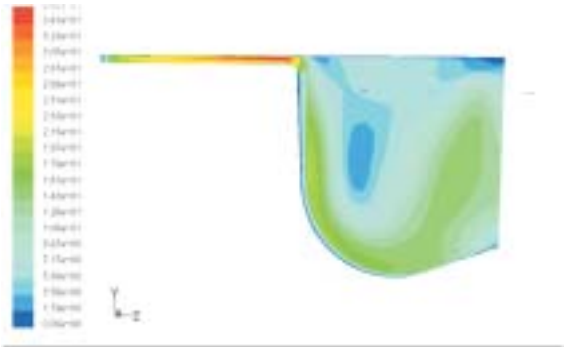

Fig. 38 Iso-tacheo-curves -10° CA before TDC, kinetic model

ture of injected ethanol $T_P = 353$ K, the ethanol rate of flow 0.067 kg/cycl.

9. Figures of the simulated velocity and concentration fields for kinetic calculation

Figs. 29 – 32 illustrate mass flow of liquid ethanol in dependence on time through a drill diameter to the right section of the piston. Fuel injection began 10° before TDC. Spray of fuel starts to deformate due to radial flow, it dependents on Reynolds number of flow. Out flow velocity is too low for ethanol to impact to the wall of combustion chamber.

Figs. 33 – 39 illustrate high-speed transformation of ethanol to carbon dioxid. Flow analysis shows the necessity of modification of time injection of fuel so that the hard combustion of ethanol is lowered. Complicated kinetic model can not be used for inconvenient computer of dynamic calculation.

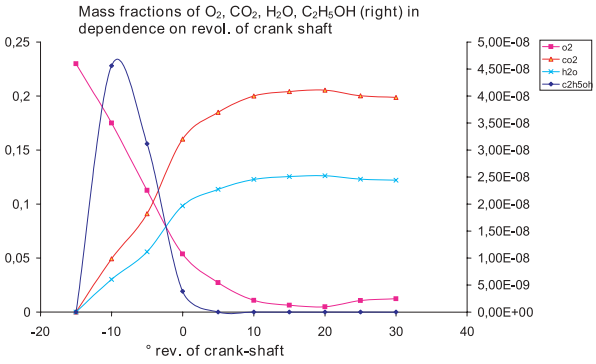

Fig. 39 Mass fractions of O_2, CO_2, H_2O, C_2H_5OH (right) in dependence on revol. of crank shaft

10. Conclusion

The impact of ethanol on exhaust emission composition was simulated using the values of pressure from the real combustion process with pure diesel fuel, ethanol added in diesel and ethanol injected in the suction manifold. The results of CO concentration show its decrease in the combustion chamber at the adding of ethanol into diesel and its increase at the injection of ethanol in the suction manifold when compared with the results calculated for pure diesel. At present the engine bench test is prepared for validation of the calculated results.

Acknowledgement

The financial support from the Science & Technology Assistance Agency, grant 20-014702 is greatly acknowledged.

References

[1] ARAI M., TABATA M., HIROYASU, H.: *Desintegrating process and spray characterization of fuel jet injected by a diesel nozzle.* SAE Paper 840275.
[2] HIROYASU H., KADOTA T., ARAI, M.: *Fuel spray characterization in diesel engines.* Symposium on Combustion Modelling in Reciprocating Engines, Michigan 1978.
[3] HALSTEAD M. P., KIRSCH L. J., QUINN, C. P.: T*he Autoignition of Hydrocarbon Fuels at High Temperatures and Pressures-Fitting a Mathematical Model,* Combustion and Flame, 30, 1977.
[4] HENEIN N. A.: *Combustion and emission formation in fuel sprays injected in swirling air,* SAE Paper 710220.
[5] VARDE K. S., POPA D., VARDE L. K.: *Spray angle and atomization in diesel sprays.* SAE Paper 841055.
[6] Fluent Inc. software manual.
[6] BRATSKY, D., LABAJ, J., STACHO, D.: *Impact of Ethanol Addition in Diesel on Power Output and Exhaust Emission Characteristics,* 5th International Colloquium, Fuels, Technische Akademie Esslingen Proceedings 2005, pp. 31–42, ISBN-Nr. 3-924813-59-0.

Andrzej Mruk*

CHARACTERISTICS OF A DIESEL ENGINE WITH A CERAMIC COATED PISTON HEAD

In this age of fuel problems, the improvement in thermal efficiency of an engine is very important. One of the ways leading to this aim consists in reducing heat losses by the application of heat-insulating coatings on the elements of the combustion chamber. The article deals with the effect of the piston head heat-insulation on a Diesel engine running indicators and presents the results of the tests.

1. Introduction

From the Analysis of the combustion engine heat balance it may be concluded that the thermal insulation of a combustion chamber should reduce energy losses caused by heat radiation, convection and flow to the cooling agent. Consequently, the improvement of engine watt-hour efficiency as well as the increase of life and resistance of its elements is expected.

Many centres, including Cracow University of Technology [3, 4, 9, 10, 11], are engaged in research into this matter, achieving different results. Both improvement and deterioration of engine running economy were noted in the case of heat insulated elements participating in heat exchange. Equally, divergent results are reported for exhaust gas toxicity.

Mostly, for insulation of combustion chamber elements, ceramic coatings made of ZrO_2 solid solutions partly stabilised with Y_2O_3, CaO, and MgO oxides or with rare earths mixture (Ln_2O_3) are used. Apart from a low thermal conduction, they are marked with variable heat loading resistance.

Analysing the share of different surface elements creating a combustion chamber in this phase of the cycle when the maximum heat quantity is generated (i.e. close by the top dead centre), it is possible to state that the share of a cylinder wall in total heat exchange surface is 10 to 30%. Consequently, the piston head and the corresponding head base surface are supposed to play the key role in heat transmission to the cooling agent. The above statements allow to conclude that the use of heat insulation on the piston head will be of great importance for the engine characteristics.

2. Experimental Tests

The investigation was carried out using a monocylinder normally aspirated engine with direct fuel injection to an open, toroidal combustion chamber, located in the piston. The nominal rotational speed of the examined engine (SB.3.1 type) was 2200 rpm. The engine was cooled with a fluid in circulation forced by a water pump.

The engine characteristics were examined by installing successively four different pistons: a standard one made of aluminium alloy (AK-12) and three others with heat insulating ceramic coatings. The coatings of zirconium dioxide (ZrO_2) partially stabilised with yttrium trioxide (Y_2O_3) were deposited by a plasma spraying method on the piston heads. The ceramic coatings differed in thickness and porosity. Therefore, different values of heat resistance and thermal conductance coefficients were noted. Heat resistance of a coating is decisive in modifying heat properties of a piston head. Consequently, for the analysis of engine characteristics, the coating heat resistance was assumed as the value determining the heat insulation of the piston.

The engine was tested on a stand equipped with an electric brake and measuring devices enabling to determine values of the following characteristics: operating (power N_e and moment M_o), economic (fuel consumption per hour and per unit) as well as the parameters connected with working medium pressure run in the engine cylinder, fuel pressure before the injector and before displacement of the injector needle depending on the crank angle. Concentration of toxic exhaust gas constituents: nitric oxides (NO_x), hydrocarbons (HC), carbon monoxide (CO) and smokiness, was examined too.

3. Results and discussion

Changes of combustion indicators, determined by a thermodynamic analysis of indicator diagrams, depending on heat resistance of the ceramic coatings deposited on the piston heads, at a rotational speed $n = 2200$ rpm and at the mean pressure $p_e = 0{,}6$ Mpa, are presented in Figs. 1 and 2.

In the case of the pistons with ceramic-coated heads, self-ignition delay is smaller than in the case of the standard pistons. It can be explained by a higher temperature in the combustion chamber

* **Andrzej Mruk**
Institute of Automobiles and Internal Combustion Engines, Cracow University of Technology, 31-864 Krakow, al. Jana Pawła II nr 37, Poland,
Tel.: + 48/126283518, Fax.:+ 48/126283520, E-mail:mruk@mech.pk.edu.pl

during injection of fuel charge and, thereby, better evaporation of fuel. However, the lowest values of a self-ignition period were obtained for ceramics marked by lower heat resistance values and, consequently, lower temperatures. It can be presumed that a large increase of temperature results in reducing the speed of fuel injection to the combustion chamber and its prolongation caused by the increase of atomiser leakage. In consequence, the advantageous effect of better evaporation is partly destroyed. The increase of leakage may occur when the fuel viscosity decreases or when the injector guide clearance increases due to a higher temperature.

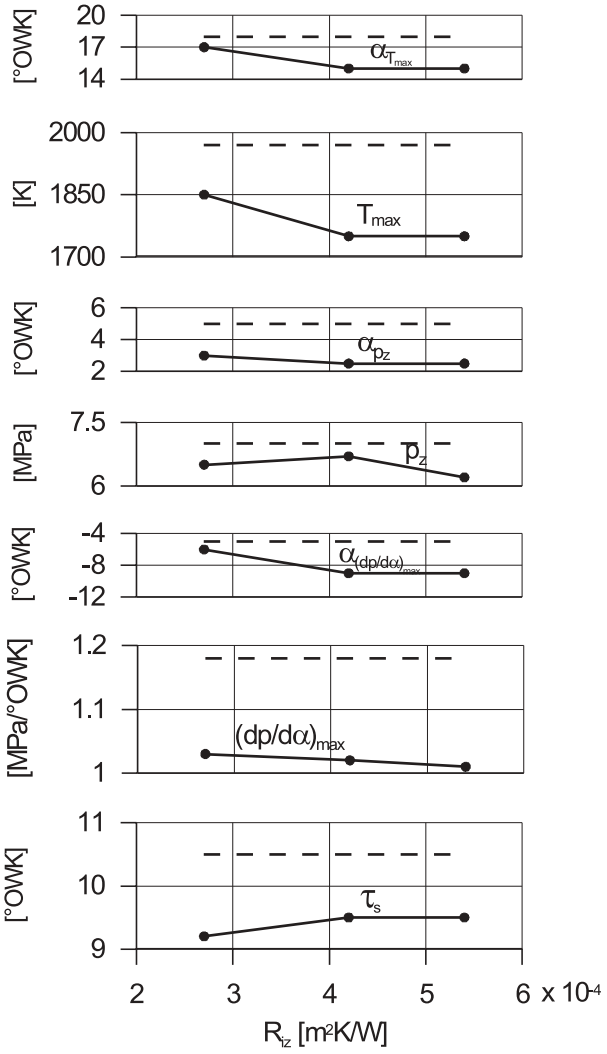

Fig. 1. Influence of heat resistance of insulating coatings on piston heads on combustion indicators; n = 2200 rpm, p_e = 0.6 MPa. Broken line – values for piston without coating.

The above hypothesis seems to be confirmed by the results of Dickey's investigation [5] where a reduction of injection pressure was found in the case of applying heat insulation in the combustion chamber.

Maximum temperatures in the cylinder determined on the basis of thermodynamic analysis of indicator diagrams decrease when heat resistance of the coatings increases. The reduction of maximum temperature values in the cylinder is accompanied by a reduction of maximum combustion pressure values, although the influence of heat resistance is not unambiguous here. Lower values of maximum temperature and pressure in the cylinder can be explained by reduction of air mass supplied to the cylinder of a normally aspirated engine resulting in incomplete deficient combustion. The rise of temperature on the inlet channel and combustion chamber surfaces causes the reduction of density and, consequently, of aspirated air mass, particularly during the period of closing the inlet valve.

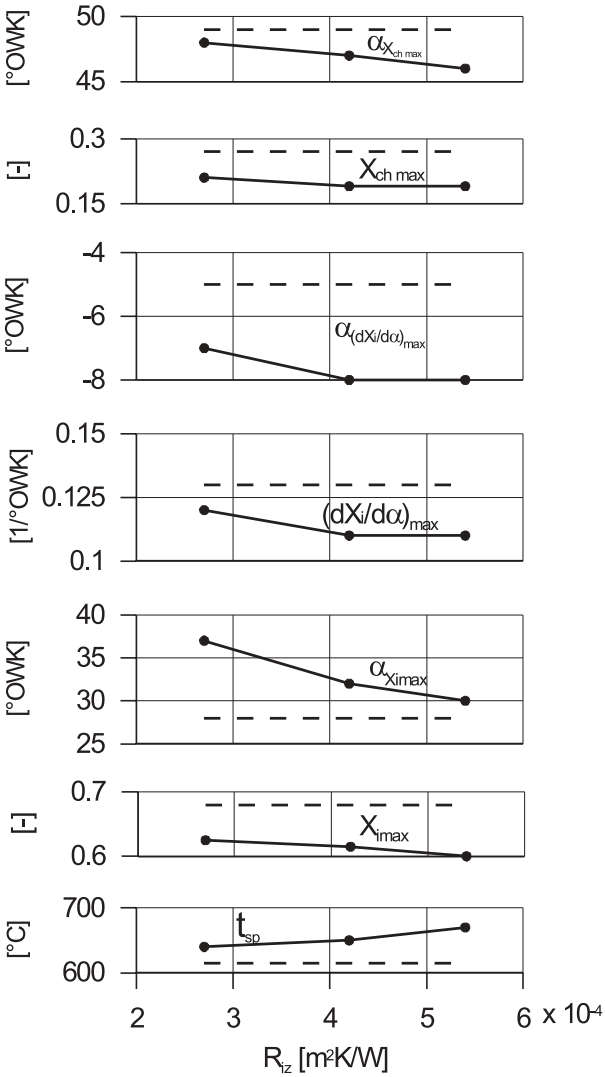

Fig. 2 Influence of heat resistance of insulating coatings on piston heads on combustion indicators; n = 2200 rpm, p_e = 0.6 MPa. Broken line - values for piston without coating.

The reduction of maximum combustion pressure may come also from the prolongation of combustion time. Alkidas [1,2] reports that the combustion time in an engine with a heat insulated chamber

may grow due to incorrect mixing of fuel and air in the combustion chamber as a result of reduced air mass and lower speed of fuel injection to the chamber as well as of elongated injection time. This interpretation seems to be convincing. Moreover, as shown in Fig. 1, the application of heat insulating coatings resulted in approximating maximum values of combustion and temperature pressure to the T.D.C. It corresponds roughly to the differences in angular variation of self-ignition delay.

The formation of the value of combustion pressure growing maximum speed $(dp/d\alpha)_{max}$ by the action of heat resistance of ceramic coatings on the piston heads is convergent with the variation of maximum pressure and temperature in the cylinder.

Maximum values of the heat evolution indicator and of maximum speed of heat absorption by a working agent $(dX_i/d\alpha)_{max}$ are lower in case of applying heat-insulating coatings. Also, when the heat resistance of ceramic coatings increases, the values of these indicators slightly decrease. It is probably due to incomplete and deficient combustion of fuel as a result of smaller air mass supplied to the cylinder. In case of applying the ceramic coatings, maximum values of X_i are located nearer by the T.D.C., whereas maximum values of $dX_i/d\alpha$ occur further from the T.D.C. It is the consequence of a shorter self-ignition delay period as well as a better evaporation and heating of the fuel. Such formation of these values is advantageous considering the distribution of heat evolution during the cycle.

The value of determined maximum coefficient of cooling losses X_{ch} is, as expected, lower in case of applying the coatings. Reduced carrying away of heat from the agent to the combustion chamber walls results in the increasing exhaust gas mean temperature.

Figs. 3 and 4 show changes of the engine working parameters depending on heat resistance of the ceramic coatings deposited on the piston heads for a rotational speed n = 2200 rpm and two different values of fuel consumption per hour, corresponding to low and high engine loadings.

As it is visible, fuel consumption per unit for an engine with the heat-insulated pistons is higher than in case of a standard engine. Only for the piston marked by the highest coefficient of heat resistance, fuel consumption was slightly lower within the range of low engine loading. These results meet other results reported [1, 5, 8, 13]. Generally, the level of exhaust gas smokiness was, at low engine loading, higher for insulated pistons, except for the piston with the highest heat resistance coefficient, where the exhaust gas smokiness was slightly lower when compared with a standard piston. In this case, it may be the effect of improving diffusive mixing efficiency as well as of better utilisation of the air during combustion process, but also of more intense oxidation of soot at higher temperatures. This conclusion could be confirmed by results achieved at higher engine loading (G_p = 6 kg/h) – Fig. 4. As shown, lower exhaust gas smokiness level was noted for all the ceramic coatings. As was expected, the application of heat insulated heads resulted in increasing exhaust gas temperature within the whole range of the engine operational loads.

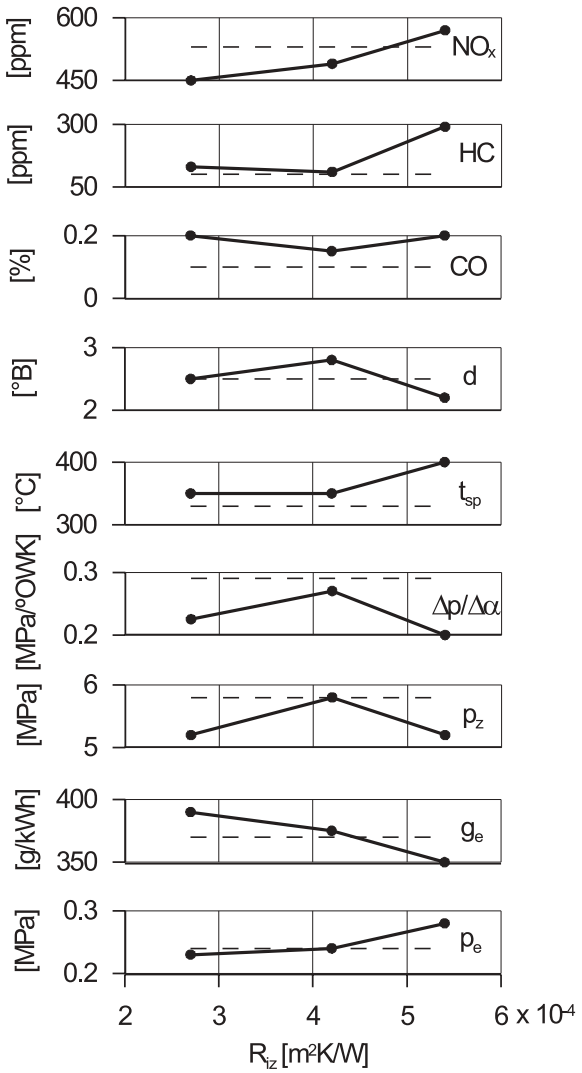

Fig. 3 Influence of heat resistance of insulating coatings on piston heads on working parameters of engine; n = 2200 rpm, G_p = 3 kg/h. Broken line – values for piston without coating.

Generally, for all the insulated pistons, the maximum speed of combustion pressure growing in the cylinder and maximum combustion pressure decreased. Furthermore, we can see clearly the relation between the hardness of engine running and the heat resistance coefficient. The higher is the heat resistance of the piston head insulating coating (less heat flows away from the combustion chamber through the piston and rings to the cylinder sleeve and to the cooling system), the lower are values of running hardness ($\Delta p/\Delta\alpha$). It can result from a lower heat evolution speed during the first phase of combustion (kinetic combustion) and elongation of the total combustion period (lower temperature in cylinder). Such interpretation is justified by the results of measurements of unburned hydrocarbons emission (increase for pistons with heat insulating coatings) and nitric oxides (decrease for heat insulated pistons). The amount of carbon monoxide was slightly higher in case of the heat insulated pistons.

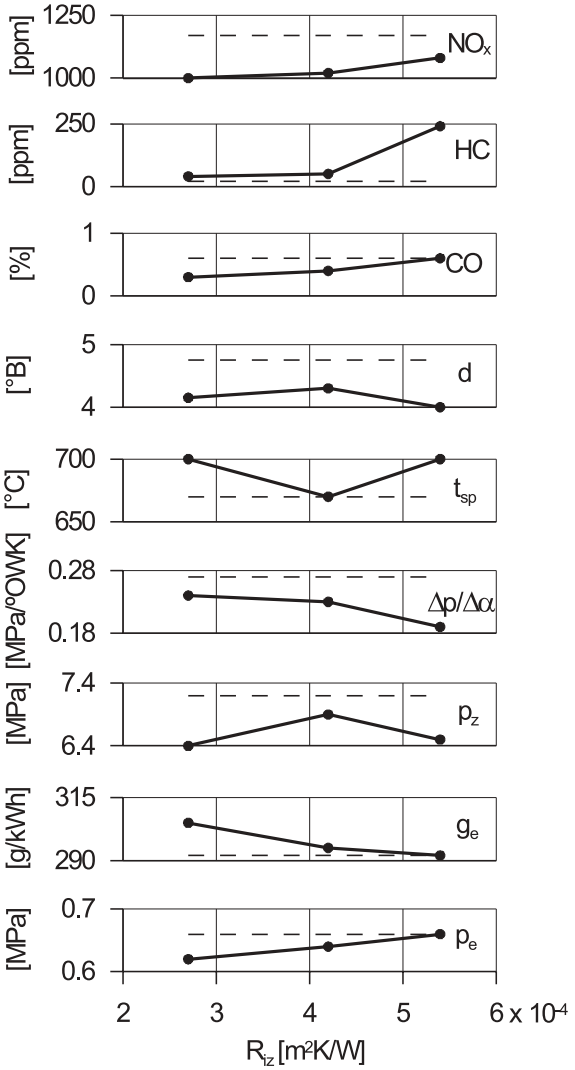

Fig. 4 Influence of heat resistance of insulating coatings on piston heads on working parameters of engine; n = 2200 rpm, G_p = 6 kg/h. Broken line – values for piston without coating.

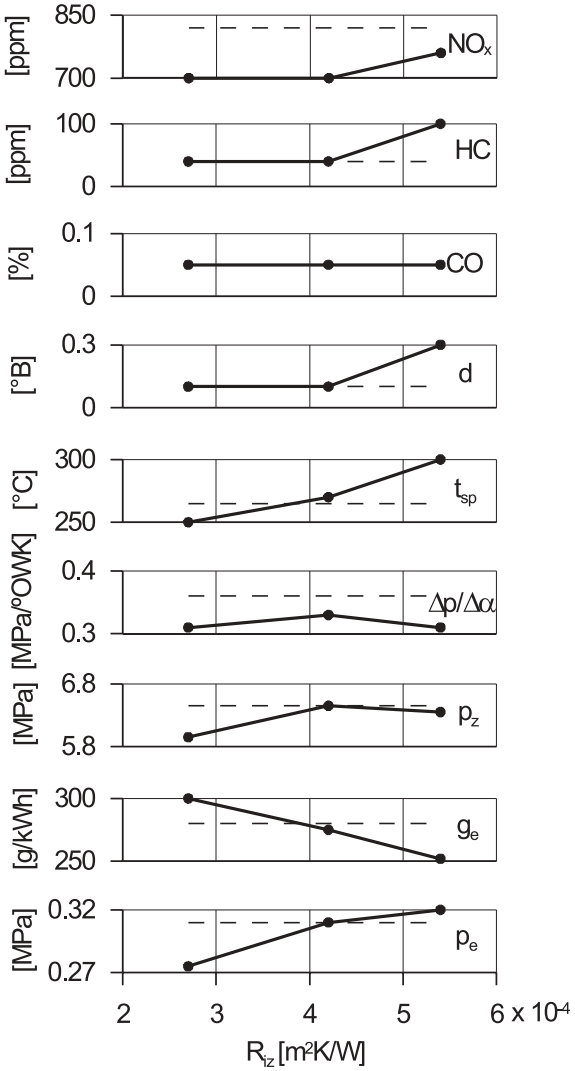

Fig. 5 Influence of heat resistance of insulating coatings on piston heads on working parameters of engine; n = 1600 rpm, G_p = 2 kg/h. Broken line - values for piston without coating.

The analysis of relations obtained for a lower rotational speed n = 1600 rpm (Figs. 5 and 6) indicates that, regarding running economy, the tendencies noted at the nominal rotational speed remained. However, the effect of the increase of heat resistance of the piston head material on the fuel consumption increase at high loads and decrease at low loads is evident.

These results confirm clearly the results achieved by G. Woschni [12, 13] and others [6, 7]. The reason for such results may be both more intensive carrying away of heat through the piston head within the range of higher temperature (high loading) and prolonged combustion period [2].

For two heat-insulated pistons maximum combustion pressure at high loads reached higher values (at n = 2200 rpm).

Since there is no clear relevance to the heat resistance value, explanation of this problem on the basis of the present investigation is not possible.

4. Conclusion

The presented results of study of the engine with piston heads covered with ceramic coatings of diverse heat resistance permit to conclude that:

- Application of heat-insulating coatings did not improve running economy of the engine, since a general increase of fuel consumption per unit was noted. In one case only, for a piston having the highest heat resistance coefficient, fuel consumption was lower; it occurred within the range of low and mean loading.

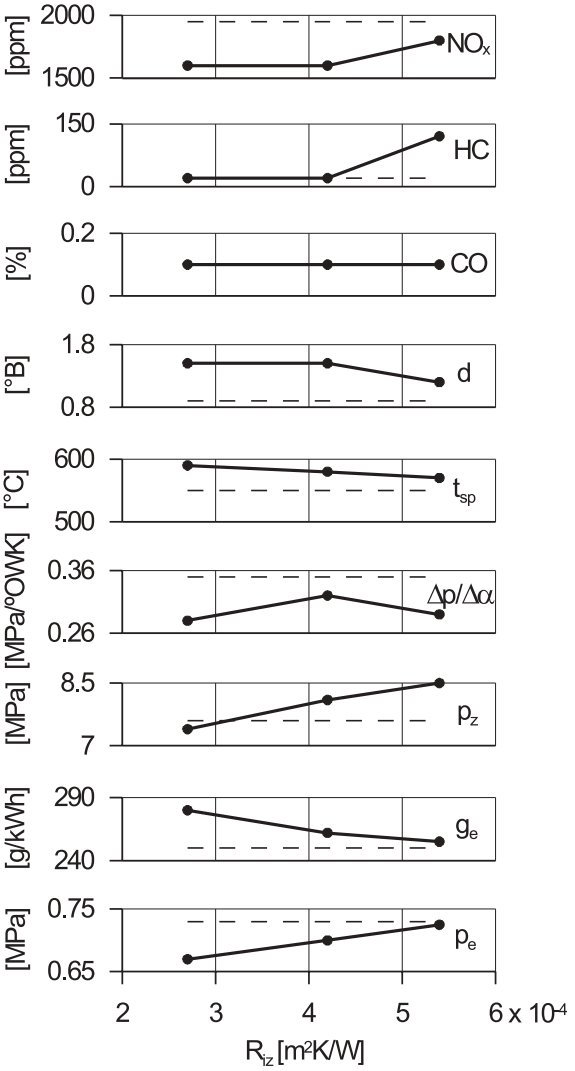

Fig. 6 Influence of heat resistance of insulating coatings on piston heads on working parameters of engine; n = 1600 rpm, G_p = 4.5 kg/h. Broken line – values for piston without coating.

- Formation of combustion indicators depends on heat resistance of the deposited ceramic coatings. The higher the heat resistance of the layer, the lower the values of maximum combustion pressure and of running hardness ($\Delta p/\Delta\alpha$). It has a connection with the reduction of heat evolution speed as well as lower maximum temperature in the cylinder. A self-ignition delay period is shorter in case of the applied ceramic coatings. The lowest values of delay were achieved at low values of heat resistance. It can be caused by reduction of speed and increase of injection time at higher temperature in the cylinder.
- Application of the heat-insulating ceramic coatings resulted, at a lower rotational engine speed, in increasing smokiness of exhaust gas, while, at a nominal rotational speed, smokiness of exhaust gas was lower. The emission of unburned hydrocarbons and carbon monoxide increases. It must be attributed to the incomplete and deficient combustion. Concentration of nitric oxide in exhaust gas decreased within the whole range of the engine loading. It is due to the reduction of maximum temperature in the cylinder.
- The temperature of engine exhaust gas grows when the heat resistance of the heat-insulating ceramic coatings on the piston heads increases.
- Analysing the influence of the heat-insulating coatings made of ZrO2 we can also consider a possibility of catalytic effect of this compound on the combustion process. It could apply particularly to the first phase of combustion – reducing the self-ignition delay.

Notation

Finally, for analysis of the results the following indicators were assumed:

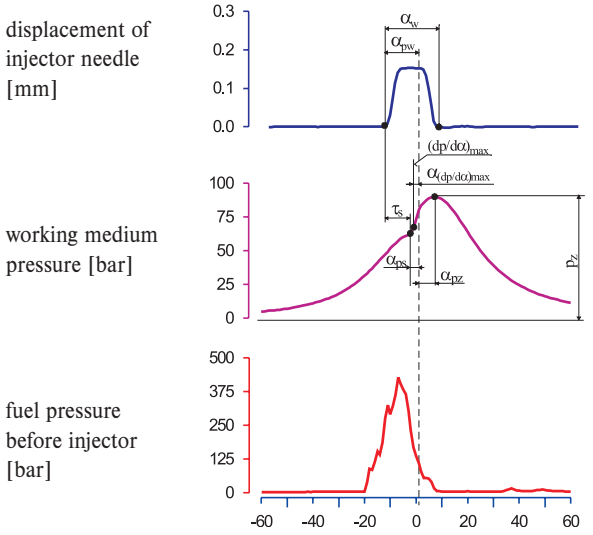

τ_s – fuel self-ignition delay, °OWK,
t_{sp} – exhaust gas temperature in the cylinder, °C
p_z – maximum combustion pressure, MPa,
p_e – mean effective pressure, MPa
T_{max} – maximum combustion temperature in the cylinder, K,
$(dp/d\alpha)_{max}$ – maximum speed of combustion pressure growing, MPa/ °OWK,
$\Delta p/\Delta\alpha$ – mean speed of combustion pressure growing, MPa/ °OWK,
X_{imax} – maximum value of heat evolution indicator,
$(dX_j/\Delta\alpha)_{max}$ – maximum speed of heat absorption by working agent, 1/°OWK,
X_{chmax} – maximum value of cooling losses coefficient,
α_{pz} – angle corresponding to the maximum combustion pressure, °OWK in relation to TDC
α_{chmax} – angle corresponding to the maximum value of cooling losses coefficient, in °OWK in relation to TDC,

α_{Tmax} – angle corresponding to the maximum temperature of the agent in cylinder, in °OWK in relation to TDC

$\alpha(dp/d\alpha)_{max}$ – angle corresponding to the maximum speed of combustion pressure growing, in °OWK in relation to TDC

α_{Ximax} – angle corresponding to the maximum value of heat evolution indicator, °OWK in relation to TDC

$\alpha_{(dXi/d\alpha)max}$ – angle corresponding to the maximum speed of heat absorption, °OWK in relation to TDC

References

[1] ALKIDAS, A., C.: *Experiments with Uncooled Single-Cylinder Open-Chamber Diesel.* SAE Transactions 1987, No. 870020

[2] ALKIDAS, A., C.: *Performance and Emission Achievements with an Uncooled Heavy-Duty Single-Cylinder Diesel Engine.* SAE Transactions 1989, No. 890144

[3] CISEK, J., MRUK, A., SZLACHTA, Z.: *Efekty zastosowania ceramicznej powłoki na denku tłoka silnika wysokoprężnego.* IV Sympozjum „Silniki spalinowe w zastosowaniach wojskowych", Jurata 1999, s.87–96.

[4] CISEK, J., MRUK, A., SZLACHTA, Z.: *Wpływ termoizolacji denka tłoka na własności silnika wysokoprężnego.* Teka Komisji Naukowo-Problemowej Motoryzacji PAN O/Kraków 15, 1998, s.105–120.

[5] DICKEY, D., W.: *The Effect of Insulated Combustion Chamber Surfaces on Directed Diesel Engine Performance,* Emissions and Combustion. SAE Transactions 1989, No. 890292.

[6] ENOMOTO, Y., FURUHAMA, S., TAKAI: *Heat Transfer on the Ceramic Combustion Chamber Wall of Diesel Engine.* CIMAC' 87, ref. D-33, Warszawa 1987.

[7] ENOMOTO, Y., FURUHAMA, S.: *Heat Transfer to Wall of Ceramic Combustion of Internal Combustion Engine.* Bulletin of JSNM 29, nr 250, 1986.

[8] HUANG, J., C., BORMAN., G., L.: *Measurements of Instantaneous Heat Flux to Metal and Ceramic Surfaces in a Diesel Engine.* SAE Transactions 1987, No 870155

[9] MRUK, A.: *Badania nad zastosowaniem termoizolacyjnych powłok ceramicznych na bazie ZrO2 w budowie silników spalinowych.* Seria Mechanika. Monografia nr 198. Wydawnictwo Politechniki Krakowskiej, Kraków 1995.

[10] MRUK, A.: *Właściwości silnika z tłokami pokrytymi powłokami termoizolacyjnymi.* Materiały konferencji KONMOT' 94, t.2, Kraków - Raba Niżna 1994, s.273-278.

[11] SZLACHTA, Z., MRUK, A., CISEK J.: *Wpływ termoizolacji denka tłoka na toksyczność spalin silnika wysokoprężnego.* Teka Komisji Naukowo-Problemowej Motoryzacji PAN O/Kraków 15, 1998, s.93-103.

[12] WOSCHNI, G., HUBER, K.: *The influence of Soot Deposits on Combustion Chamber Walls on Heat Losses in Diesel Engines.* SAE Transactions 1991, No 910297.

[13] WOSCHNI, G., KOLESA, K., SPINDER, W.: *Isolierung der Brennraumwande – Ein lohnendes Entwicklungsziel bei Verbrennungsmotoren ?.* Motortechnische Zeitschrift 47, n. 12, 1986, s. 495–500.

Peter Palček – Mária Chalupova *

BREAKDOWN OF THE IMPELLER WHEEL OF A TG2 KAPLAN TURBINE

The paper deals with the investigation of the breakdown of the impeller wheel of a TG2 Kaplan turbine with the power of 36 MW that was operating for only 6.5 years. To find the cause, both methods of investigation of mechanical properties and analyses of microstructure and micrographics were used. On the basis of the results of individual analyses we found out that the primary cause of the impeller wheel breakdown was inconvenient material of the servomotor rod.

1. Introduction

Nowadays, Slovak hydro-electric power plants present a significant source of energy. Beside the fact that they belong to renewable resources, they serve as peak power plants. Regarding their important function in electric power production and relatively high installation costs, they are constructed in order to feature a long operating life. However, in some exceptional cases a failure in part of the energy chain may occur. Breakdowns of the impeller wheel of a turbine are particularly serious, as their dismantling is very complicated, time and money demanding and it can cause a failure of other parts of the power plant, or serious ecology damage.

The paper deals with breakdown of the impeller wheel of a Kaplan turbine. The nominal performance of the turbine is 36 MW. The damaged turbine signed as TG2 was operating from April 1998. Till its breakdown the turbine ran for 23557 hours. During the operation no extreme states were found. The failure occurred suddenly on the servomotor of the impeller wheel that provided speed and performance regulation. At the breakdown oil from the hydraulic circuit of the servomotor penetrated into the area of the generator. After detecting the failure, the turbine was safely shut down in compliance with the standards.

The servomotor is placed in the middle of the impeller wheel and it is composed of the rod, piston, cylinder, tail mechanisms and hydraulic distribution. The rod together with the piston are firmly joined to the body of the impeller wheel. The cylinder is double-acting and with the help of the tail mechanisms it provides the turbine with vanes coiling. When the secondary regulation is engaged in operation, the servomotor can get a signal to switch the vanes in 15 s periods. When the servomotor fails, the turbine loses the possibility of regulation and there is threat of the machine collapse. Regarding the servomotor placing, it was necessary to dismantle the regulator, generator, impeller wheel and also the turbine chamber.

2. Experimental part

To find the reasons of the breakdown, the following procedures were chosen: dismantling of the hydraulic circuit, dismantling of the generator rotor, extraction of the impeller wheel, dismantling of the servomotor, visual checking of the whole wheel and finally, the analysis of the damaged part material.

Basic operational parameters of the impeller wheel:

Number of operation hours	23557 h
Speed frequency	150 min^{-1}
Number of revolutions to failure	212013000
Impulse of secondary regulation	4 min^{-1}
Number of servomotor throws	35335500
Area of piston	795000 mm^2
Pressure of servomotor oil	6 MPa
Maximum force from piston	4771000 N
Rod material	StE 500
Weight of piston	915 kg
Piston material	St 52-3N
Weight of rod	1434 kg
Nominal stress in rod	63 MPa
Weight of cylinder	3511 kg

3. Visual checking

After extracting the turbine impeller wheel from the chamber and dismantling its bottom it was found out that the rod of the servomotor was extruded downwards by about 4.2 cm (Fig. 1). On its upper part it can be seen that there is a fracture of the whole rod cross-section just under its flange (Fig. 2). The fracture has a fatigue character in the constitutive part of its cross-section (Fig. 3), while the initiation of the fracture was from the gasket and slot from

* **Peter Palček, Mária Chalupová**
Department of Materials Engineering, Faculty of Mechanical Engineering, University of Žilina, E-mail: peter.palcek@fstroj.utc.sk

various parts over the whole perimeter of the crossing area. The parts of the damaged gasket (Fig. 4) and forged pieces of metal caused by the crack growth were on the surface of the fracture. The thickness of these pieces ranged from 5 to 14 μm (Fig. 5).

Fig. 1 The rod extrusion from bottom bearing

Fig. 2 The fracture of the rod under its flange

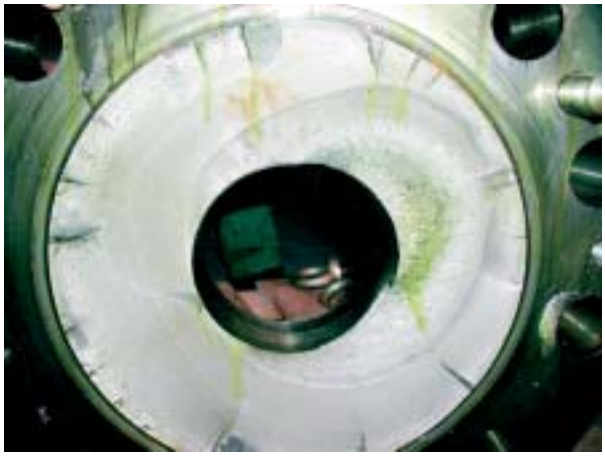

Fig. 3 The fracture of the rod

Fig. 4 The parts of gasket between the rod and the body of the turbine rotor

Fig. 5 Forged pieces of the rod

Fig. 6 Extruded material on the edge of the vane

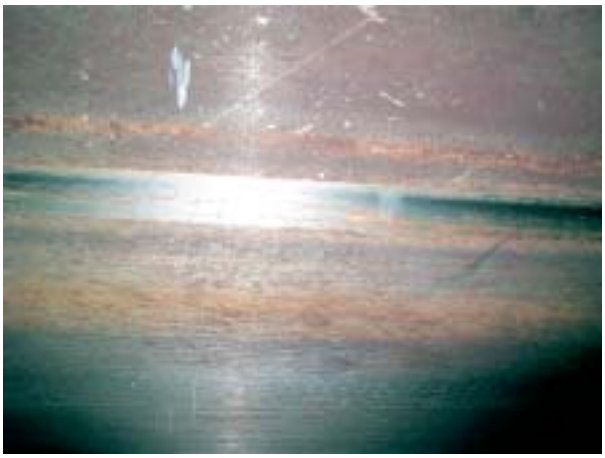

Fig. 7 The failure of the chamber surface of the turbine by wear from vanes

Fig. 8 The crack in the piston of the servomotor

By inspecting the impeller wheel we found out that there are areas without biological corrosion on the external circumference of the vanes. It means that the vanes had a direct contact with the turbine chamber when moving. This presumption is confirmed by the extrusion of material on the whole circumference of the vanes (Fig. 6) and by a continuous glossy track created by a mechanic contact with the vanes (Fig. 7).

By dismantling the servomotor cylinder it was found out that there is a crack on the piston. The crack is growing in the direction to the external diameter approximately to the two thirds of the diameter (Fig. 8). On the crack tip it is visible that the material of the piston is plastic (Fig. 9). This is typical for crack growing. On the contact area of the matrix that secures the position of the piston on the rod and transmits the forces from the piston to the rod, the maps with a changed surface quality were found out (Fig. 10). It is typical for contact fatigue.

After complete dismantling of the impeller wheel it was found out that the rod is damaged by longitudinal lines and there is a large failure by contact fatigue – pitting (Figs. 11 and 12) on the functional areas of the rod.

On the basis of the visual checking and positive findings it was possible to state that the fatigue failure of the rod affects more than 85% of the supporting cross-section and the fatigue fracture was initiated at various places on the rod circumferences. Mechanic contact of the vanes with the turbine chamber verifies disalignment of the impeller wheel with the bearings or it means that there was an ample allowance in the main bearing. Contact fatigue on the

Fig. 9 The detail of the crack end on the piston

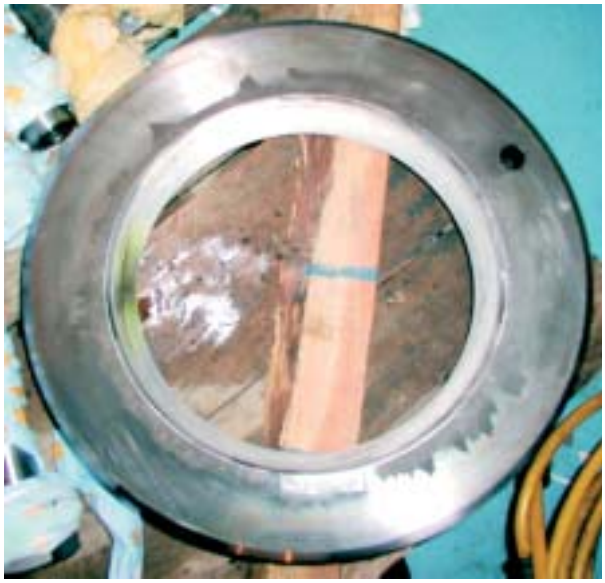

Fig. 10 Pressing of the matrix surface

Fig. 11 Deep pittings on the functional surface of the rod

Fig. 12 Deep and shallow pittings on the functional surface of the rod

functional areas of the rod and impeller wheel proves that the rod has a relatively big side oscillation that caused contact wearing and contributed to the total fracture of the rod. The side oscillation operated as an additional tension (bending) and it was superimposed on the longitudinal tension from the piston. The oscillation could be caused by asymmetry of the loading from the piston or by the impact of centripetal forces caused by oscillation of the whole impeller wheel.

The failure of the piston by the crack could be caused by concentration of tensions in the slot for spring, by a directed structure after rolling or by a structural non-homogeneity of the piston material. The contact fatigue on the rod matrix verifies a mutual micro motion between the piston and matrix (pulsating tension) that could contribute to the origin of additional loading of the piston.

5. Analysis of chemical composition

According to the design documentation rod was produced by forging from StE 500 material and the piston was produced by hot rolling from St 52-3N material. The specimens extracted from the failed flange of the rod were used for the chemical analysis. The chemical composition of the rod according to the norm according to the certification of a supplier and according to the results of the chemical analysis is shown in Tab. 1

The results of the given analyses show that the chemical composition of the rod corresponds to the norm for StE 500 material with an exception - the content of copper. Copper as a pearlite creating element increases air-corrosion resistance and in the listed content, it should not affect mechanical properties significantly.

Chemical composition of the rod according to the norm and according to the certification Tab. 1

[wt %]	C	Mn	Si	P	S	Cr	Ni	Mo	Al	Cu
StE500	0.21	1.0–1.70	0.16–0.60	0.035	0.03	0.3	1.00	0.1	0.02	0.20
Certificate	0.190	1.13	0.25	0.011	0.010	0.05	0.08	0.01	0.025	0.20
Positive	0.225	1.235	0.255	0.013	0.0085	0.045	0.07	0.0095	0.018	0.235

4. Analysis of the material of the damaged part

It was necessary to find out whether there had not been any substitution for material to find the reason of the damage and failure of the rod and piston. According to the given agenda, the rod and the piston were produced from normal, low-carbon steels of standard quality.

These analyses were performed in the frame of the experimental part: chemical composition determination, investigation of mechanical properties, metallographic analysis and micrographic analysis. Despite the fact that the piston of the servomotor was also damaged, the paper deals only with the analysis of the damage and failure of the rod as the primary cause of the breakdown.

6. Mechanical properties

Fundamental mechanical properties of StE 500 steel Tab. 2

Property	Re [MPa]	Rm [MPa]	A [%]	Z [%]	Specimen diameter [mm]
StE 500	410	570–740	17	–	10
Certificate	438	587	28	57	10

Mechanical properties of the rod material according to the norm for steel StE 500 and according to the supplied certificate are shown in Tab. 2. From the comparison of these parameters the

material should correspond to the requirements of the norm and to the requirements for the loading intensity. Regarding the fact that the rod material has a ratio of *Rm*/Re >1.4, it was assumed that in the consequence of cyclic loading the hardness would be slightly increased. This assumption was not confirmed by the hardness and toughness tests.

At the evaluation of the rod material properties, the hardness of the material was the first property to be investigated. It was necessary to perform a tensile test (manufactured specimen had a diameter of 10 mm) regarding the fact that hardness according to Brinel reached the maximum values HBS 2.5/62.5/10 = 136, this corresponds to the tensile strength of 470 MPa and does not correspond to the values given in the norm. The recorded values are in Tab. 3.

Recorded tensile strength of rod material Tab. 3

Property	Re [MPa]	Rm [MPa]
Specimen1	318	484
Specimen 2	316	494
Specimen 3	315	–

From the recorded values it is clear that the measured tensile strength is lower minimally by 100 MPa than the one declared for rupture strength Rm and for yield stress Re. It, therefore, means that the state of the rod material is unsatisfactory.

At the static tensile test, by gradual loading, it was found out that the cracks appeared on the surface of the tested rod. The cracks were just under the yield stress. These cracks could be observed without a microscope. Because of this, the surface of one tested rod (specimen 3) was polished and observed by a raster electron microscope after loading. The character of the failure is recorded in Figs. 13 to 16.

In the area of larger cracks (Figs. 13 and 14) a creation of slip lines – plastic deformation on the crack tip is observed. The creation of cracks is probably conditioned by presence of inclusions in the material structure. These inclusions are non-coherent and hard. They cracked by loading and they got separated from the basic material (Figs. 15 and 16) and it means that they served as micro cracks nuclei.

7. Metallographic analysis

The specimens for the metallographic analysis were extracted in a way to be characteristic for the microstructure of the steel in a vertical direction to the surface of the rod flange (cross-section) and in a parallel to the rod surface (longitudinal section). The specimens were prepared by standard metallographic methods. The microstructure was evaluated by an optic microscope NEOPHOT 32 (Figs. 17 and 18) and by an electron microscope TESLA BS 343 (Figs. 19 to 22).

Steel structure is irregular, ferritic-pearlitic, created by grains of different sizes. Pearlite is lamellar in many cases, but it also exists in a spheroidic shape that corresponds to soft annealing. The size of ferritic grains is also very different. Moreover, it exists in the shape of Widmannstätten structure in many cases. Spheroidic pearlite is created by soft annealing that is realized at heating of material just under AC1 and leaving it at this temperature for some hours. In the case of the evaluated rod, a partial spheroidization occurred by slow cooling of the rod after forging. On the other hand, ferrit in the shape of Widmannstätten structure is created by rapid cooling

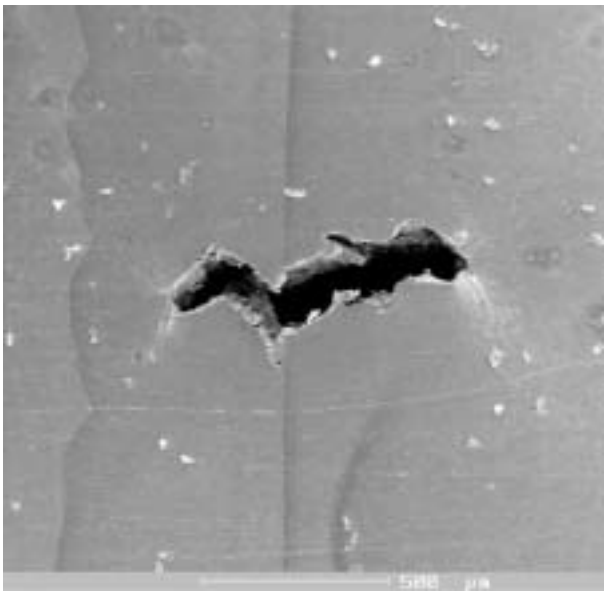

Fig. 13 A crack on the surface of the testing rod, REM

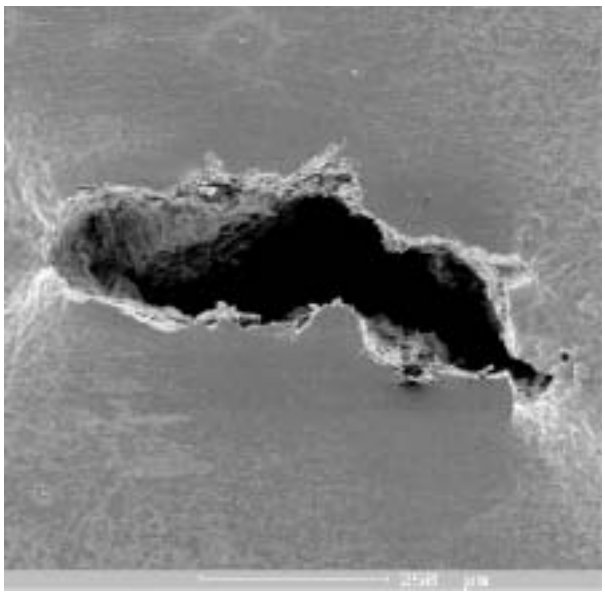

Fig. 14 A different crack, plastic deformation on the crack tip, REM

Fig. 15 The separation of an inclusion from basic material, REM

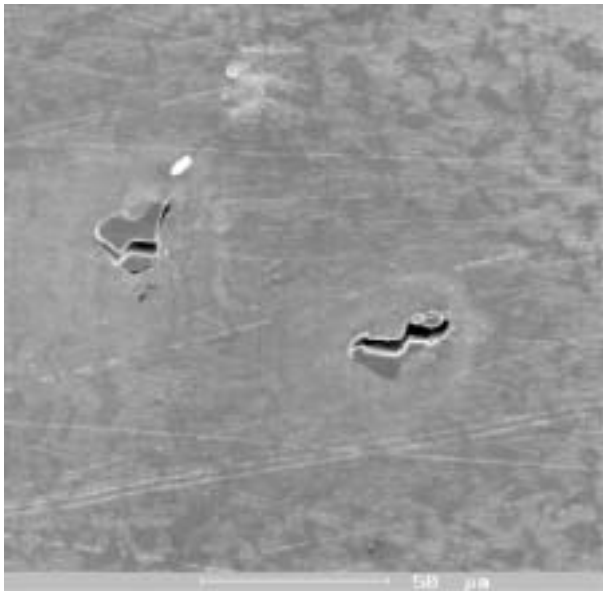

Fig. 16 Cracked inclusions on the surface of the testing rod, REM

from high temperature that occurs at over-heating over permissible hardening temperatures. Both processes, i.e. over-heating over hardening temperatures as well as slow cooling contribute to the creation of irregular grain.

The electron microscope evaluation was focused on the documentation of the size and shape irregularity of the grains of ferrit and pearlite and on the evaluation of the shape and occurrence of inclusion in the structure. The REM evaluation confirmed that the structure of the material is ferritic-pearlitic, very irregular (Figs. 19 and 20) and there are grains of a very small (6 μm) size and of very large sizes (45 μm).

Pearlite is of a lamellar character in some grains and globular in others. Sporadically, Widmannstättenic ferrit was observed in the areas with near by big grains. Except for very irregular grains, inclusions of various shapes and parameters occurred in the structure (Figs. 21 and 22), while they nearly always had a non-coherent interface. The separation of inclusions from the matrix is probably caused by a long-term dynamic loading with a relatively high amplitude (in the relation to fatigue properties of the evaluated steel).

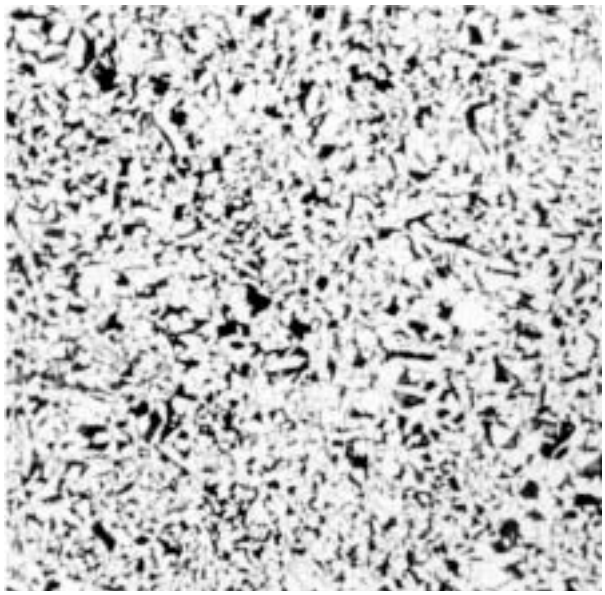

Fig. 17 Ferritic-pearlitic structure, a longitudinal section, 100x, etch. 3% NITAL

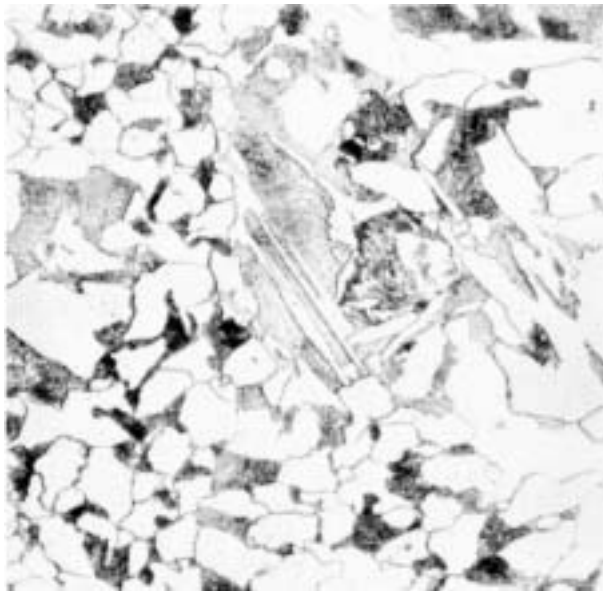

Fig. 18 Ferritic-pearlitic structure, a diagonal section, 400x, etch. 3% NITAL

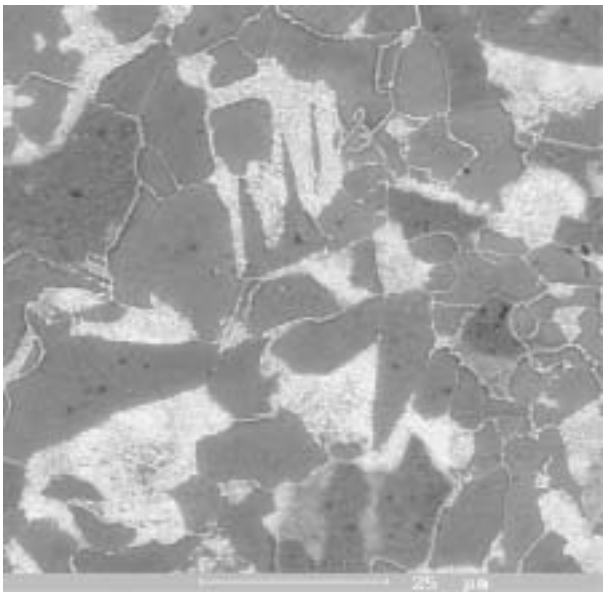

Fig. 19 Ferritic-pearlitic structure, a longitudinal section , REM

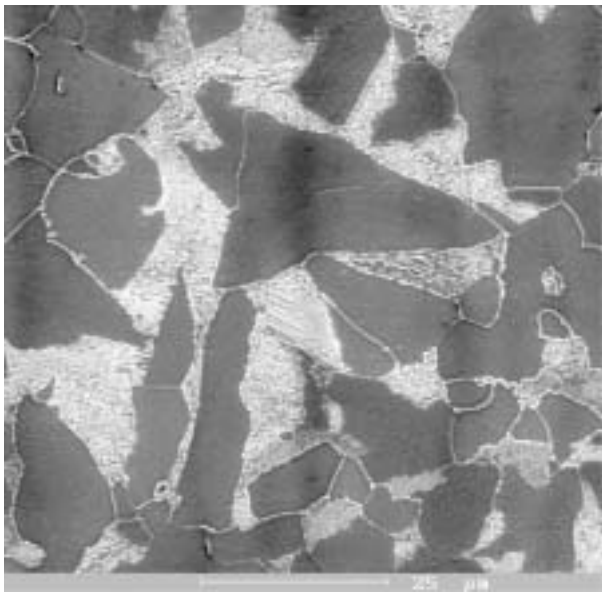

Fig. 20 Ferritic-pearlitic structure, a diagonal section , REM

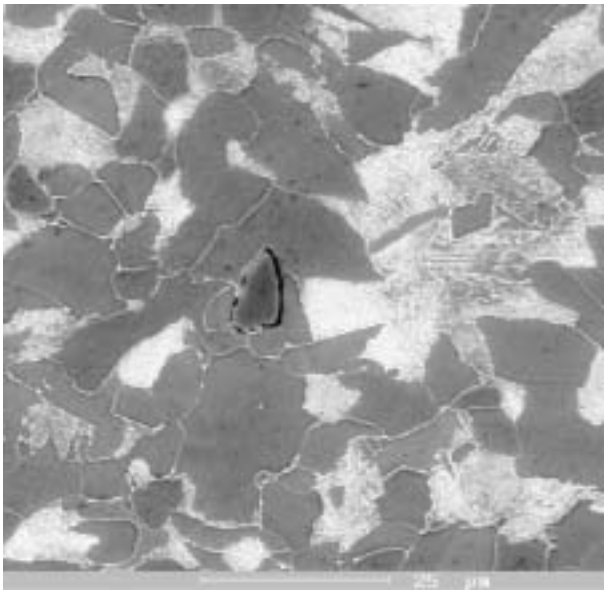

Fig. 21 The presence of an inclusion in the material structure, irregular size of grain, REM

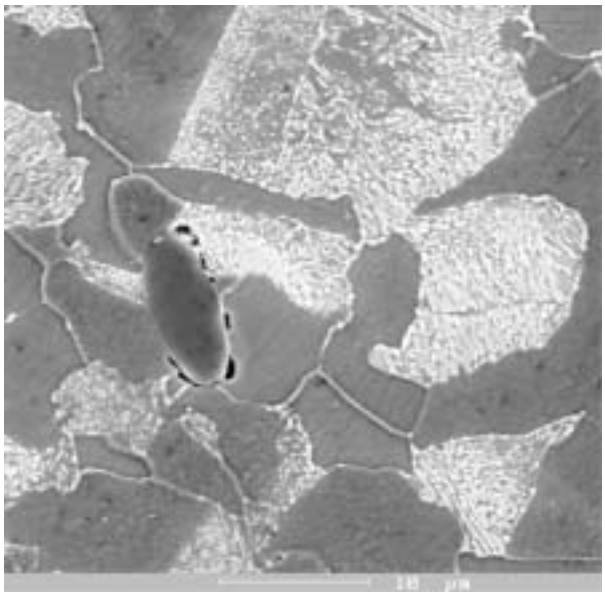

Fig. 22 The detail of ferritic-pearlitic structure with occurrence of an inclusion, REM

9. Fractographic evaluation

The specimen for the fractographic evaluation was extracted in the way to record the place of a supposed beginning of the crack growth, its gradual progress to the final fracture (Figs. 23 to 28). There were two sources on the evaluated fracture area (Fig. 23) from where the crack began to grow. In Fig. 23 the source is on the surface, the second source is superficial (Fig. 24). Most probably there was a bigger inclusion that served as a crack nucleus. But we cannot confirm this as the fracture area is damaged by oxides and pressing on this particular place. The pressing and partial oxidation was observed on the whole fracture area.

The character of the fatigue fracture area in the direction from the source to the force fracture is shown in Figs. 25 and 26. The whole fatigue fracture is characteristics by a transcrystalline fatigue failure with the occurrence of relatively deep secondary cracks (Fig. 25). At bigger magnifications typical fatigue signs – striations were observed (Fig. 26).

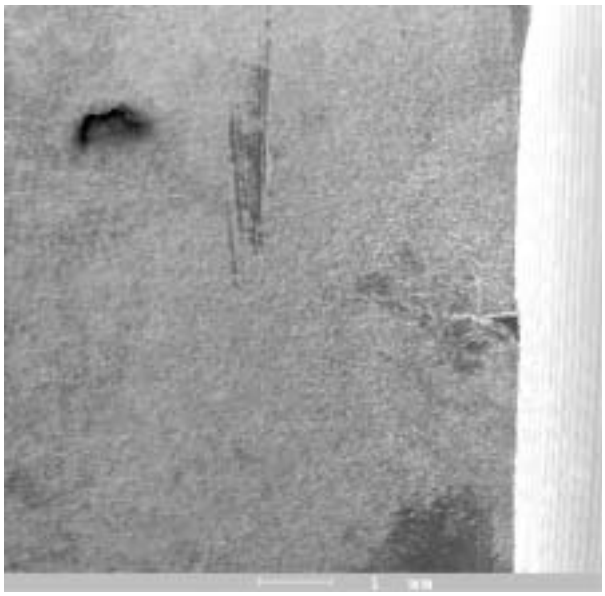

Fig. 23 The beginning of the crack growth – one of the sources, REM

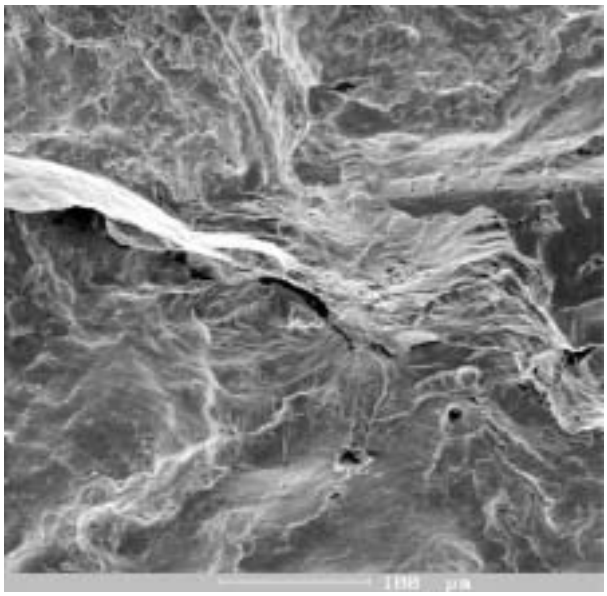

Fig. 24 The detail of a sub-surface source, REM

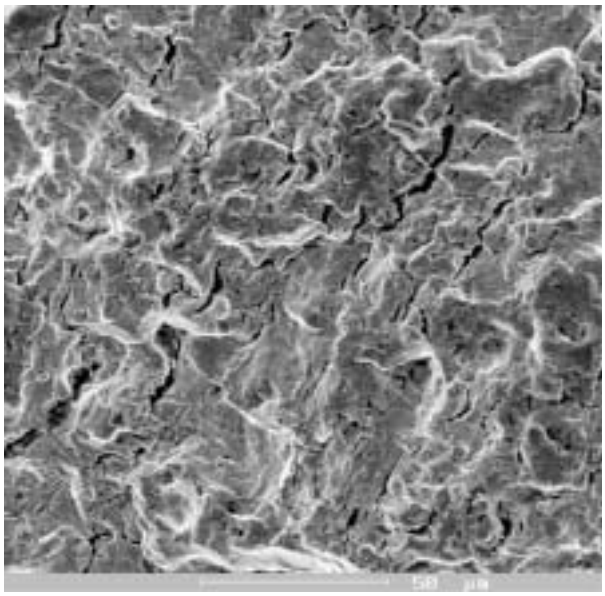

Fig. 25 The character of fatigue fracture area further from the source, REM

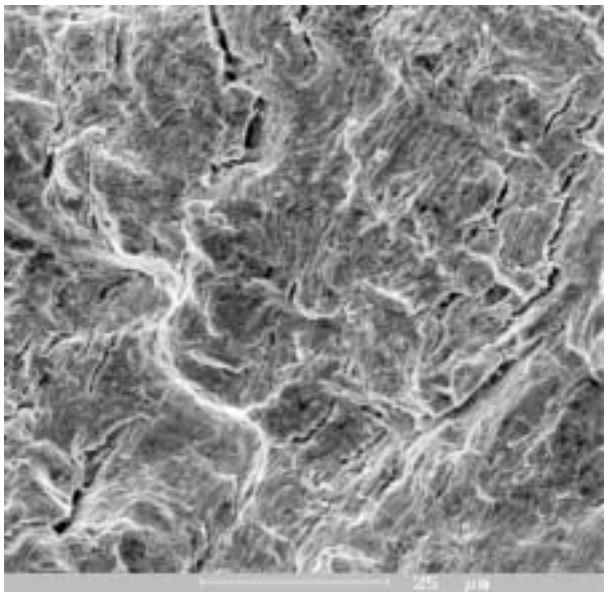

Fig. 26 A transcrystalline fatigue failure with the occurrence of striations and cracks, REM

The area of fracture is characteristics with a transcrystalline ductile failure with dimple morphology (Figs. 27 and 28), while the dimples were very heterogeneous which is related to the material heterogeneity. Big dimples correspond to ferrit, small dimples are pearlitic.

10. Conclusion

From the manifestation of the failure and appearance of functional surfaces of individual parts of the rod and piston results that the rod was loaded by additional loading – probably by bending – that caused the failure of the functional areas of the rod and impeller wheel by contact fatigue. Apart from the above mentioned the rod has an unsatisfactory geometry of the gasket slot under the flange. The vanes of the impeller wheel had a mechanical contact with the turbine chamber. It means that the turbine did not have perfect bearings.

On the basis of the experimental evaluation of the state of the rod material from the impeller wheel of a TG2 turbine it is possible to state that according to the recorded chemical composition the

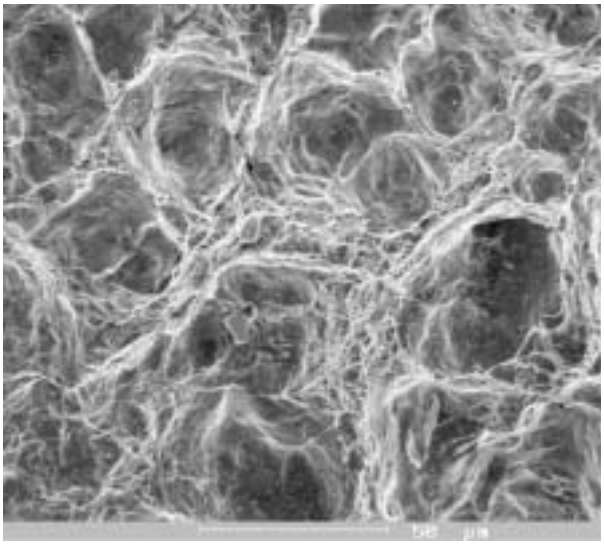

Fig. 27 The area of fracture, a transcrystalline ductile failure with dimple morphology, REM

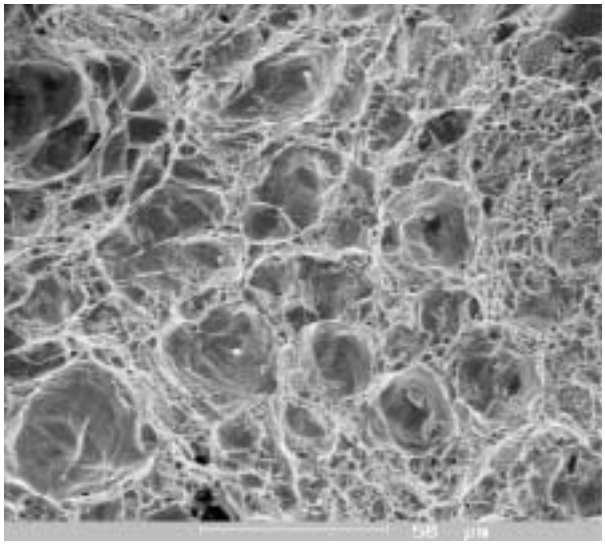

Fig. 28 The area of fracture – big dimples are ferritic, small are pearlitic, REM

rod material corresponds to the quality of StE 500 steel (Tab. 1), but its tensile strength reaches the values Rm = 489 MPa a Re = 317 MPa, i. e. by 100 MPa lower than the norm for StE 500 steel. This is inaccessible for the use.

The metallographic evaluation shows that the microstructure of steel is irregular, ferritic-pearlitic created by grains of various sizes (Figs. 17 to 22) while pearlite is lamellar in many cases but it appears also in a spheroidized shape and in many cases in Widmannstätten structure. It results from these facts that the inadmissible state of the structure was caused by wrong the heat regime at the production. The inclusions occurring in the structure were separated from the basic material and they operated as the crack nuclei (Figs. 15 and 16). At mechanical loading, the cracks were created around the inclusions at the tension just over the yield stress.

The fatigue fracture started from several sources on the rod circumference which is related to the inconvenient structure and state of the material (Figs. 23 to 26). The fatigue fracture is characteristics by a transcrystalline fatigue failure with ductile and fragile striations (Figs. 25 and 26) while there are many secondary cracks on the fatigue fracture area. The area of force fracture is characterized by a transcrystalline ductile failure with dimple morphology while the dimples have a very distinct diameter (Figs. 27 and 28).

The individual findings lead to the following conclusions. The failure of the impeller wheel was cause by:

- a failure of the rod construction (high values of local tensions)
- a failure of material (strength characteristics lower by 20% than the norm)
- an mistakes at installation (vibrations and oscillation of the whole impeller wheel).

This work has been supported by the Scientific Grant Agency of the Ministry of Education of the Slovak Republic and Slovak Academy of Sciences, grant No. 1/3155/06

References

[1] SKOČOVSKÝ, P., BOKŮVKA, O., PALČEK, P.: *Material Science (in Slovak)*, EDIS, ŽU Žilina, 1996.
[2] DRASTÍK, F. et al..: *Atlas of Metal Applications in the Engineering, Electrical Engineering and Chemical Industry (in Czech)*, SNTL, Praha 1980.
[3] MITURA, K., LANDOVÁ, S.: *Inclusions in the Steels (in Czech)*, SNTL Praha, Praha 1986
[4] SKOČOVSKÝ, P., PALČEK, P., KONEČNÁ, R., VÁRKOLY, L.: *Structural Materials (in Slovak).* EDIS ŽU Žilina, 2000.
[5] PLUHAŘ, J., PUŠKÁR, A., KOUTSKÝ, J., MACEK, K., BENEŠ, V.: *Physical Metallurgy and Threshold States of Materials (in Czech),* SNTL/ALFA, Bratislava, 1987.
[6] KOUTSKÝ, J., JANDOŠ, F., KAREL,V.: *Fracture of Steel Parts (in Czech),* SNTL, Praha, 1976.
[7] JECH, J.: *Heat Treatment of Steels (in Czech)*, SNTL Praha, 1983.
[8] PALČEK, P., HADZIMA, B., CHALUPOVÁ, M.: *Material Properties (in Slovak).* ŽU v Žiline, Žilina 2004.
[9] BOK(VKA, O., NICOLETTO, G., KUNZ, L., PALČEK, P., CHALUPOVÁ, M: *Low and High – frequency fatigue testing.* EDIS ŽU Žilina, October 2002. (ISBN 80-8070-011-7).
[10] PALČEK, P., CHALUPOVÁ, M., NICOLETTO, G., BOK(VKA, O.: *Prediction of Machine Element Durability. Education Aid for Multimedia Lectures.* ES ŽU Žilina, 2003.

Paweł Droździel *

THE INFLUENCE OF VEHICLE MAINTENANCE CONDITIONS ON CHOSEN ELECTRIC PARAMETERS OF STARTER DURING COMBUSTION ENGINE START-UP

Necessary mechanical energy needed for initiation of self-dependent combustion engine work is transferred by crankshaft driving using an electrical starter. Changes of values of the static resistant moment and start-up resistant moment in the engine influence current input by the electric starter during start-up of the combustion engine. Overloads observed in the vehicle electric power system are the results of high value of current intensity input by the electric starter. It seems very important to find the answer how the vehicle maintenance conditions influence the chosen working electric parameters of the starter during the combustion engine start-up. This article presents the results of investigations of starting working electric parameters during a combustion engine start-up, made during the vehicle maintenance.

1. Introduction

Necessary mechanical energy needed for initiation of self-dependent combustion engine work is transferred by crankshaft driving using an electrical starter supplied from the accumulator in modern vehicles. Initiation of the engine start-up begins when the operator applies voltage at the starter. Interconnection of the pinion with the flywheel gear ring of engine crankshaft circle occurs. Passing from standstill to motion state of elements and groups of engine needs overcoming a great resistance of static friction forces from the electric starter. Later the engine start-up resistant moment has less value than at the starting point of the movement. This moment is characterized by significant variability connected with kinematics of the pistons to-and-fro motion and changeable pressure during air-fuel mixture compression and expansion in the engine cylinders [3, 4, 5].

Changes of values of static resistant moment and start-up resistant moment influence the current run input by the electric starter during start-up of the combustion engine. On the beginning of the engine start-up the maximal value of current intensity input by the electric starter (with electric power 3–4,5 kW) can exceed 300 A. During the next stage of start-up current intensity drops more than twice. Overloads observed in the vehicle electric power system are the results of high value of current intensity input by the electric starter. The voltage drops corresponding with them can cause abnormalities in the vehicle electronic systems work. The value of current intensity input by the electric starter during the engine start-up depends on many factors such as: technical state of the engine start-up system, state of the accumulator load, properties of lubricant, the length of pauses in the vehicle operation, engine temperature etc. [1, 3, 6].

The user of the vehicle has an influence on some of these factors but most of them are relative only to external conditions of the vehicle maintenance. It seems very important to find the answer how the vehicle maintenance conditions influence working electric parameters of the starter during the combustion engine start-up. It is not only important for a vehicle operator but, first of all, for a designer of modern combustion engine start-up systems. This article presents the results of investigations made during the engine maintenance.

2. Research methodology

The researches included the 443 115 142 723 starter produced by the Czech company MAGNETON. It is an electric series motor designed for a short-term operation. The pinion of the starter which initiates the motion of the engine crankshaft circle is drown out electromagnetically by a switch with two windings: retracting and supporting. When the starter is switched on both windings work. When the current flows along the starter winding the retracting winding is switched off. Constant work of the starter cannot be longer than 5 seconds. Maximal current input by the starter is 140 A and minimal rotational speed is 5000 rpm during a test without loading. On the other hand current input by the starter is 550–600 A, minimal rotational speed is 1500 rpm and voltage drop on the starter clamp is 10V during a test with loading. The chosen technical data of the starter are shown in tab. 1.

The investigation starter is installed in the 4-cylinder diesel engine 4CT90. This engine is produced by the engine factory "Andoria" located in Andrychów, Poland. The engine displacement: indirect injection, 2.417 dm^3, stroke/diameter 95/90, maximum power: 63.5 kW at 4100 rpm, maximum torque: 195 Nm at 2500 rpm. This engine was equipped with the injection pump MOTORPAL Jihlava type PP4M7P1g 3176, produced in the Czech Republic. The 4CT90 engine is installed in a delivery truck (maximum

* **Paweł Droździel**
Department of Machine Design, Mechanical Faculty, Lublin University of Technology, ul. Nadbystrzycka 36, 20-618 Lublin, POLAND,
E-mail: p.drozdziel@pollub.pl

Technical data of the starter 443 115 142 723 company MOTORPAL Tab. 1

Nominal voltage [V]	12
Nominal power [kW]	3
Moment on pinion [Nm]	min 44.1
Rotations on nominal Power [rpm]	1700^{+100}
Voltage on „30" starter clamp on nominal power [V]	10
Current of starter without loading [A]	140
The direction of rotations	Right
Wright [kg]	5.3
Number of teeth in pinion [-]	9
Module pinion pitch [-]	3

authorized total weight < 3.5 t) LUBLIN III. The investigated vehicle was maintained by the Polish Post in Lublin Province during spring, summer and autumn seasons.

A special recorder was constructed to register selected parameters of LUBLIN III operation and activity of the 4CT90 engine and its starter. The following parameters were recorded: time and date of switching on electrical supply in the vehicle, number of crankshaft revolutions and drive shaft, pressure and temperature of the engine oil, coolant temperature, toothed bar position of the injection pump. The starter electric parameters were recorded: intensity of the current consumed by the starter at the engine start-up and voltage applied at the starter. The current consumed by the starter as well as voltage at the starter were recorded every 25 ms from the very beginning of the engine start-up cycle, after the value of the starter current had exceeded the threshold (50A). All the parameters were transferred to a PC computer where they were processed by the programme converting raw data into text-saved measurement results. Then they were transmitted to other computer programmes to analyse the data [2].

3. Statistical analysis of experimental results

The results of the research on selected parameters of the LUBLIN III vehicle operation, the 4CT90 engine start-up and electric parameters of its starter were analysed by a computer programme STATISTICA. The following electric and working parameters of the investigated starter: maximal current intensity (I_{max} in A) in a first step of start-up, voltage (U_{max} in V) at the maximal current intensity, power (P_{max} in W) consumed by the starter at the maximal current intensity, mean current intensity (I_{mean} in A), which occurs when the starter drives the engine crankshaft during the start-up, mean voltage (U_{mean} in A)and mean power (P_{mean} in W), time (t_{start} in sec) of the engine start-up and time (t_{work} in sec) work of starter were distinguished.

The time of the engine start-up is stated from the moment of applying the voltage on the starter to the moment when current intensity input by the starter reaches the value which appears during work without loading. The time of the starter work is connected with time of applying the voltage at the starter.

The histogram of maximal current intensity I_{max} in the first step of start-up is presented in Figure 1. This bar chart was approximated using an extreme value distribution with the following coefficients: position – 292.74; scale – 46.392. Fig. 2 presents a bar chart of the mean current intensity I_{mean}, which occurs when the starter drives the engine crankshaft during the start-up. This bar chart was approximated using the extreme value distribution with the following coefficients: position – 144.33; scale – 3.004.

The histogram of power P_{max} consumed by the starter at the maximal current intensity is presented in Figure 3. This bar chart was approximated using a lognormal distribution with the following coefficients: scale – 7.806; shape – 0.1379. Fig. 4 presents the bar chart of the mean power P_{mean} consumed by the starter, which occurs when the starter drives the engine crankshaft during the start-up. This bar chart was approximated using the normal distribution.

The histogram of time of the engine start-up t_{start} is presented in Fgure 5. This bar chart was approximated using an extreme value distribution with the following coefficients: position – 0.3275; scale – 0.0874.

Further part of the data analysis deals with preparing the matrix of the correlation coefficients r between the specified starter para-

Statistical parameters of analyzed variables Tab. 2

Random variable	Mean value	Standard deviation	Median	Mode	Mean error	Skewness	Kurtosis	Maximal value	Minimal value
Max current I_{max} [A]	318.15	52.73	314.00	286.00	1.565	0.354	−0.399	484.00	188.00
Max voltage U_{max} [V]	7.84	0.60	7.86	7.86	0.017	−0.225	0.146	10.20	6.00
Max power P_{max} [W]	2477.70	341.14	2449.44	2350.92	10.126	0.304	0.000	3801.60	1515.00
Mean current I_{mean} [A]	146.25	5.05	145.00	146.00	0.178	3.046	13.219	180.;00	139
Mean voltage U_{mean} [V]	9.32	0.36	9.36	9.44	0.012	−0.446	0.572	10.39	7.72
Mean power P_{mean} [W]	1362.56	55.06	1363.68	1368.80	1.945	−0.057	0.996	1582.63	1134.84
Time t_{start} [sec]	0.379	0.165	0.350	0.350	0.004	5.284	38.238	0.100	2.300
Time t_{work} [sec]	0.487	0.206	0.425	0.400	0.006	3.830	23.307	0.125	2.700

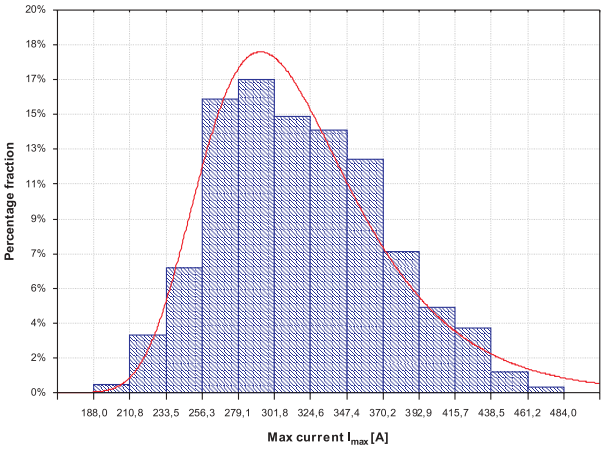

Fig. 1 Statistical distribution of maximal current intensity I_{max} in first step of start-up

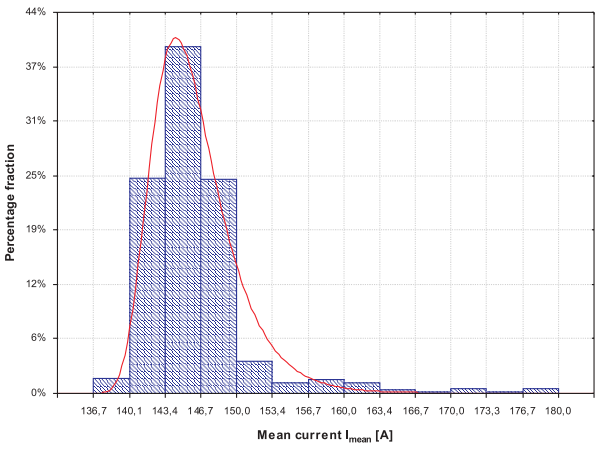

Fig. 2 Statistical distribution of mean current intensity I_{mean}, which occurs when starter drives engine crankshaft during the start-up

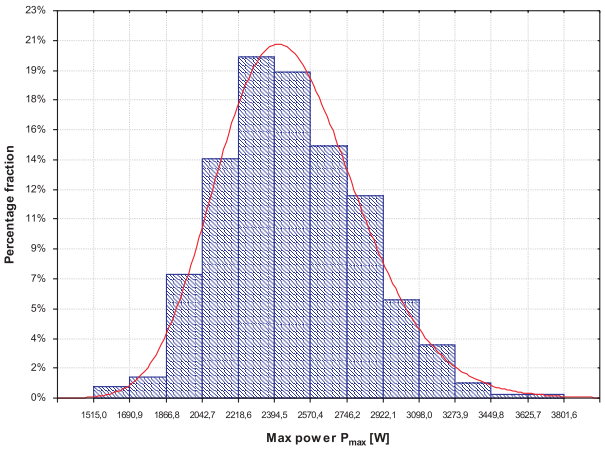

Fig. 3 Statistical distribution of power consumed P_{max} by the starter at the maximal current intensity

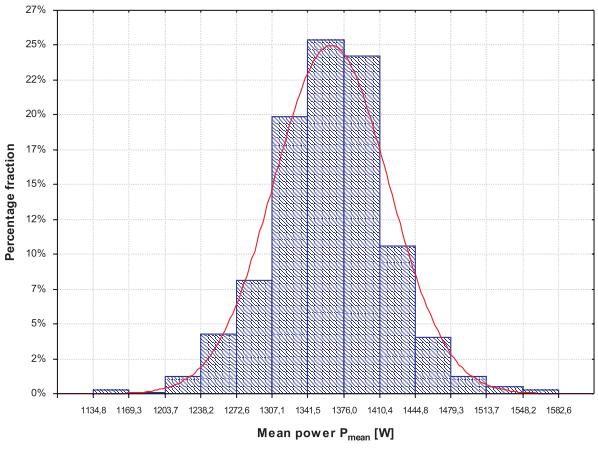

Fig. 4 Statistical distribution of power consumed P_{mean} by the starter, which occurs when starter drives engine crankshaft during the start-up

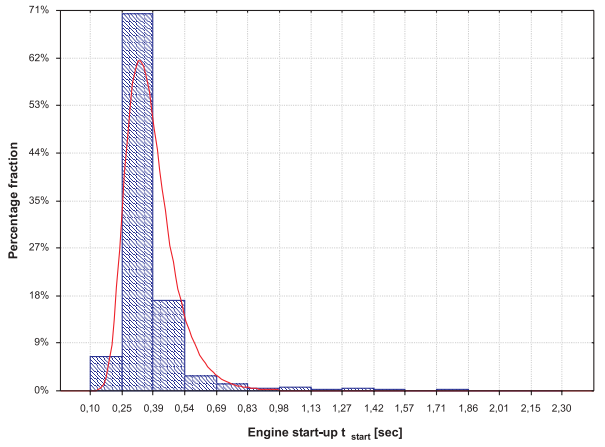

Fig. 5 Statistical distribution of the engine start-up t_{start}

meters and the other chosen engine and vehicle parameters. The following engine and vehicle parameters: temperature of cooling agent (T_{agent} in °C) at the moment of the engine start-up, time of the engine operation (t_{oper} in min) before its next start and the length of pauses in the vehicle operation (t_{pause} in min), when the 4CT90 engine is switched off were chosen to calculate the correlation coefficients.

Figures 6-9 show scatter diagrams for chosen variables with the equation of regression function, for which the correlation coefficients $r \geq |0.4|$ which indicates a significant correlation between the analysed variables.

Figure 6 presents scatter diagrams for the maximal current intensity I_{max} in the first step of start-up and power consumed P_{max} by the starter and linear function of regression with the confidence interval for forecast mean observation with a prediction interval for single observation for the declared confidence level

	I_{max}	U_{max}	P_{max}	I_{mean}	U_{mean}	P_{mean}	t_{start}	t_{work}	T_{agent}	t_{oper}	t_{pause}
I_{max}	1.00	– 0.56	0.88	0.05	0.16	0.20	– 0.02	0.00	0.00	0.03	– 0.01
U_{max}	– 0.56	1.00	– 0.11	– 0.28	0.40	0.16	– 0.20	– 0.28	0.39	0.14	– 0.22
P_{max}	0.88	– 0.11	1.00	– 0.10	0.42	0.32	– 0.14	– 0.16	0.23	0.11	– 0.14
I_{mean}	0.05	– 0.28	– 0.10	1.00	– 039	0.44	0.53	0.60	– 0.69	– 0.13	0.70
U_{mean}	0.16	0.40	0.42	– 0.39	1.00	0.65	– 0.35	– 0.43	0.54	0.19	– 0.34
P_{mean}	0.20	0.16	0.32	0.44	0.65	1.00	0.09	0.07	– 0.03	0.08	0.23
t_{start}	– 0.02	– 0.20	– 0.14	0.53	– 0.35	0.09	1.00	0.89	– 0.59	– 0.10	0.65
t_{work}	0.00	– 0.28	– 0.16	0.60	– 0.43	0.07	0.89	1.00	– 0.73	0.17	– 0.70
T_{agent}	0.00	0.39	0.23	– 0.69	0.54	– 0.04	– 0.59	– 0.73	1.00	0.31	– 0.71
t_{oper}	0.03	0.14	0.11	– 0.13	0.19	0.08	– 0.10	0.17	0.31	1.00	– 0.13
t_{pause}	– 0.01	– 0.22	– 0.14	0.70	– 0.34	0.23	0.65	– 0.70	– 0.71	– 0.13	1.00

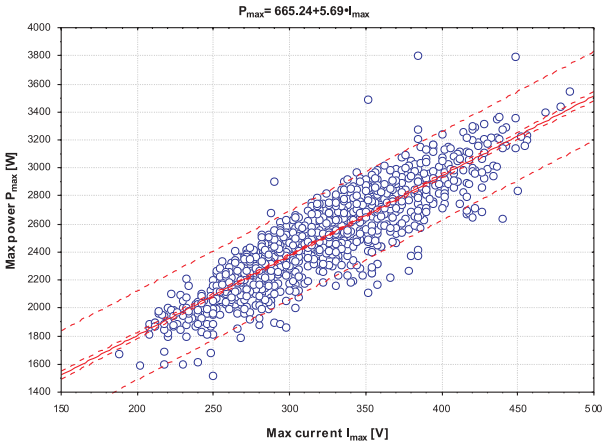

Fig. 6 Scatter diagram for the maximal current intensity I_{max} in first step of start-up and power consumed P_{max} by the starter

95%. Statistical analysis using Statistica computer programme (declared significant level $\alpha = 0.05$) showed that the random error of estimation for slope of the straight line is equal 0.091 and *t*-Student statistics ($t = 62{,}58$). The mean random deviation of a free term estimation is equal to 29.357, the value of *t*-Student statistics ($t = 22.660$). The critical significant level α_{kr} is to equal 0.00 in both cases. It shows that the point estimation of regression coefficients is statistically significant. The value of the coefficient of determination r^2 is high and equals to 0.7756, which proves that the line function of regression fits well to the data.

Also the relationship between the mean current intensity I_{mean} and the mean power P_{mean}, which occur when the starter drives the engine crankshaft during the start-up seems to be linear what is shown in Fig. 7. The random error of estimation for slope of the straight line is equal to 0.3446 and the *t*-Student statistics ($t = 14.092$). The mean random deviation of a free term estimation is to equal 50.4198, the value of *t*-Student statistics ($t = 12.940$). The critical significant level α_{kr} is equal to 0.00 in both cases. It shows that the point estimation of regression coefficients is statistically significant. Unfortunately the value of the coefficient of determination r^2 is low and equals to 0.1990 which testifies weak variability of the mean power P_{mean} line regression model. The values of analyzed parameters (I_{mean} and P_{mean}) which occur during the first daily engine start-ups (if $I_{mean} > 155$ A) indicated influence on regression dependency for these parameters.

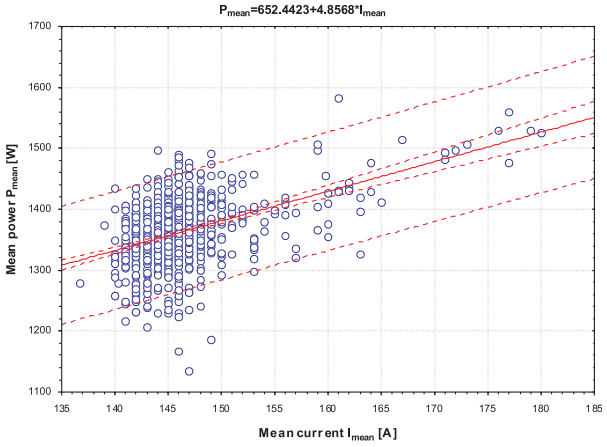

Fig. 7 Scatter diagram for the mean current intensity I_{mean} and mean power P_{mean}, which occur when starter drives engine crankshaft during the start-up

The influence of values of the analyzed parameters which occur during the first daily engine start-ups is also observed in the relationship between the variable representing the engine thermal state (temperature T_{agent}) and the mean current I_{mean} which occurs when the starter drives the engine crankshaft during the start-up. The value of the correlation coefficient $r_{Tagent,Imean} = -0.69$. It means that as the engine start-up temperature grows the movement resistance drops. Figure 8 shows scatter diagrams for the temperature of the cooling agent T_{agent} at the moment of the engine start-up and the mean current intensity I_{mean}, which occurs when the starter drives the engine crankshaft during the start-up and the polynomial regression function. The statistical analysis showed that the mean random deviation of the free term estimation is equal to 1.632, with

the value of *t*-Student statistics ($t = 114.78$). The mean random error for the regression coefficient is equal to 0.000011 when $(T_{agent})^3$, with the value of *t*-Student statistics ($t = -9.5302$). The mean random error for the regression coefficient is equal to 0.00195 when $(T_{agent})^2$, with the value of *t*-Student statistics ($t = 11.6980$) and the mean random deviation of estimation for the slope of the straight line is equal to 0.1052 when T_{agent}, with the value of *t*-Student statistics ($t = -15.9818$). The critical significant level α_{kr} is equal to 0.00 in these cases. The estimation point of the regression coefficients is statistically significant. The value of the coefficient of determination r^2 is high and equals 0.6451, which leads to the conclusion that the polynomial function of the regression fits the data well.

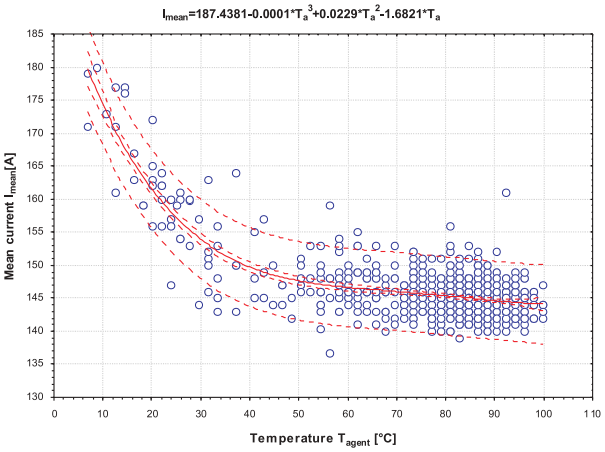

Fig. 8 Scatter diagram for the temperature of cooling agent T_{agent} at the moment of engine start-up and mean current intensity I_{mean}, which occurs when starter drives engine crankshaft during the start-up

The correlation coefficient $r_{Tagent,tstart} = -0.59$ between the variable representing the engine thermal state (temperature T_{agent}) and the variable describing the time of its starting t_{start} shows, which seems to be evident, that as the start-up temperature increases, the engine needs less time to start to operate independently at idle running. It is the result of the first spontaneous ignition of the fuel-air mixture in the engine cylinder. The scatter diagram with the regression curve for the temperature of the cooling agent T_{agent} at the moment of the engine start-up and the engine start-up time t_{start} shown in Fig. 9 confirms that regularity. The mean random deviation of the free term estimation is equal to 0.0632, with the value of *t*-Student statistics ($t = 23.00$). The mean random error for the regression coefficient is equal to 0.00001 when $(T_{agent})^3$, with the value of *t*-Student statistics ($t = -5.6092$). The mean random error for the regression coefficient is equal to 0.000073 when $(T_{agent})^2$, with the value of *t*-Student statistics ($t = 7.0154$) and the mean random deviation of estimation for the slope of the straight line is equal to 0.0039 when T_{agent}, with the value of *t*-Student statistics ($t = -10.0395$). The critical significant level α_{kr} is equal to 0.00 in these cases. It shows that the point estimation of the regression coefficients is statistically significant. The value of the coefficient of determination r^2 is average and equals 0.6451, which leads to the point that the polynomial function of regression fits the data satisfactorily.

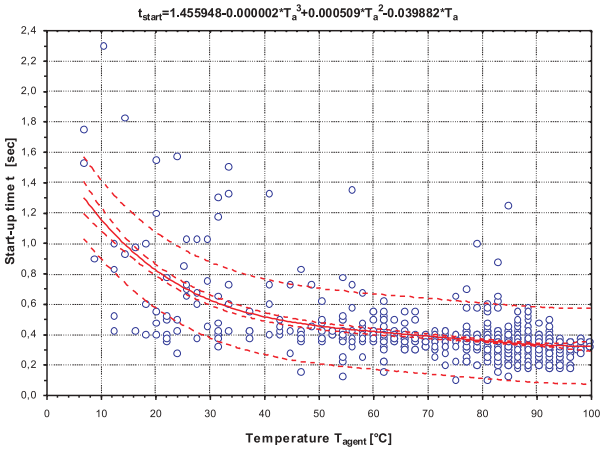

Fig. 9 Scatter diagram for the temperature of cooling agent T_{agent} at the moment of engine start-up and engine start-p time t_{start}

The engine start-up time t_{start} is connected with the mean current I_{mean} which occurs when the starter drives the engine crankshaft during the start-up. The value of the correlation coefficient $r_{Imean,tstart}$ is equal to 0.53. It is obvious that this connection is the result of the engine thermal state during the start-up. The decisive parameters that influence the engine thermal state are pauses in the vehicle operation t_{pause}, when the 4CT90 engine is switched off. It's shown by the correlation coefficient $r_{tpause,Tagent} = -0.71$. The mean current I_{mean} and the time of engine start-up t_{start} are relative to the pauses in the vehicle operation t_{pause}, when the 4CT90 engine is switched off. The correlation coefficients $r_{tpauset,Imean}$ is equal to 0.70 and $r_{tpauset,start}$ is equal to 0.65. The influence of the pauses in vehicle operation t_{pause} at the engine start-up time t_{start} is shown in Fig. 10.

The statistical analysis showed that the random error of estimation for the slope of the straight line is equal to 0.00003, with the *t*-Student statistics ($t = 23.1154$). The mean random deviation of the free term estimation is equal to 0.004242, with the value of *t*-Student statistics ($t = 83.2188$). The critical significant level α_{kr} is equal to 0.00 in both cases. It shows that the estimation point of the regression coefficients is statistically significant. The value of the coefficient of determination r^2 is insignificant and equals 0.3241, which provides the fact that the line function of regression doesn't fit the data. It is the result of the engine first daily start-ups which appear after at least 7 hours' pauses in the vehicle operation t_{pause}, when the 4CT90 engine is switched off.

Finally we should remark that the intensity of the mutual connections between the specific starter parameters and other chosen variables of the engine 4CT90 and LUBLIN III vehicle depend on the analyzed parameters occurring during the first daily start-ups.

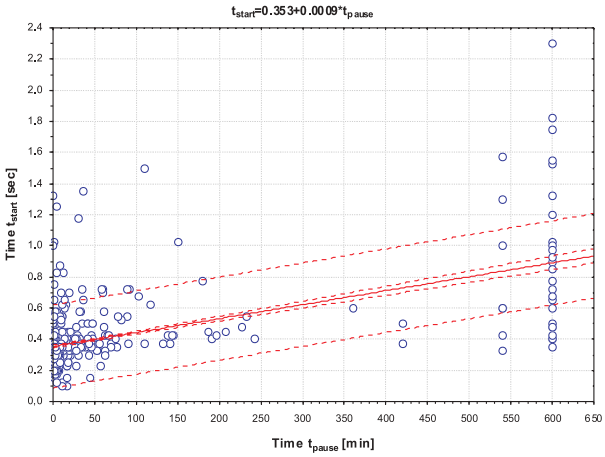

Fig. 10 Scatter diagram for the length of pauses in a vehicle operation t_{pause}, when the 4CT90 engine is switched off and engine start- up time t_{start}

4. Summary

Taking into account the correlation and the regression statistical analysis of the results of 4CT 90 engine start-up maintenance investigations we can state:

1. The crucial factor of vehicle work, influenced by the thermal state of the engine, the electrical parameters, is the time of pauses in vehicle operation, when the engine is switched off.
2. Proper organization of LUBLIN III vehicle trips and short time of pauses in the vehicle operation, when the engine is switched off, results in the fact that high temperatures occur of 4CT90 engine start-ups. That is why short start-up times are common and we can observe only unimportant overloads in engine start-up system.
3. The first daily start-ups are the separate group of start-ups which influence the correlation and the regression connections between the vehicle maintenance conditions and the electric starter parameters. The electric overloads during first daily start-ups are rather long and have the highest possible values.

References

[1] DROŹDZIEL P.: *The investigations of the 4CT90 start-up engine during the operation of LUBLIN car (in Polish).* The maintenance of combustion engines, no. 6. Publisher Szczecin University of Technology. Szczecin, 2002, p. 45–50.
[2] DROŹDZIEL P., LIŠČÁK Š.: *The chosen problems of commercial truck maintenance,* EDIS- Žilina University publisher, Žilina, 2005.
[3] KOZIEJ E.: *The electric machine of vehicles (in Polish).* Publisher WNT. Warszawa, 1986.
[4] MYSŁOWSKI J.: *The start-up of a diesel engine (in Polish).* Publisher WNT. Warszawa, 1996.
[5] PSZCZÓŁKOWSKI J.: *The characteristics of start-up of diesel engines (in Polish).* Publisher SEPP „Cogito". Zbąszynek, 2004.
[6] WAJAND J. A., WAJAND J. T.: *The combustion piston engine average - and high-speed (in Polish).* Publisher WNT. Warszawa, 1997.

Tomáš Lack – Juraj Gerlici *

THE USAGE OF ARCS RADII PROFILE VARIATION FOR THE SYNTHESIS OF RAILWAY WHEEL AND RAIL HEAD PROFILES

The presented article deals with one of the ways of profile geometry design of a railway wheel and railhead. The base for the creation of new profiles is an interactive attitude based on the modification of "the original shape which is defined by section of a railway wheel profile", with to each other connected and exactly defined arcs radii. It is possible to change them according to shape needs of the final geometrical characteristics.

1. Introduction

The wheel/rail geometry is one of the main parameters dramatically influencing track forces and vehicles dynamic. The resulting wheel geometry in service conditions depends upon the new assumed profile, the track geometry distribution, the creep coefficients and forces, the rail average material and mechanics, the wheel material and mechanics, the lubrication. The evolution of wheel profile used to be validated in exemplar application cases, on the basis of available results or through dedicated measuring campaign.

In the article we will deal with the railway wheel/rail contact from the point of view of wheels and rails profiles geometry.

2. Railway wheel/rail contact in the frame of railway vehicles interoperability request

Problems of the railway wheel /rail contact represents a basic point of any analysis which is connected with the moment of a railway vehicle on a track, with safety, speed, with comfort of people and goods transport.

It is connected with the construction of new railway vehicles, with the reconstruction of the old ones, with the approval (refusal) of vehicles into operation, with their evaluation as well as with the evaluation of track quality and their maintenance. It has a direct influence on the position of rail transport in the frame of the whole transport system, on economics, ecology and so on.

Profiles shapes (we understand a profile curve course which a rail and wheel have in a lateral cross section, or at a rail in a cross section which is perpendicular on the rail axis and at a wheel with a plane which is crossing the wheel centre point and which is perpendicular on a plane of a wheel lateral cross section) as we know them today have been developing since the beginning of railway.

The shape of wheel tread and rail head profiles has been developed together with the satisfaction of needs on the goods and people transport when looking at the enhancement of wheelset loading for heavy haul transport and speed for passenger and heavy haul transport as well.

Nowadays several basic wheels and rails profiles types are used on various European railways. It depends on a specific railway company of the given country whether one type of rails equipped with a standardised profile or several types of profiles are used in its railway corridors.

The aim of each railway company is (or should be) that the wheel/rail contact couple provides the best presuppositions for a smooth, safe (stable) and quiet vehicle running on a track with a minimum wheels and rail wearing, with a minimum negative force influence of a wheel on the track.

The fact that various types of rails with different types of profiles, with different slopes are used at separate companies complicates the situation. The track gauge complicates it to a smaller degree.

Today there is an extremely up to date need for the security of vehicles interoperability in its greatest extend in order to use in reality one of the greatest advantages of railway transport (economic transport of a huge volume of goods over long distances). The fulfilment of the need places a higher requirement on the sphere of usage (design or choice of the right, for the given railway company so -called optimum profile).

It arises from the variety of inputs and transport needs of separate railway companies that it is not easy at all to find one profile which solves all the problems.

It is possible to use a proved and verified standard in a higher degree when building new modern tracks and railway corridors.

* **Tomáš Lack, Juraj Gerlici**
Department of Transport and Handling Machines, Faculty of Mechanical Engineering, University of Žilina, Univerzitná 8215/1, SK-010 26 Žilina.
E-mail: tomas.lack@fstroj.utc.sk, juraj.gerlici@fstroj.utc.sk.

As a result of real conditions of a railway track in certain European regions at specific utilisation (the way of operation, loading, accessibility, simplicity and economic demands for the track maintenance), it has a sense to adapt, for example, a wheels profile to rail head profiles or for a certain track type to vehicles equipped with a certain wheels profile to find a rails profile which improves a mutual vehicle/rail interaction.

In order to declare a profile or a couple of profiles (wheel/rail) for a better one than another profiles couple, it is necessary to analyse both the existing and new state on the base of unambiguous criteria.

Such input criteria, after fulfilment of which verification in operation must of course follow, are geometrical characteristics.

When assessing characteristics in the article we take into consideration neither the wheelset rotation around its axis which can happen at a lateral movement of a wheelset in a rail, nor the wheelset angle of attack; their influence in this case seems to be of minimum importance [4, 5].

3. Wheel and rail profiles geometry analysis

The geometric shape of theoretical wheels and rails profiles is usually defined in a table way, with radii (and centres) of to each other linked arcs, or by functional dependence of a vertical profiles points position with regard to the lateral coordinate y.

The profiles acquired from the measurements have a base in points which are determined with couples of coordinates. It is often necessary to smooth such profiles for further assessment.

The role of the smoothing is to keep the profile geometry characteristics and to minimize influence of possible imperfections of measurements. Theoretical profiles are not smoothed. Profiles and arcs radii values from which the profiles are created with regard to the lateral coordinate y are graphically depicted in Fig. 1 and Fig. 2. Theoretical profiles: wheel profile DIN5573 (marked S1002) and rail UIC60 are analysed separately in the figures.

In Fig. 3 there is a course of theoretical wheel profile arcs radii values of S1002 in the contact points with regard to wheelset lateral movement y.

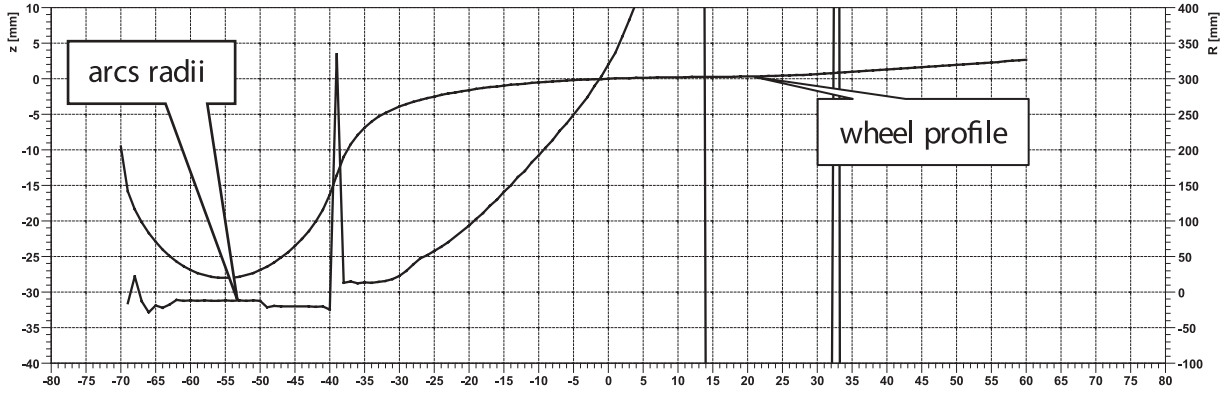

Fig. 1 Course of theoretical wheel profile arcs radii values of S1002 with regard to a lateral profile coordinate y

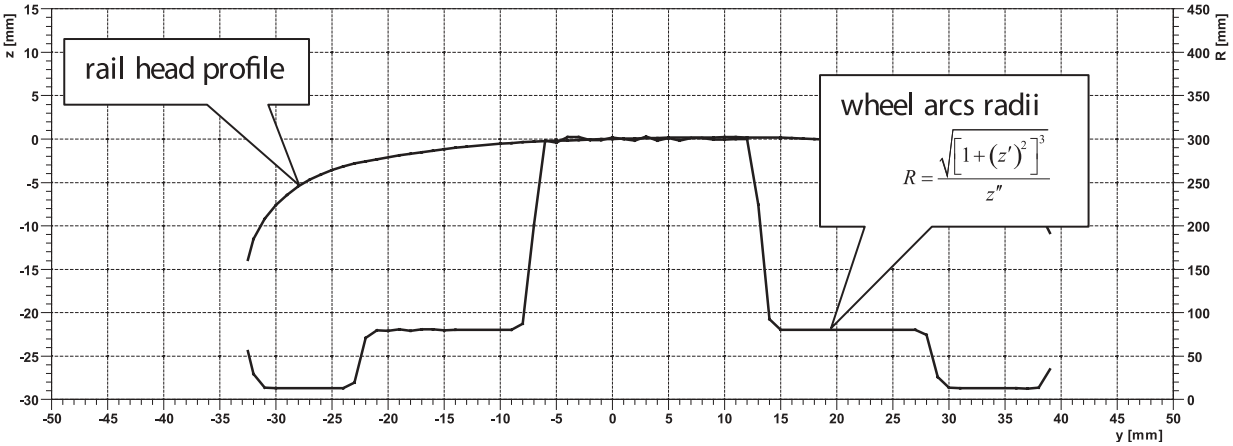

Fig. 2 Course of theoretical rail head profile arcs radii values of UIC60 with regard to a lateral profile coordinate y

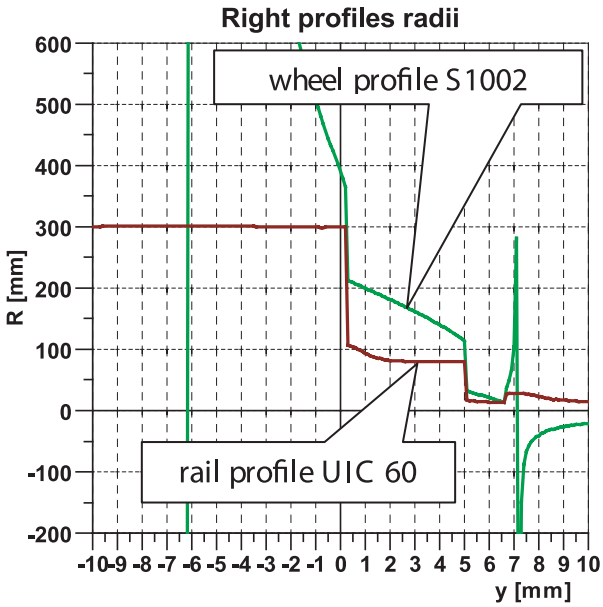

Fig. 3 Course of theoretical wheel profile arcs radii values of S1002 and rail UIC60 in the contact points with regard to wheelset lateral movement (y)

4. Wheelset and rail geometric characteristics

Wheelset and rail geometric characteristics help to specify the geometric binding of a wheelset and rail. With the help of them, it is possible relatively quickly to assess some parameters of the binding which help to estimate as a vehicle or better to say a wheelset can behave in a real operation.

Under the name of geometric characteristics we understand the following: contact points distribution between a wheel and rail at a lateral movement of wheels profiles of a wheelset over rail heads profiles, delta r function, tangent gamma function and equivalent conicity function. The basic presupposition for the characteristics evaluation is detailed knowledge of a wheel and rail profiles geometric shape.

To make the information complete, it is necessary to mention separate geometric characteristics. On the base of their shape we will suggest a railway wheel profile shape (to the given rail profile) or a rail head profile shape (to the supposed railway wheel shape).

They are as follows:

Contact points between the wheel and rail determine the contact points position at a wheel profile lateral movement over the rail profile. If we can presuppose that left and right wheel profiles (as well as rail profiles) are identical, the final curve course is symmetrical with regard to the rail axis.

Delta r function is a difference between an instant diameter of running of one wheel of a wheelset and instant diameter of running (course) of other wheel of a wheelset at the lateral movement of a wheelset on a rail. The Delta r function course shape indicates the rotating tendency of a wheelset at its lateral movement in a rail or kinematics running ability of a wheelset through the track arc.

Tangens gamma function is a difference between the value of the normal line tangent angle of the tangential contact area in the contact point and vertical axes of a rail. It determines the rate of binding intensity which comes back the wheelset after its lateral deviation into a centred equilibrium position on the rail. The tangent gamma function has (like the delta r function) anti-symmetrical course for the same wheels and rails profiles and it crosses the horizontal coordinate axis in its zero point.

Equivalent conicity is the reference conicity which equals the curving profile of a wheel when taking into consideration the amplitude of a coned wheel movement. According to the definition of UIC519 it is such conicity of a simple cone wheelset profile which the wheelset should possess in order to have the same kinematics characteristics as a wheelset with a curved profile at a certain oscillation amplitude.

It is possible to find more detailed information about separate characteristics, their definitions, meaning and the way of calculation under various possible conditions in references [4, 5, 6, 9, 21] of the article.

5. New optimum profiles statement

It is not possible to state a generally optimum profile for all types of tracks and railway wheels. The main reason is that in operation there are tracks with various gauges, various rail heads profiles on which vehicles with various railway wheels profiles move. Vehicles move at various speed, with various wheel forces, they transport various goods and more over we require various kinematics behaviour. That is why it is very difficult to state unambiguous criteria which we could define and compare when taking into account all vehicles.

We have chosen geometric characteristics of a railway wheelset and rail, we will state our optimum real or rail profile on the base of their specific shape.

5.1 Criteria for the search of an optimum profile

We have stated the following conditions as criteria for optimizing process:

- *delta - r function shape* without jump change of the course,
- *requested equivalent conicity,*
- *fluent distribution of contact points on the wheel and rail surface,*
- *exclusion of two- point- contact*

The difference function course shape (delta-r) without jumps indicates continual increase in lateral forces in the wheel and rail contact point without kick bounces and additional dynamic exciting of the vehicle mechanical system. This phenomenon is shown on the value of safety against derailment.

The size of instant equivalent conicity value is connected with the size of wavelength of periodic oscillation movement which a wheelset performs. A low conicity value presupposes a higher wavelength value. Sufficient wavelength size is extremely important for a high-speed railway operation. The size of equivalent conicity is projected into the stability of vehicle movement and riding comfort of passengers.

The determining value of equivalent conicity is stated at the movement amplitude of 3 mm.

Contact points distribution across the profile has a crucial influence on wearing (resistance against wearing) of wheel and material and at the same time the geometric stability of their profiles.

From the nature of the way of geometrical characteristic evaluation it is clear that it is not possible to suggest profile geometry directly on the base of contact points position setting. Various authors [1, 17, 20, 23] have applied various procedures where continual profile shape modification on the base of a geometric characteristic was the starting point.

5.2 Profiles creation method through arcs radii profile variation

We used the method of arcs radii profiles variation for the creation of new profiles which are suitable for the given criteria.

The base of the activity is an interactive attitude which is based on the modification of the original shape defined by parts of railway wheel profile with to each other linked exactly defined arcs radii which can be changed according to the need for the final geometric characteristics shape.

5.2.1 Arcs radii profile variation

The basic procedure is as follows:

1. We have the profile of the rail of UIC 60 1:40.
2. We have a requested shape of geometric characteristics: it is low equivalent conicity ≤ 0.05 in the given case.
3. We choose a "suitable" wheel profile: we will choose the up to now used profile of S1002.
4. We perform numerical division of the whole existing wheel profile in order to obtain simple geometric parts, (depicted in Fig. 4).
5. We create the radii function $R(y)$ (in dependence on the lateral wheel profile coordinate), (depicted in Fig. 5).
6. We set the starting conditions in the equation (10): in the given example, it is the first derivation = tangent value in the starting point = 0.05.
7. We change the selected radius (from the original S1002 profile radii) and compute the equation (3).

When the new profile is derived, the geometric characteristics are evaluated and the results are assessed. If the results meet our

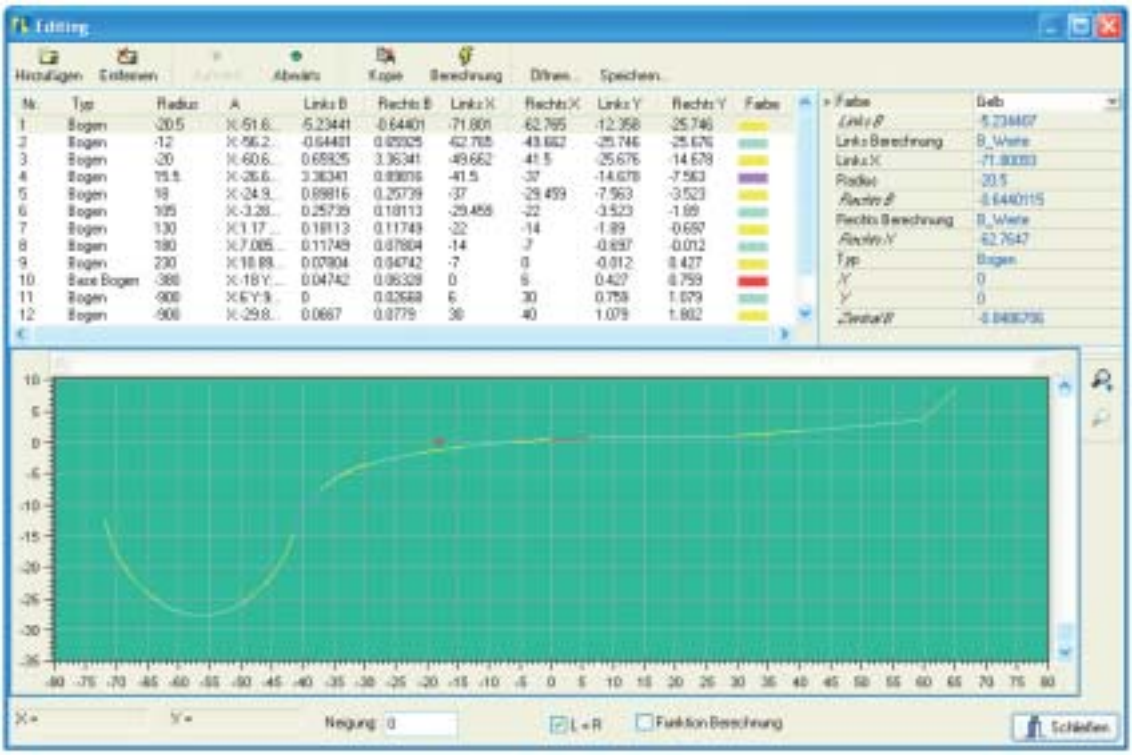

Fig. 4 Wheel geometry profile radii setting

expectations, the profile is accepted, if the results do not fulfill our expectations, the selected radius (radii) is (are) changed and computations have to continue. In this case, there is a need for knowledge and for experience and skills in the radius selection and radius value for the determination of the change.

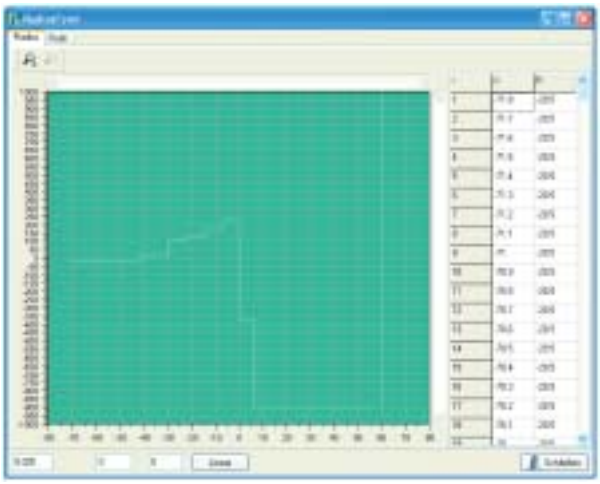

Fig. 5 Arcs radii values course of the suggested wheel profile

5.2.2 Profile creation on the base of the given functional dependence of radii depending on the coordinate y

Nyström method which is described in the relationship from 4 to 7 was used for the solution of the differential function (3) arising from the relationship for curvature. Its application for the solution of the function (3) is in relationships (8) and (9). The starting conditions are defined in the equation (10).

The radii function R depends on the lateral movement y, z is a vertical profile coordinate.

$$R = R(y) \tag{1}$$

$$\frac{1}{R(y)} = \frac{z''}{[1 + (z')^2]^{3/2}} \tag{2}$$

$$z'' = \frac{[1 + (z')^2]^{3/2}}{R(y)} \tag{3}$$

Basic relationships for the solutions of a differential function by Nyström method

$$k_1 = f(y_m, z_m, z'_m)$$

$$k_2 = f\left(y_m + \frac{h}{2}, z_m + \frac{h}{2} \cdot \left(z'_m + \frac{h}{4} \cdot k_1\right), z'_m + \frac{h}{2} \cdot k_1\right)$$

$$k_3 = f\left(y_m + \frac{h}{2}, z_m + \frac{h}{2} \cdot \left(z'_m + \frac{h}{4} \cdot k_1\right), z'_m + \frac{h}{2} \cdot k_2\right)$$

$$k_4 = f\left(y_m + h, z_m + h \cdot \left(z'_m + \frac{h}{2} \cdot k_3\right), z'_m + h \cdot k_3\right) \tag{4}$$

$$k = \frac{1}{6} \cdot (k_1 + k_2 + k_3) \tag{5}$$

$$k' = \frac{1}{6} \cdot (k_1 + 2 \cdot k_2 + 2 \cdot k_3 + k_4) \tag{6}$$

k_n are auxiliary variables for determination of profiles points vertical coordinate,
h is computational step, we used $h = 0.005$ mm.

$$y_{m+1} = y_m + h$$

$$z_{m+1} = z_m + h \cdot (z'_m + h \cdot k) \tag{7}$$

$$z'_{m+1} = z'_m + h \cdot k'$$

An application of Nyström method for the solution of the equation (3)

$$k_1 = \frac{[1 + (z'_m)^2]^{3/2}}{R(y_m)}$$

$$k_2 = \frac{\left[1 + \left(z'_m + \frac{h}{2} \cdot k_1\right)^2\right]^{3/2}}{R \cdot \left(y_m + \frac{h}{2}\right)}$$

$$k_3 = \frac{\left[1 + \left(z'_m + \frac{h}{2} \cdot k_2\right)^2\right]^{3/2}}{R \cdot \left(y_m + \frac{h}{2}\right)} \tag{8}$$

$$k_4 = \frac{\left[1 + (z'_m + h \cdot k_3)^2\right]^{3/2}}{R(y_m + h)}$$

The initial conditions:

$$z(y_0) = z_0$$

$$z'(y_0) = z'_0 \tag{9}$$

were specified in the following way:

$$y_0 = 0$$

$$z_0 = 0 \tag{10}$$

$z'_0 = tg$ profile tangent slope

The initial condition secures that the beginning of the profile coordinate system is placed in a horizontal direction into the plane

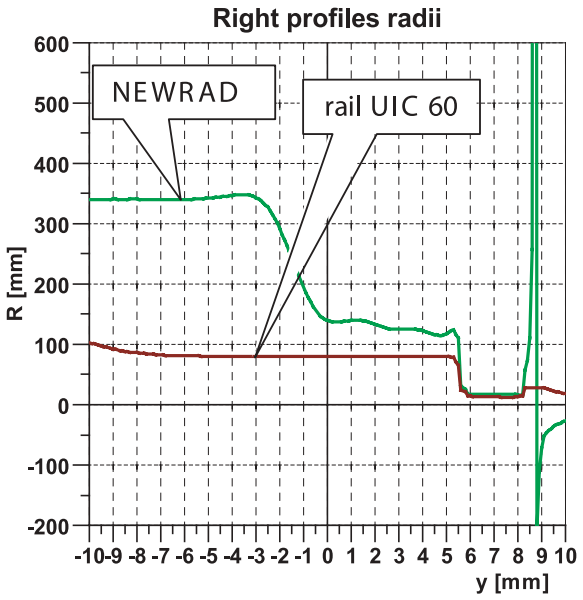

Fig. 6 Profiles radii NEWRAD and UIC60 at contact points

of the nominal wheel radii circle and the profile crosses the beginning.

The first z'_0 coordinate derivation determines the tangent value of the profile tangent slope in the point $[y_0, z_0]$. The profile is created by the solution of the differential equation (3) continually from the point $[y_0, z_0]$ to the left side and then from the point $[y_0, z_0]$ to the right side.

5.2.3 Results of application of the chosen method

The wheel profiles (NEWRAD) corresponding to our needs thanks to their properties were created on the base of the chosen input parameters at the defined optimizing criteria.

5.3 Arcs radii profile variation for the creation of an outer rail profile for a track in a left arc

It is possible to create a rail profile (NEWRAIL) in the similar way like the wheel profile (NEWRAD) was created. Let us suppose

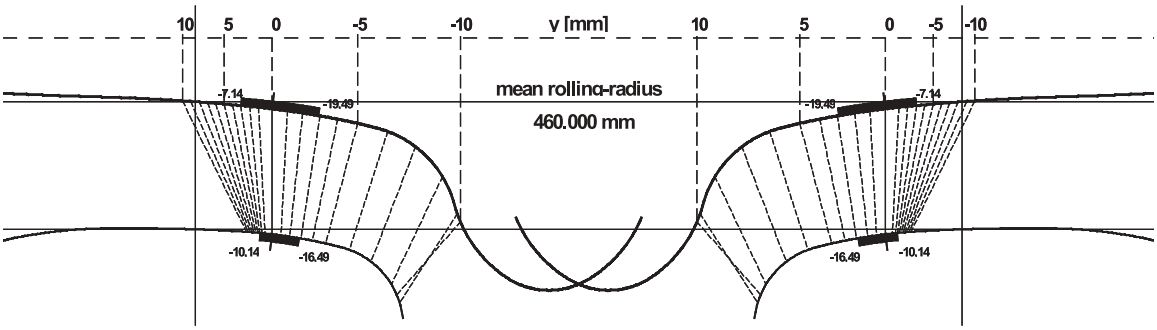

Fig.7 Contact points at profiles combination NEWRAD/UIC60/1:40/1435 with marking of contact points interval at a wheelset lateral movement in a rail with amplitude of 3 mm

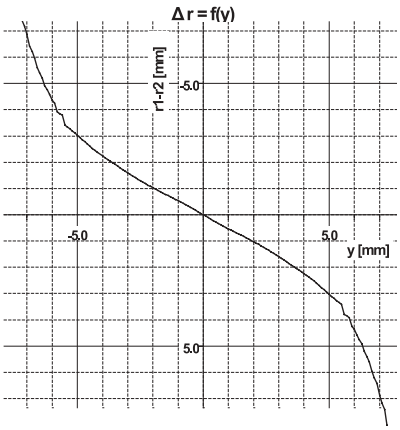

Fig. 8 Delta r function for the profiles combination NEWRAD/UIC60/1:40/1435

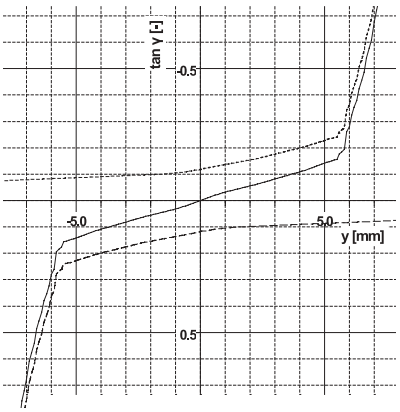

Fig. 9 Tangent gamma function for profiles combination NEWRAD/UIC60/1:40/1435

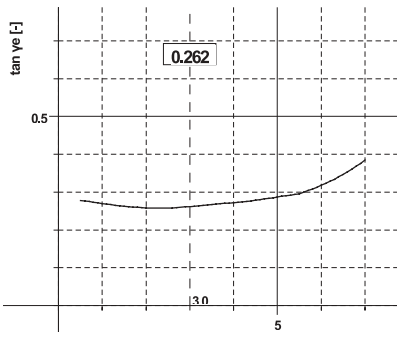

Fig. 10 Equivalent conicity function for the profiles couples NEWRAD/UIC60/1:40/920/1435

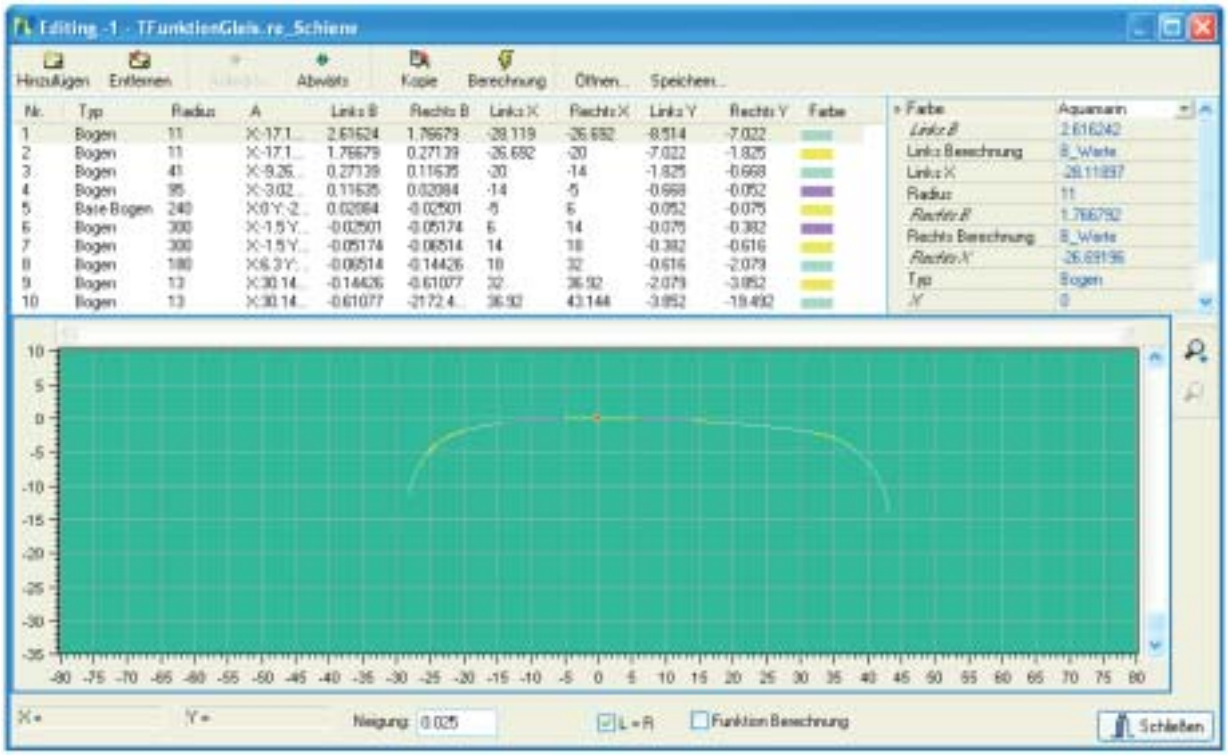

Fig. 11 Dialog window for geometry radii setting of separate rail profile parts

that it is necessary to create an outer rail profile for a track in a left arc in order to fulfil the basic criteria.

We require the following criteria for the new profile: fluent distribution of contact points at a wheelset lateral movement in a rail, no jump course changes of the difference delta r function, low equivalent conicity, the best possible wheelset kinematics movement ability even in the case of small arcs at a small lateral movement, exclusion of two-point-contact. The principal objective of the activity is similar to the one at the wheel profile, it is an interactive attitude based on the modification of the "original shape" which is defined by rail profile parts with to each other linked exactly defined arcs radii. It is possible to change the radii size according to the need of a final geometric characteristics shape. The basic profile is divided into parts with precisely defined geometry (radius). The radii function which is dependent on (see part 3) is created.

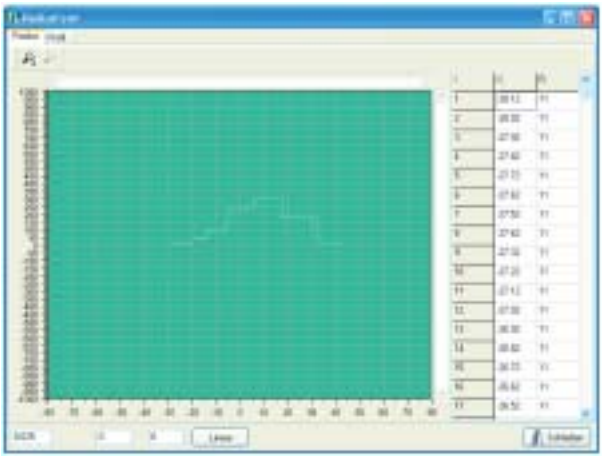

Fig. 12 Depiction of rail head profile arcs at contact points

We will modify the function. The differential equation (3) is solved. We set the initial conditions which place the profile into the beginning of the coordinate system and tilt it in this point according to our needs. We calculate the points position of the new profile. We calculate the geometric characteristics. If the shape of the characteristics is not suitable we modify the radii function and repeat the procedure.

INNERRAIL is an inner rail, NEWRAIL is an outer rail of the track. We suggest and analyse the profile for the outer rail.

It is clear from Fig. 17 that the wheel equipped with the S1002 profile can move in a kinematic way through the rail arc radii with an outer rail profile NEWRAIL with the value of approximately 600 m. This happens at the given configuration already at zero lateral displacement. It can move in a kinematic way through the radius smaller than 150 m at lateral displacement of 5 mm. It is not possible when combining the wheel profile S1002 and the profile UIC60 (Fig. 18).

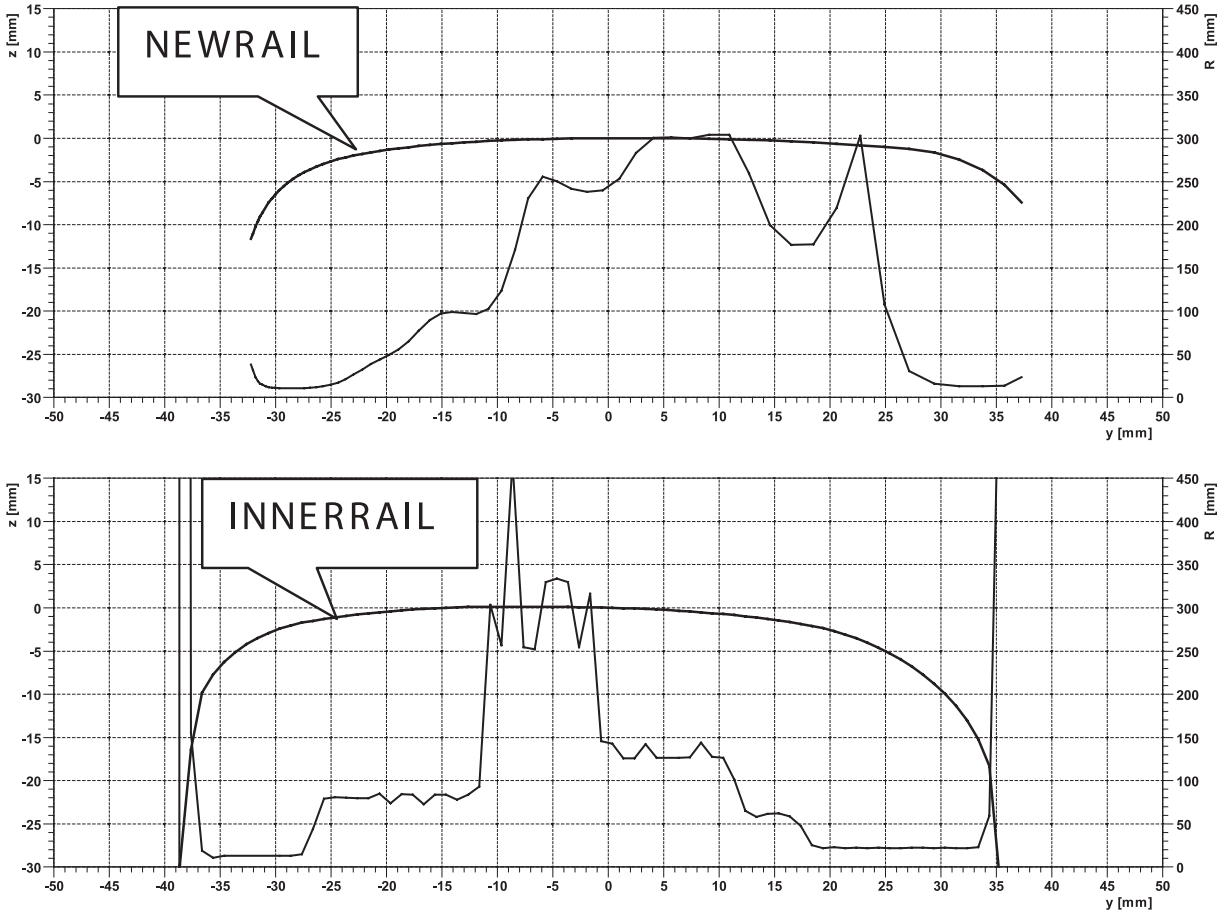

Fig. 13 Profiles and profiles radii NEWRAIL and INNERRAIL

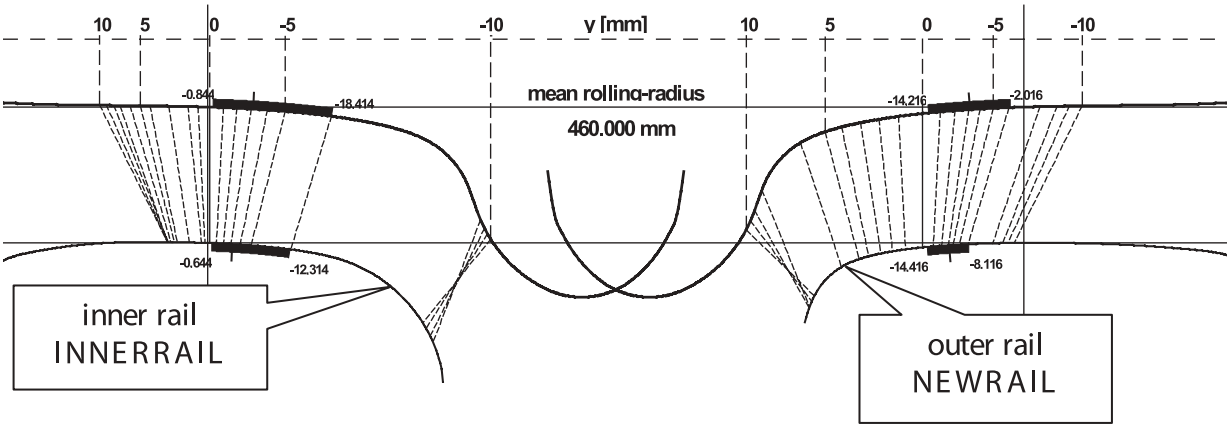

Fig. 14 Depiction of wheelset contact points with profiles S1002 and rails profiles INNERRAIL a NEWRAIL

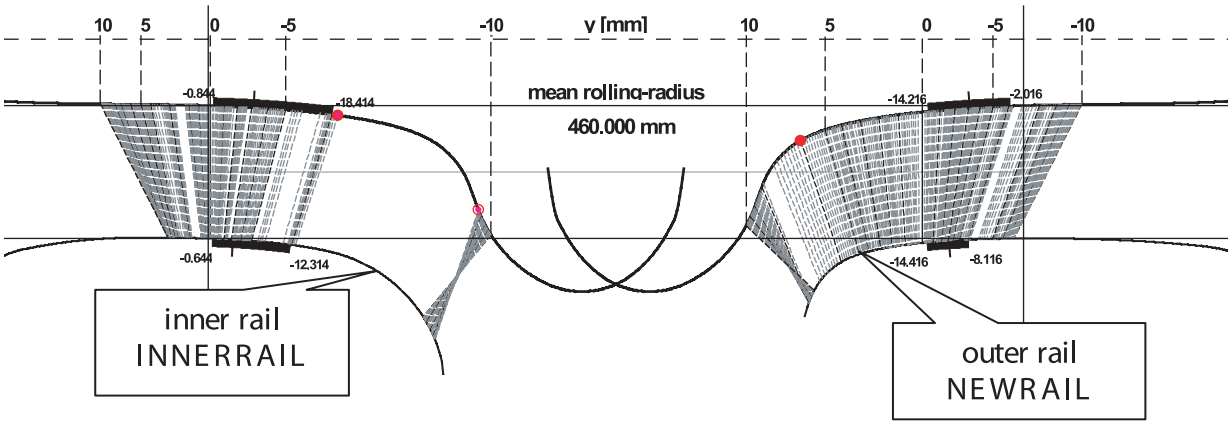

Fig. 15 Detailed view of wheelset contact points distribution with profiles S1002 and rail profiles

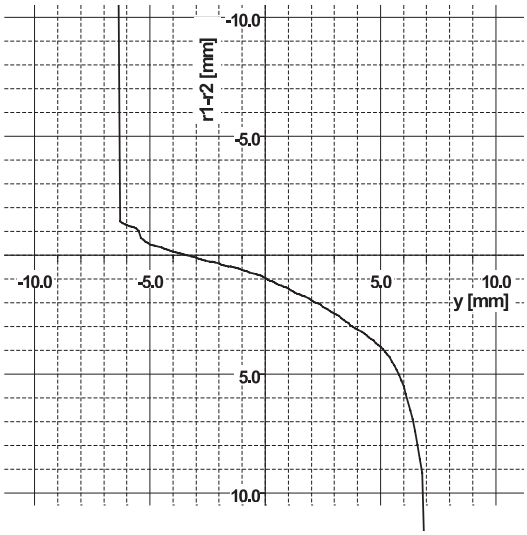

Fig. 16 Delta r function for the given profiles configuration

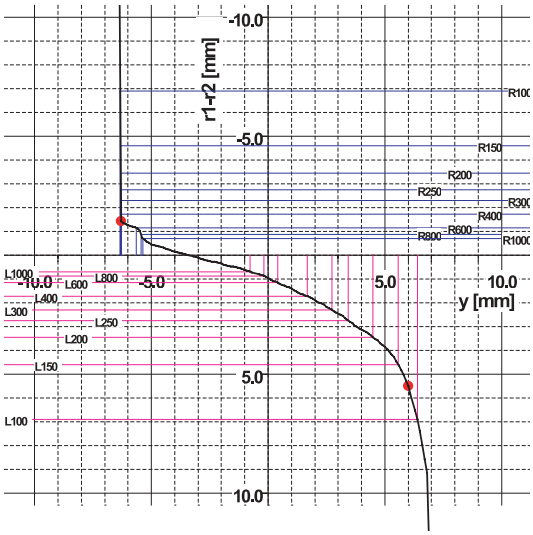

Fig. 17 Delta r function with marked radii for a kinematic movement through a track arc for the rail profile NEWRAIL and wheel profile S1002

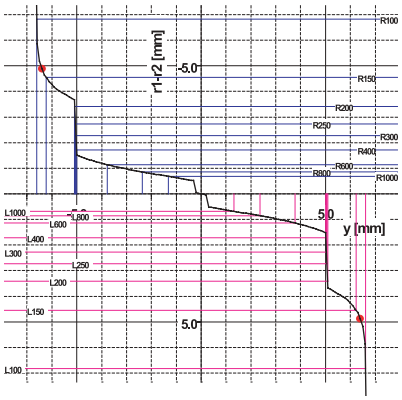

Fig. 18 Delta r function with marked radii for a kinematics movement through a track arc for the rail profile UIC60 and wheel profile S1002

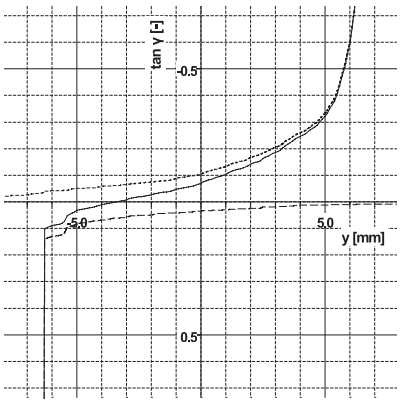

Fig. 19 Tangent gamma function for the given profiles configuration

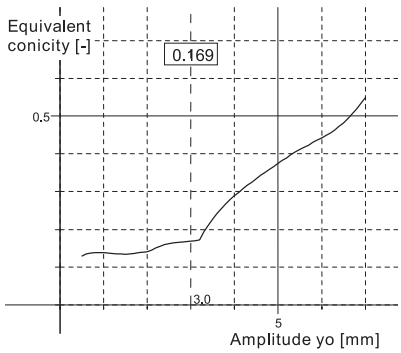

Fig. 20 Equivalent conicity

The tangent gamma function in Fig. 19, similarly like the delta r function, has the horizontal axis cross section point shifted against the beginning of the coordinate system.

6. Conclusions

The article deals with one of the ways of profile geometry design of the railway wheel and rail, or rail head profile on the base of the chosen criteria. On the base of the geometric characteristic shape definition we suggested a railway wheel profile shape (to the given rail profile) NEWRAD and a railhead profile shape (to the supposed railway wheel shape) NEWRAIL.

So from the above mentioned arises that the wheel profiles NEWRAD with characteristics according to Fig. 7–10 and the rail head profiles NEWRAIL with characteristics according to Fig. 14–20 (excluding Fig. 18) are the solution for the following criteria: fluent distribution of contact points at the wheelset lateral movement in a rail, no jump course changes of the difference delta r function, low equivalent conicity, the best possible wheelset kinematics movement ability even in the case of small arcs at a small lateral movement, exclusion of two-point-contact.

The profiles on the base of the assessed characteristics represent an approach to an optimum solution for certain presupposed operational conditions and required manner of vehicle running.

A profile with different geometry will be a result in a case of change of initial parameters which can be represented, for example, by a change of geometry of one from contact couple profiles or a change of vehicle operation manner (a need for different equivalent conicity).

Acknowledgement

The work was supported by the Scientific Grant Agency of the Ministry of Education of the Slovak Republic and the Slovak Academy of Sciences in Project No. 1/3169/06 "Properties Research of Rail Vehicles in Movement with Emphasis on the Solution of a Wheel and Rail Contact at the Wheelset Rolling in the Rail via Computer Simulation" and in Project No. 1/2116/05: "Interdisciplinary Solution of Modern Rail Transport Means by Usage of Virtual Models and Experimental Methods".

Translation: PaedDr. Marta Kadorová

References

[1] BERGANDER, B., DENDL, G., NEFTZGER, A., NICKLISCH, D.: *Die Entwicklung von Rad- und Schienenprofilen.* In: ZEVrail Glasers Annalen 127. Str. 482–503. Georg Siemens Verlagsbuchhandlung, 2003.

[2] BUßMANN, C., NEFTZGER, A.: *Die Entwicklung von Schienenprofilen unter dem Einfluß von Verschleiß und die Auswirkungen auf das quasistatische Kurvenlaufverhalten eines Fahrzeuges.* In: VDI Berichte NR.820, Systemdynamik der Eisenbahn, 1990.

[3] GERLICI, J., LACK, T.: *Railway wheel and rail geometry influence on ride properties of the vehicle. (In Slovak)* 16. International conference "Current problems in rail vehicles – PRORAIL 2003", EDIS – Publishing house of University of Žilina, 2003.

[4] GERLICI, J., LACK, T.: *Railway wheelset and track contact. (In Slovak)* Monograph, p. 200, ISBN 80-8070-317-5, EDIS – Publishing house of University of Žilina, 2004.

[5] GERLICI, J., LACK, T. at.: *Transport Means properties Analysis. Vol. I.* Monograph, p. 214, ISBN 80-8070-408-2. EDIS – Publishing house of University of Žilina, 2005.

[6] GERLICI, J., LACK, T., KADOROVÁ, M.: *Calculation of the Equivalent Conicity Function with a Negative Slope.* Communications – Scientific papers of the University of Žilina, 2/2004, pp. 49–56, ISSN 1335-4205, EDIS – Publishing house of University of Žilina, 2004.

[7] HAYASHI, T, TOYAMA, M., HINO, K., ISA, M.: *Development of wheel tread nicknamed "CS Tread" for narrow gauge lines.* In: World congress on railway research Tokyo, Japan. Pp. 195–198., 1999.

[8] IZER, J.: *Effective and equivalent conicity of the wheel tread profile of railway wheelset. (In Czech)* In: PRORAIL'95 Current problems in rail vehicles. VŠDS Žilina, 1995.

[9] LACK, T., GERLICI, J.: *Contact area and normal stress determination on railway wheel / rail contact.* Communications – Scientific papers of the University of Žilina, 2/2005, pp. 38–45, ISSN 1335-4205, EDIS – Publishing house of University of Žilina, 2005.

[10] LACK, T., GERLICI, J.: *Profiles synthesis through radii variation of arcs profile. (In Slovak).* Current problems in Rail Vehicles. Pp. 115–135. ISBN 80-7194-780-6. DFJP UP, DP Česká Třebová 2005.

[11] LEHNA, H., THEILER, A.: *Radprofiloptimierung bei der Verkehrsbetrieben Zürich. (2003)* In: Rad Schiene. Pp. 42–50. 6. Internationale Schienenfahrzeugtagung, Dresden, 2003.

[12] MÜLLER, R.: *Die Problematik der Berührungsgeometrie Rad/Schiene.* In: ZEV+DET Glas. Ann. 118, 3 März, Georg Siemens Verlagsbuchhandlung, 1995.

[13] MÜLLER, R.: *Zusammenwirken von Rad- und Schienenprofilen.* In: Rad Schiene 2003. Pp. 30–34. 6. Internationale Schienenfahrzeug-tagung, Dresden, 2003.

[14] NEFTZGER, A.: *Geometrie der Berührung zwischen Radsatz und Gleis.* ETR – Eisenbahntechnische Rundschau, DK 681.938:625.1/.2.031.3, Heft 3. Pp. 113–122, 1974.

[15] PREN 13715:1999, *Bahnanwendungen, Radsätze und Drehgestelle, Räder - Radprofile.* Deutsche Fassung prEN 13715:1999.

[16] RIEČANOVÁ, Z. AT AL.: *Numerical methods and mathematical statistics. (In Slovak).* University textbook. 063-559-87 NMA. Alfa Bratislava, 1987.
[17] SASAKI, K., KAGEYAMA, K., ASANO, K., OKUMURA, M.: D*evelopment of the wheel tread profile for commuter train (Investigation of the wear profile of the wheel tread and the rail head. (2000)* In: Proc. the 5-th International Conference on Contact Mechanics and Wear of Rail/Wheel Systems CM2000 (SEIKEN Symposium No. 27), pp. 265–270, Tokyo.
[18] SÁGA, M., LETRICH, M., KOCÚR, R.: *An Analysis of Vehicle Vibration with uncertain system parameters.* Communications – Scientific papers of the University of Žilina, 1/2005, pp. 16–21, ISSN 1335-4205, EDIS – Publishing house of University of Žilina, 2005.
[19] SCHEUNEMANN, E., KOLBE, T., MÜLLER, R.: *Geometrie Rad /Schiene, ein gemensames Thema für Fahrzeug und Fahrweg.* In: ZEV+DET Glas. ZEVrail Glasers Annalen 129, Tagungsband SFT Graz 2005. Pp. 168–189. Georg Siemens Verlagsbuchhandlung, 2005.
[20] SHEN, G., AYASSE, J., B., CHOLLET, H., PRATT, I.: *A unique design method for wheel profiles by considering the contact angle function.* In: Proc. Instn. Mech. Engrs. Vol 217 Part F.: J. Rail and Rapid Transit. F01902, pp. 25–30. IMechE, 2003.
[21] UIC CODE 519: *Method for determining the equivalent conicity. (2003)* Draft of January 2003 Original version, 2003.
[22] UIC-KODEX 510-2 VE: *Wagen. Bedingungen für die Verwendung von Rädern verschiedener Durchmesser in Laufwerken unterschiedlicher Bauart.* 4. Ausgabe. Übersetzung, Oktober 2002
[23] WALENTA, R., HAIGERMOSER, A.: *Berührungsgeometrie von Rad und Schiene. Neue Methoden zur Untersuchung und Optimierung.* In: ZEV+DET Glas. Ann. 121 (1997) Nr. 2/3 Februar, Georg Siemens Verlagsbuchhandlung, 1997.

Peter Horbaj – Jozef Víglaský – Dušan Mikolaj *

COOLING WORKING ROLLS OF THE FINISHING SECTION OF WIDE-STRIP HOT ROLLING MILLS

The contribution deals with heat nucleation in rolling on the hot wide strip mill as well as into following transfer to the rolls without friction heat being involved. This work has resulted in the computer program owned by author. It represents the most accessible computer technique and the dependence of the accepted heat amount on the revolutions and angle of bite, as well as the dependence on the temperature of the roll surface which may participate in the initiation and widening of the surface friction coefficient and roll stand sequence.

Key words: *cooling working rolls, finishing section, wide strip, hot rolling mills*

1. Introduction

Due to the stringent demands on the quality of rolled sheets it is necessary to gradually modernise rolling trains. An important role in every rolling mill train is played by the working rolls whose quality also determines the final quality of products, their cost and output of the rolling mill train. The finishing lines of the wide-strip rolling mill trains consist of six-seven stands. In the pass, the finishing line used cast iron rolls with a non-specified hardened working layer. The use of these rolls had a number of disadvantages [1], [2]:

- high specific consumption of rolls per unit mass of rolled material;
- reduced hardness of the surface of the body of the roll and associated negative effect on the dimensions and surface quality of the rolled strips.

Because of this it was necessary to find and use rolls of higher quality. The cast iron rolls with the hardened layer were replaced by centrifugally cast rolls with a higher chromium content.

2. Cooling working rolls

After introducing the rolls it was necessary to pay special attention to cooling the rolls. This is associated with utilisation of theoretical information on heating and cooling the rolls and practical experience obtained in operation with them. The need to examine this problem is also indicated by the fact that these rolls are subjected to high demands caused by changes in the thermal-physical properties in comparison with the cast iron rolls with a non specified hardened layer.

The surface temperature of the roll is an important quantity in cooling the rolls which influences the deformation of the working rolls, their wear and quality of the surface, as well as dimensions and quality of the surface of rolled strips. According to service experience obtained in rolling mill trains using rolls with a high chromium content, the surface of the roll is not excessively damaged by cracks formed under the effect of heat if the surface temperature of the roll does not exceed 60°C in removal from the stand. Regardless of this fact, this temperature cannot be regarded as an absolute value. Concerning continuous welding process the extent of temperature variations decreases and the temperature of the roll increases. As a result of a reduction of the temperature variations, the thermal shock to which the working rolls are subjected decreases. Practical experiences show that temperature variations have far worse consequences for damaging the surface of the roll than the roll temperature.

'The cooling of the rolls is also significantly influenced by the amount and pressure of cooling and the position of collectors. The majority of rolling mill trains use a large number of high-pressure spraying nozzles for cooling the working rolls. These nozzles are installed in the so-called cooling connectors. However, incorrect application of the high-pressure nozzles may limit the cooling effect of water. To obtain the most effective cooling effect, the pressure and the angle of the cooling jet should be selected in such a manner as to avoid reflection of water droplets with a high energy from the surface of the roll. This would reduce the contact time of cooling water with the surface and, consequently, reduce the cooling effect The nozzles distributed in a relatively stable position form different cooling zones on rolls with different diameters because the distance between the nozzles and the cooled surface of the roll changes.

The highest temperature of the working roll is recorded in the area of contact with the strip. In this zone, higher temperatures are found only in a very thin layer. It is therefore essential to ensure that the heat received by the roll from the strip is removed as soon

* **Peter Horbaj[1], Jozef Víglaský[2], Dušan Mikolaj[1]**
[1]Faculty of Mechanical Engineering, Technical University in Košice, Vysokoškolská 4, 04200 Košice, Slovak Republic, E-mail: peter.horbaj@tuke.sk, dusan.mikolaj@tuke.sk,
[2]Faculty of Environmental and Manufacturing Technology, Technical University in Zvolen, T. G. Masaryka 24, 960 53 Zvolen, Slovak Republic, E-mail: viglasky@vsld.tuzvo.sk

as possible, i.e., immediately after the completion of contact between the roll and the strip. The heat received by the roll must be removed to avoid its further penetration into the roll. This can be ensured by correct distribution of the cooling collectors. In many cases, even if the pressure conditions are maintained and the amount of cooling water is sufficient, with the correct distribution of collectors, rolls in certain stands of the finishing line can be overheated, i.e. the surface temperature exceeds the allowed value. This results in insufficient cooling which requires detailed analysis of the thermal processes taking place during cooling of the rolls.

In cooling the rolls it is necessary to take into account the fact that the amount of heat received by the roll from the strip must be equal to the amount of removed heat. If this equilibrium is disrupted, i.e., if the amount of removed heat is lower, heat would build up in the roll and, in the final analysis, the roll temperature would increase.

In analysing the amount of heat received from the surface it is necessary to take into account the following heat sources and solutions of the equations, Fig. l:

1. The equation of heat conduction in the roll.
2. The equation in of heat conduction in the strip which takes into account the development of heat caused by plastic deformation.
3. The equation of heat conduction through the oxidation film existing between the roll and the strip-takes into account heat caused by friction.

For different rolling conditions we calculated the transfer of heat to the roll which does not include the friction heat [3]. The basis for compiling the mathematical model of the temperature field of the roll in hot rolling is the differential equation of heat conduction in the roll:

$$\frac{\partial^2 \Theta(\rho, \varphi, Fo)}{\partial \rho^2} + \frac{1}{\rho};$$

$$\frac{\partial \Theta(\rho, \varphi, Fo)}{\partial \rho} + \frac{1}{\rho^2} \cdot \frac{\partial^2 \Theta(\rho, \varphi, Fo)}{\partial \varphi^2} = \frac{\partial \Theta}{\partial Fo} \qquad (1)$$

In solving equation (1) it is necessary to know the initial and boundary conditions:

- *initial condition*

$$\Theta = \Theta_0 \quad \text{for} \quad Fo = 0$$

- *boundary conditions*

$$\Theta = \Theta(\varphi) \cdot e^{i.Pd.Fo} \quad \text{by} \quad \rho = 1 \qquad (2)$$

$$\Theta(\rho, \varphi, Fo) = \Theta[\rho, (\varphi + 2k \cdot \pi), Fo] + K \cdot \Delta t \qquad (3)$$

where exponent i is an argument which expresses the complexity and periodicity of the boundary conditions. The first term on the right hand side of the equation (3) represents the periodicity of the function and the second term the temperature increase on the surface as a result of deformation.

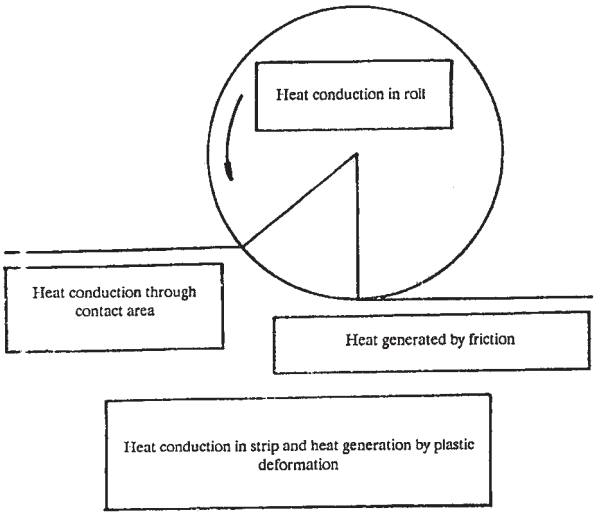

Fig. 1 Heat sources

The constant K can be determined by means of experiments. The value Δt expresses the temperature increase during deformation. At 700–1300 °C the deformation energy is completely transformed to thermal energy. The increase of the energy of the stressed state can be regarded as negligible. The value Δt is determined from (4):

$$\Delta t = \frac{p_s \cdot \ln h_{i-1}/h_i}{c_k \cdot \rho_k} \qquad (4)$$

where the values of the mean deformation resistance p_s for different stands in the line, for different diameters of the working rolls, for different revolutions of the working rolls and different temperatures can be found in the literature [4].

Figure 2 shows the diagram of distribution of the boundary conditions on the surface of the upper working roll. In the zone of contact between the roll and the rolled strip φ_1 the temperature on the surface of the roll is equal to the strip temperature t_p. In the cooling zone φ_3 the temperature is determined by the temperature of cooling water t_v. In the zones φ_2 and φ_4 it can be assumed that the surface is insulated from water with wipers. During rolling the roll rotates at the angular speed ω_0 and, consequently the equation (1) must be solved for the rotating system. The differential equation (1) together with the unambiguity conditions (5) and (6) makes it possible to obtain a solution describing the radial non stationary temperature field of the rotating roll.

Fig. 3 shows the distribution of the boundary conditions of the surface of the rotating roll with the angular speed ω_0. The vertical axis gives the temperature distribution Δt which varies from t_o to t_p. In the zone of angle φ_2 the temperature decreases exponentially. In the zone of angle φ_3 the roll is cooled with water at such a rate that the surface temperature of the roll can be regarded

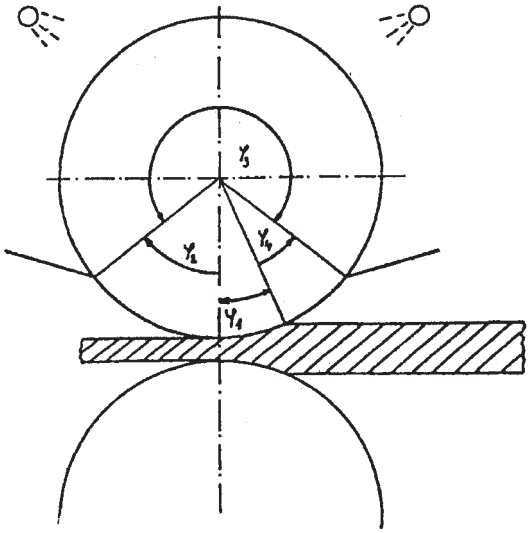

Fig. 2 Distribution of boundary conditions on the surface of the working roll

as equal to the temperature of the cooling water. In the zone φ_4 the temperature of the surface exponentially increases, as in the zone φ_2. As a result of transformation of the equations, the final equation of the amount of heat received in the strip by the two rolls has the form:

$$Q(\varphi_0) = 2\lambda \cdot b \cdot \sqrt{Pd}\,(tp - \bar{t}) \cdot \left(\varphi_1 + \frac{\varphi_2}{2}\right) \qquad (5)$$

In the quasistationary conditions, the amount of heat supplied to the rolls is equal to the amount of heat taken away during a single revolution:

$$Q(\varphi_0) = Q(\varphi_m)\,. \qquad (6)$$

The area $S_1 + S_2$ in Fig. 3 corresponds to the supplied heat and $S_3 + S_4$ to the heat removed.

On the basis of the above results we compiled a program for calculating the amount of received heat in different rolling conditions. Fig. 4 and 5 show the dependence of the amount of received heat for the finishing line of the wide-strip hot rolling mill train. The amount of received heat was calculated on the basis of the our programme "Calculation of heating of rolls"[1]. Fig. 4 can be used to compare the amount of received heat for different revolutions in the individual stands. The graph indicates clearly the degree of loading of the individual stands. Fig. 5 shows the dependence of the amount of heat on the angle of engagement. This heat does not yet include the friction heat.

Fig. 6 shows the distribution of the surface temperature of the rolls in relation to the friction heat which is proportional to the rolling speed. An increase of the temperature of the finishing line is caused by the formation of heat as a result of friction due to higher rolling speeds. In higher loading of the mills, *A* (high rolling speed), the curve increases above the optimum temperature of the surface

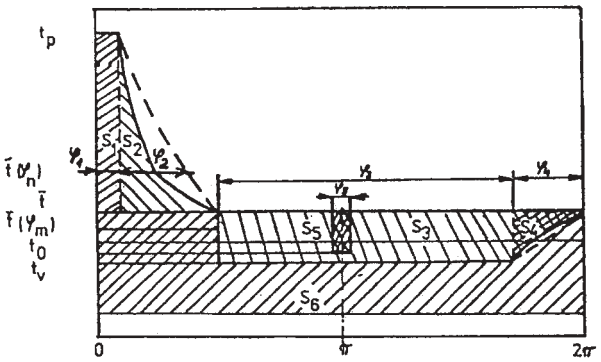

Fig. 3 Distribution of boundary conditions on the circumference of the roll

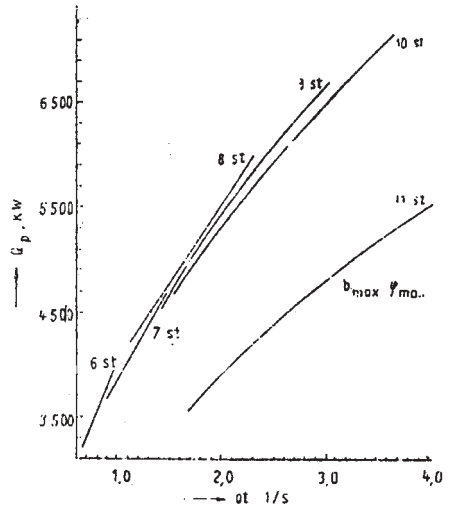

Fig. 4 Dependence of the amount of received heat on revolutions

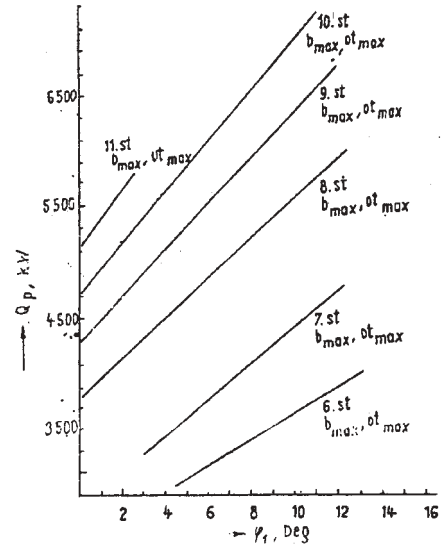

Fig. 5 Dependence of the amount of received heat on the angle of engagement

of the rolls and the rolls can be subjected to a considerable risk of damage in comparison of the values obtained under the normal rolling conditions, *B* (normal rolling speed) [5]. The optimum surface temperature of the roll is represented by the value specified by the manufacturer.

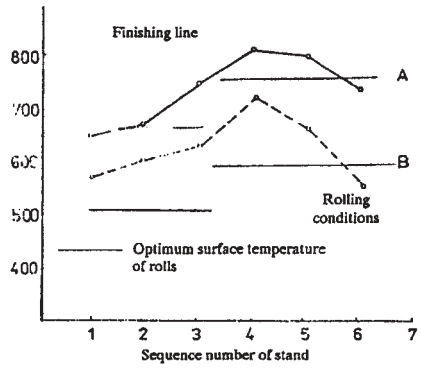

Fig. 6 Dependence of the surface temperature of rolls on the rolling speed in the individual stands of rolling trains

Fig. 7 shows the dependence of the maximum surface temperature of the roll on the friction coefficient at different rolling speeds. As indicated by Fig. 7, the friction coefficient determined from the literature data, for example [6], has strong effect on the surface temperature of the roll.

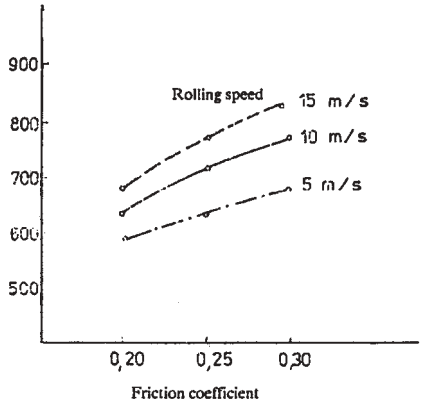

Fig. 7 Dependence of surface temperature on friction coefficient

3. Conclusion

The following conclusions can be drawn:

- Special attention must be given to the thermal loading of the individual stands of the finishing lines of the wide – strip hot rolling mills (it is necessary to take into account all heat sources which change in relation to different rolling conditions);
- It is necessary to consider the pressure conditions and the distribution of cooling water supplied to the individual rolls of the finishing line as well as the distribution of water at the inlet and outlet for the individual stands;
- Special attention must be given to the risk of overheating the rolls in service in the rolling conditions in which the individual stands are subjected to the maximum loads. In the future it would be necessary to examine new systems of cooling the rolls in the finishing line, for example, cooling by means of the water wall, or water with a low pressure using collectors with a slit along the entire width. Water is then trapped at a low energy and the water film should remain on the surface curve as long as possible [7] and [8].

In conclusion it can be said that to propose suitable conditions of cooling the individual stands, the calculations must be supplemented by the amount of heat formed under the effect of friction in relation to the rolling speed and the friction coefficient.

After determining this heat it will be necessary to determine accurate conditions of cooling which ensure sufficiently effective cooling of the rolls [10, 11, 12, 13].

Symbols:

$\Theta(\rho, \varphi, Fo)$ – relative temperature $\Theta = t - t_{min} / t_{max} - t_{min}$
$t(\rho, \varphi, Fo)$ – surface temperature of the roll
$\rho = r / R$ – relative dimensionless radius
R – roll radius, $0 \leq \rho \leq 1$
$Fo = a \,.\, \tau / R^2$ – Fourier criterion
$Pd = \omega_0 \,.\, R^2 / a$ – Predvoditelev's criterion
a – heat conductivity coefficient, $m^2.s^{-1}$
b – the width of rolled strip, m
c_k – specific heat capacity of the material, $kJ.kg^{-1}.K^{-1}$
h – the thickness of the rolled strip, m
h_i – the thickness of the rolled strip after *i*-th pass, m
h_{i-1} – the thickness of the rolled strip after *i*-1-th pass, m
p_s – mean deformation resistance, Pa
t_P – strip temperature, °C
t – mean temperature in the range $\varphi_m = \varphi_3 + \varphi_4$, °C
Δt – temperature increase in deformation, °C
λ – heat conductivity coefficient, $W.m^{-1}.K^{-1}$
ρ_k – density of material, $kg.m^{-3}$
τ – time, s
ω – angular speed, s^{-1}

Acknowledgements

This research has been sponsored by the grant from the Scientific Grant Agency of Ministry of Education of the SR and Slovak Academy of Sciences, under the contracts No. 1/1105/04 VEGA "Research effect of composition of biogas, sludge gas and landfill gas on operating characteristics of a cogeneration unit", as well as Dutch-Slovak project PSO 98/SK/2/16 "Replacement of brown coal fired boilers by a biomass-fired boiler at the School Forest Enterprise of TU in Zvolen".

The authors are greatly indebted to the mentioned institutions for sponsoring this research work.

Reference

[1] ČIŽMÁR, J., HORBAJ, P.: *Cooling working rolls of the finishing section of wide-strip hot rolling mills (in Slovak),* Hutnícke listy, 54/1990, No. 9, pp. 639–644
[2] NOVÁK, J., PAVLENKO, S.: *Automation of pipeline energetics systems component manufacturing.* In: Automation 2001, Warszawa, Poland, March 2001, pp. 75–82
[3] SHICKOV, A. N.: *Temperature conditions in sheet rolling rolls (in Russian)*, Verlag Leningrad University, Leningrad, 1974
[4] RAUDENSKÝ, M.: *Simulation of thermal processes in products of hot rolling (in Czech)*, Hutnícke listy, 52/1988, No. 9, pp. 623–626
[5] OSAMU, K. et. al.: *Relation between Calculated Surface Temperature and Deteration of Hot Strip Work Rolls,* Transaction of the Iron and Steel Institute of Japan, No. 12, 1980
[6] *Cooling Water Volume of Hot Strip Mill Finishing Stands.* Report on Hot Strip Mills in the USSR and other industrial countries, VSŽ a.s., Steelworks, Košice, 1987
[7] ANDREJČÁK, I., MOLNÁR, V.: *Technology of pressurized casting (in Slovak),* ES FVT Prešov, pp. 71, ISBN 80-7099-419-3
[8] KIZEK, J., LAZIČ, L.: *Simulation method for optimization of a mixture of fuel gases.* Metalurgija, 38/1999, No. 2, pp. 109–113
[9] VÍGLASKÝ, J.: *Technical-economic evaluations of solar air collector application at a sawn timber kiln (in Slovak),* TU Zvolen, Report No. 02-522-804/3, 1989, p. 53.
[10] RUŽINSKÁ, E.: *The modificated Black Liquors for Preparation of perspective Wood-based Composite Materials.* Proceedings from 7th International Scientific Conference „CO-MAT-TECH". STU MTF in Trnava, 1999, pp. 170–175.
[11] RUŽINSKÁ,E.: *A Perspective Wood-based Composite Materials. Part I.: Study of Preparation and Evaluation of Selected Properties of Adhesive Mixtures.* Proceeding from 4th International Scientific Conference „Wood and Fire Safety". Štrpské Pleso - Patria, 2000, pp. 297–304.
[12] RUŽINSKÁ, E.: *Effective Utilization of Kraft Black Liquors for Wood-based Composite Materials.* Proceedings from 13th International Conference "Pulp & Paper 2002". Brno, 2002, CD, 6 p.
[13] RUŽINSKÁ, E.: *Thermal characteristics of Modified Kraft Black Liquors and Sulphate Lignins. Part I. Thermogravimetry (TG, DTG).* Proceedings from international conference "Fire Engineering 2002". Lučenec, Hotel Reduta, 2002, pp. 337–340.

Jozef Blaho – Jozef Víglaský – Peter Horbaj *

OLDER LOW-EFFICIENT BOILERS BROWN COAL-FIRED, GENERATED EMISSIONS AND DIFFUSION OF IMISSIONS

At thermooxidizing processes generating energy from natural solid fuels, heat as its main product is accompanied with side products – solid waste and emissions, resulting in unfavourable effects on the environment. This contribution deals with the results of measurements and analyses regarding an old-fashioned type boiler unit fired by solid fuel. It showed low efficiency of older brown coal fired boilers currently used in many small companies. All of them generate pollutants - gaseous as well as solid emissions polluting the environment. Thus, they cause environmental damage in spite of their meeting emission and imission limits within their category. The imission value of tar component at low temperature of flue gases in fireplace and short time of flue gas remaining in fireplaces causes the presence of some components over the permissible imission limit.

Key words: emissions, imissions, brown coal, solid fuel-fired small-size boilers

1. Introduction and background

In spite of significant accomplishments that were achieved in the reduction of emissions and imissions in Slovakia during the last decade, there are still many small and midsize sources of emissions that abundantly contribute to the environmental pollution. It is especially old fired heating equipment fuelled with fossil fuels mainly occurring in villages that are not gas connected, but heated by old boilers fuelled with fossil fuels with the heat capacity up to 2 MWth. According to the legislative statutes [1, 2], small sources of pollution do not have determined exact emission limits. That is why entrepreneurs, mainly physical persons, are not obliged to respect certain rules while building such appliances and are not even fined for the air pollution. Midsize sources with lower capacity – up to 2 MWth have only limited concentrations of sulphur and nitrogen oxides, while sulphur oxides are limited by the concentration of 2500 $mg.m^{-3}$ only under those circumstances when emission flow of sulphur oxides is above 20 kg an hour, which is not reached by these kinds of appliances. The emission limit of nitrogen oxides in this category of combustion appliances is 650 $mg.m^{-3}$, which is difficult to achieve because with this pollutant, the concentration in the combustion products is quantitatively dependent either on the temperature that is measured in the combustion chamber of the boiler, or on the content of fixed organic nitrogen in the fuel. To create nitrogen oxides from the air by oxidation of the airborne nitrogen are, as a rule, needed temperatures over 1100 °C. However, this temperature cannot be achieved while using small sources fuelled with fossil fuels and smaller boiler units of older types with the heat capacity up to 2 MW. It happens where combustion products from the combustion area usually flow through the flue or directly through the combustion pipe into the chimney. That is why nitrogen oxides in the combustion products whose temperature in older appliances is below 800 °C do not originate from the airborne nitrogen but from fuel only. Nitrogen in fossil natural fuel can be found especially in heterocyclic components of compounds and also in wood as proteinaceous residues and amino derivative polysaccharides. There is about 0.7 % of nitrogen in wood, while the occurrence of nitrogen in coal is more variable, usually a bit higher, however, it depends on the locality of mining. That is why the content of nitrogen oxides in the combustion products of coal is usually higher than in the combustion products of wood. The low temperature of the combustion process as well as a short time of flue gas remaining during the combustion of the fossil fuels in the chamber, cause a defective combustion of the gassed fuel. This will result in poor quality of combustion products which can even be visually seen as the presence of a higher portion of soot in combustion products that escape through the chimney into the air, or particularly when analytically evaulating combustion products components. Gaseous combustion products from organic nitrogen are found as nitrogen oxide if the temperature is low. Oxidation of nitrogen oxide materialises only in the atmosphere.

In particular, it is pointed out that there are inappropriate conditions for inlets of primary and secondary air into firing space with regard to the amount of gasified fuel. Inflow of air and directions of its flow are also important. Poor mixing gases in the firing space causes inappropriate combustion, which will give a high content of carbon monoxides as well atmospheric oxygen in different locations of the firing space. At the older low-efficient boilers there is a characteristic short flow distance of combustion gases in the firing

* **Jozef Blaho[1], Jozef Víglaský[2], Peter Horbaj[3]**
[1]Faculty of Ecology and Environmental Sciences, Technical University in Zvolen, Kolpašská 9 B., 969 01 Banská Štiavnica, Slovak Republic, E-mail: blaho@vsld.tuzvo.sk
[2]Faculty of Environmental and Manufacturing Technology, Technical University in Zvolen, T. G. Masaryka 24, 960 53 Zvolen, Slovak Republic, E-mail: viglasky@vsld.tuzvo.sk
[3]Mechanical Engineering Faculty, Technical University in Košice, Vysokoškolská 4., 042 00 Košice, Slovak Republic, E-mail: peter.horbaj@tuke.sk

space, which results in influencing also its good mixing with air in the firing space. It results in a low thermal efficiency, but also in reduced heating value.

Relatively low temperature of fuel gasification as a short time of gassed products remaining in combustion area cause defective combustion. Resulting in dark smoke during such combustion conditions will cause following reactions: there will be an emission of inorganic residues (in the combustion area) along with condensed aromatic organic compounds, often with the content of fixed oxygen that make these inorganic residues visually black. The chemical structure of these substances is very various and also changeable (it depends on conditions of combustion process and combusting fuel) and they are called tarry substances. Many of them belong amongst persistent organic compounds (POC) that are distinguished for their longevity in the atmosphere and their physiological influence on living creatures, also plants and animals is often considered as a carcinogenic, mutagenical, or teratogenic one.

2. Materials and methods

Some measurements were undertaken to find out combustion products and their diffusion into the atmosphere from an operation of a boiler unit VSB-4 made in ŽD Bohumín in 1972 with a capacity of 0.25 MWt per hour, working under usual conditions. There is a combustion product ventilator installed in this boiler that is normally used for inundating. The ventilator was not operating during the measurement of the combustion products. During the measurement of emissions and also at usual operation which is carried out only during the winter heating, brown coal type O_2E with a content of ash 12.5 % and sulphur up to 1 % was used.

The measurement was carried out in a walled flue pipe and places of the measurement were determined according to the rules of STN ISO 10 780 [5] and STN ISO 9096 [6]. The flow of the combustion products was calculated from measured physical quantities (dynamic, static and atmospheric pressures, temperature of the combustion products) by Pitot-Prandtl tube and digital micromanometre and density of the combustion products was calculated from the chemical structure of the combustion products (containing oxygen, nitrogen and carbon dioxide, or water vapour). Concentration of combustion gases was calculated from the chemical composition of combustion gases (content of oxygen, nitrogen and carbon dioxin, or water steam).The concentrations of oxygen and carbon oxide were determined by a gas analyser FY IMR 1200 with electrochemical sensors, while carbon dioxide was deducted by analogy. The sulphur oxides were determined by the classical method after sampling into 3 % hydroperoxide according to STN 83 4711 [9]. The sample of fossil pollutants was taken by Ströhlein apparatus STG 4E and determined by the gravimetric method according to [6]. The qualitative characteristics of fossil emissions was done by determination of a soluble portion of fossil elements in carbon disulphide and the consequential analysis were determined by the gaseous chromatography method of dividing on a capillary column of medium polarity. The programmed change of column temperature was used for separation. The graphic record is presented in Figure 1.

The diffusion of a few volatile organic components (VOC) from a defective combustion of coal was determined according to Szabu programme MODIM 1.20 d [12].

Within Szabu programme MODIM 1.20 d [12], the author applied methodology of the MLVH (1979) for interpolation of a wind rose.

3. Results

The results of concentration and flow of the emissions of basic polluting substances from brown coal combustion in older combustion equipment presented in tables 1–3 are indicated under reference conditions according to the legislative directives [10]. The content of soluble substances from isolated SPM by an organic solvent (CS_2) was 92.5 %, concluding that an average content of inorganic residues in combustion products was 54 $mg.m^{-3}_{r}$. Supposing that during the combustion process while the low temperatures are present, the content of condensed organic substances emitted into the atmosphere of average concentration was 604 $m.g^{-3}$, which is emission flow of 531 $g.h^{-1}$ from one boiler. Even if volatile organic compounds (VOC) are not the subjects of evaluation of the combustion product quality according to contemporary applicable legislation, it is interesting to notice their quantity as well as quality arising from the process of an inferior combustion action. The highest concentration of vaporous organic substances of the human breathing zone during average climatic conditions (3.1 $m.s^{-1}$ wind speed, 10 °C air temperature, NE prevailing air circulation) was 10 $\mu g.m^{-3}$ at a distance of 450–600 m from the chimney in SW direction during an actual average meteorological situation. The worst concentration of the VOC during unfavourable climatic conditions (calm, stagnation of air layers) is assumed to happen at a distance of 120–320 m from the chimney. In this case the calculated concentration of the VOC in the combustion products was 174 $\mu g.m^{-3}$. The coefficient "S" used as a criterion for the calculation of minimal height valued at 10 $\mu g.m^{-3}$ for naphthalene and its derivatives, while toluene and xylene valued 200 $\mu g.m^{-3}$. These characteristics can be compared with the value of IHk. Owing to the fact that tars from brown coal mainly contain naphthalene and its derivatives, it can be assumed that there is a contravention of imissive limit.

4. Discussion

The entrepreneurs of air polluting sources are by laws related to the atmosphere supposed to use BAT (Best Available Technology) when building new mechanisms, i.e. No. 478/2002 [1]. This concept was developed as a directive concerning the atmosphere and known as BATNECC (best available technologies not entailing cost). In the quoted Act the BAT is defined as the best available technology economically achievable, in section § 6, segment 5.

Sample ID : slp
Sample : decht1-1
From : Friday, 21th May, 1999 18:12:04
Primary : decht01
Project : slp

Analyst : J.B.
Printed : Tuesday, 13th July, 1999 10:27:09
Calibration : (none)
Style : report

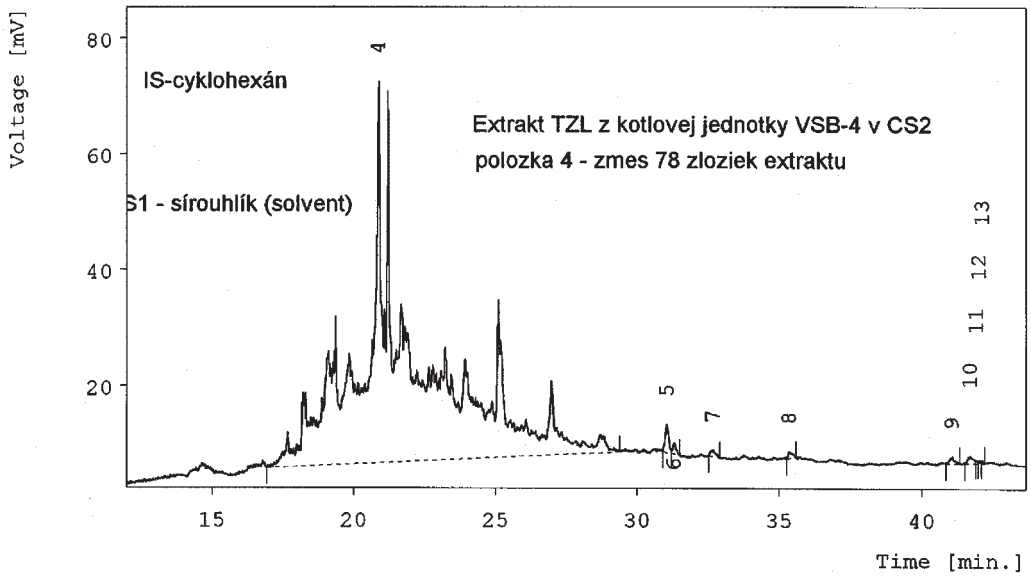

Result Table - Calculation Method Uncal

Peak No.	Reten. time	Area [mV.s]	Height [mV]	W05 [min.]	Area [%]	Height [%]
2	4.147	1551.3123	679.386	0.040	17.406	89.716
4	20.887	7238.4257	65.806	0.133	81.217	8.690
5	31.080	42.4467	4.740	0.147	0.476	0.626
6	31.333	15.9550	1.931	0.120	0.179	0.255
7	32.700	13.8741	1.094	0.233	0.156	0.145
8	35.380	11.9369	1.061	0.220	0.134	0.140
9	41.113	14.3074	1.097	0.180	0.161	0.145
10	41.760	20.3331	1.185	0.260	0.228	0.156
11	41.967	0.3798	0.157	0.040	0.004	0.021
12	42.073	1.5540	0.341	0.087	0.017	0.045
13	42.180	1.8781	0.463	0.067	0.022	0.061
-	Total	8912.4031	757.260			

Fig. 1 The arrangement of VOC which were isolated from solid particles absorbed on filter during SPM sample take-off by the gas chromatography method applied.

Legend: • IS-cyklohexán: cyclohexane • S1 - sírouhlík: carbon disulphide (solvent) • Extrakt TZL z kotlovej jednotky VSB-4 v CS_2: Extract of SPM (Solid Polluting Matters) from VSB-4 boiler unit sample taken from chimney in carbon disulphide (CS_2) • Polozka 4 - zmes 78 zloziek extraktu: Item 4 is mixture of 78 components found in an SPM extract.

According to Virčíková [11] the BAT parameters are as follows: emissive limit (or other characteristics if a polluting substance emitted from a source has no emissive limit) + general conditions of operation + technical parameters of operation + precautions to avoid dangerous and accidental

situations + comprehensiveness of air protection solution + security of emissions diffusion + comparability with an air protection standard of developed industrial countries. The BTA criteria are determined by the general obligatory directives dealing with the air protection, technical norms (STN, OTN ŽP, EN, ISO), directives issued by the EU and by the norms of developed countries (e.g. EPA, VDI etc.), and by standard condition of the technology.

The heat production from the fossil fuels, including various kinds of coal, also brings certain obligations for investors in terms

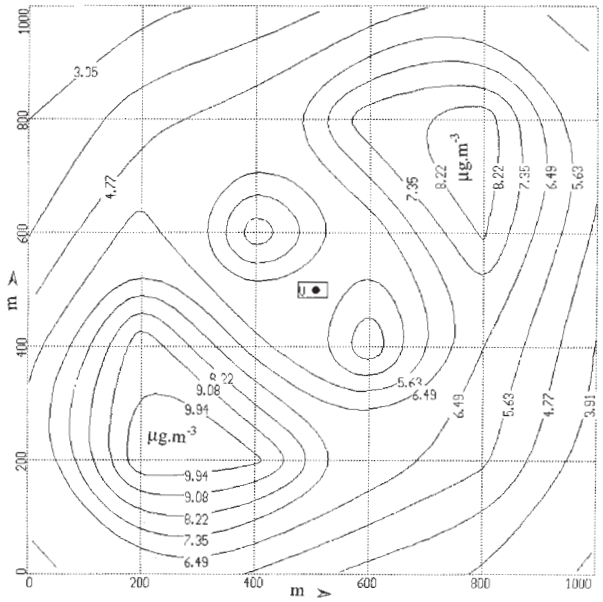

Fig. 2 Isolines of VOC imission concentration gained by brown coal burning technology at low temperature in VSB-4 boiler unit evaluated in the area with average climatic conditions

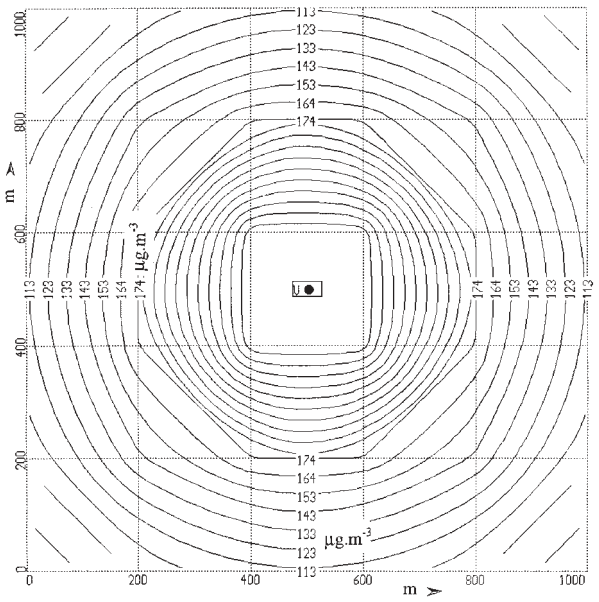

Fig. 3 Isolines of VOC imission concentration in human breathing zone under inclement climatic conditions for their scattering

Concentration and emission flow, emission limits (by reference conditions – 101.325 kPa, 0 °C normalised to 6 % oxygen in waste gas). Table 1
Fuel: brown coal

No.	Polluting mater	Concentration ($mg.m^{-3}_r$)		Emission flow ($kg.h^{-1}$)
		Measured *)	emission limit	
1.	Solid Polluting Matter (SPM)	658	undefined	0.579
2.	Sulphur Oxide	1406	2 500[1)]	1.2373
3.	Nitrogen Oxides	268	650	0.2358
4.	Carbon Oxide	2590	Undefined	2.2792

Explanatory notes: *) – results are given as arithmetic average of 12 measurements and analysis from two flue-gas off-takes,
1) – at mass flow SO_2 over 20 kg/h.

Basic statistic characteristics of measured emission source – mass concentration of flue-gas components and volume flow Table 2
Measurement 1

Emission source	Measured characteristics *1)		Arithmetic average (x)	Number of measurements	Maximal value	Minimal value	Decisive deviation (S_x)	Error band $L_{1,2}$ *2)
Boiler K_2	Flow [$m^3.h^{-1}$] (Reference Conditions)		882	6	940	838	40	985 – 780
	Concentration SPM	[$mg.m^{-3}$]	972	6	1063	502	189	1340 – 380
	Concentration SO_2	[$mg.m^{-3}$]	1441	6	1733	1103	184	1913 – 968
	Concentration NO_x	[$mg.m^{-3}$]	238	6	256	205	17	282 – 194
	Concentration CO	[$mg.m^{-3}$]	3195	6	3695	2420	435	4313 – 2007

Explanatory notes: *1) under reference conditions (dry gas, 0 °C, 101 325 Pa, content of O_2 = 6 % V). Average temperature of flue-gases in chimney was 54 °C
*2) error band $L_{1,2} = x \pm t * S_x$, where x – arithmetic average, t – coefficient of Student difference, S_x – decisive deviation

Basic statistic characteristics of measured emission source – mass concentration of flue-gas components and volume flow Table 3
Measurement 2

Emission source	Measured characteristics *1)		Arithmetic average (x)	Number of measurements	Maximal value	Minimal value	Decisive deviation (S_x)	Error band $L_{1,2}$ *2)
Boiler K_2	Flow [$m^3.h^{-1}$] (Reference conditions)		877	6	917	821	30	954 – 800
	Concentration SPM	[$mg.m^{-3}$]	344	6	410	267	59	462 – 226
	Concentration SO_2	[$mg.m^{-3}$]	1371	6	1468	1320	85	1590 – 1153
	Concentration NO_x	[$mg.m^{-3}$]	299	6	359	251	34	386 – 212
	Concentration CO	[$mg.m^{-3}$]	1985	6	2241	1827	200	2500 – 1471

Explanatory notes: *1) under reference conditions (dry gas, 0 °C, 101 325 Pa, content of O_2 = 6 % V). Average temperature of flue-gases in chimney was 65 °C

of legislative norms and statutes. The evaluated apparatus for the heat production – VSB-4 boiler unit determined for the combustion of fossil fuel, according to the BAT requirements, fulfils only requirements concerning emissions limits and their diffusion which are not too strict for low efficiency heating equipment. According to the accomplished measurements it is obvious that the entrepreneur did not achieve the required temperature parameters of combustion products in the chimney, resulting in low temperature of the combustion products in the combustion area of boiler and also defective combustion process resulting in high concentration of carbon dioxide and polluting fossil fuels resulting in SPM (Fig. 1). According to the GC analysis, the character of these organic substances is similar to purposely made tars from brown coal, whose main components are aromatic hydrocarbons, heterocyclic oxygenous, nitrogenous, and sulphuric compounds. Their physiological influence on human and other organisms (e.g. animals, plants etc.) differs in comparison with inorganic compounds of ash. According to figures in tables 2 and 3 it is obvious that higher occurrence of the defective combustion products (carbon dioxide, SPM of organic origin) appears during the low temperature combustion.

Therefore, it is very important for every entrepreneur to respect operational directives and requirements to improve operational quality of the combustion processes and reduce the amount of polluting substances in combustion products that are emitted into the atmosphere [13, 14].

5. Conclusion

During brown coal combustion at a low temperature, the emissions of polluting substances are emerged and they contain larger amounts of defective combustion products, such as carbonic dioxide and organic gases and vapours of higher aromatic hydrocarbons, heterocyclic compounds and their derivatives, which after refrigeration are transformed into soot-like substances that are soluble in organic solvents. Their amount and qualitative composition depends on the type of combusted coal and conditions of combustion process. During the defective combustion process, the emerging VOCs, pollute the atmosphere, increase the amount of smog in the atmosphere, influence production of ground ozone and they can also cause physiological changes and health problems [15–18].

Acknowledgements

This research was partly sponsored by grants from the Scientific Grant Agency of Ministry of Education of the Slovak Republic and the Slovak Academy of Sciences, under the contract No. 1/2382/05 VEGA; EC Projects: PN 116441-CP-1-2004-1-FR-MINERVA-M, title: BIO-eTRAIN "The Implementation of an eLearning University for Bioenergy"; Project N°: 012429 – BIOPROS "Solutions for the safe application of wastewater and sludge for high efficient biomass production in Short-Rotation-Plantations"; Leonardo da Vinci Project: EnTraCoP – Enhancing the Teaching of Collaborative Planning in Natural Resource Management, the Agreement n° 2005 FI- 05-B-F-PP-160633. Project "FET-EEU" full title: Future Energy Technologies for Enlarged European Union; Proposal/Contract no.: 510417. The authors are greatly indebted to the mentioned institutions for helping to sponsor this research work.

References

[1] Anonymous: Complete version of the Act No. 478/2002 digest, 20 August 2002, *concerning air protection against polluting matters (Act for atmosphere) resulting from later changes and updating* (in Slovak)

[2] Regulation of ME of the SR No. 112/1993 digest 27 April 1993, *Allocation of areas requiring special air protection, and operation of smog precautionary and control systems in version of later changes and statutes* (in Slovak).

[3] The statute of the government of the SR No. 706/2002 executing the Act No. 478/2002 *digest, the Air protection against polluting matter (Act for atmosphere air) in wording of later regulations*. In Slovak.
[4] Technical standard OTN ŽP 2002: 96 Air protection. *Single-shot measurement of emission and imission polluting surrounding air.* Requisites of measurement report (in Slovak).
[5] Slovak technical standard STN ISO 10 780. *Stationary sources of polluting. Measurement of speed and volume flow in pipes* (in Slovak.)
[6] Slovak technical standard STN ISO 9096. *Stationary sources of pollution. Stating of concentration and mass flow of solid polluting matter in flowing gas* (in Slovak). Manual gravimetric method.
[7] *Uncertainty determination of analytical measurement* (in Slovak). Eurachem Slovakia. Bratislava, editted by J. Garaj. 1995, pp. 96. In Slovak.
[8] BLAHO, J.: *Emission of polluting matter generated by VSB-4 boiler brown coal fired* (in Slovak). Measurement report, Ekolab Zvolen, 30 p. In Slovak, 1999.
[9] Slovak technical standard 83 4711, the part 1. *Measurement of emission: Sulphur Oxide, Sulphuric acid and total sulphur oxide content from polluting air sources* (in Slovak).
[10] Regulation No. 41/1997 digest, *Quantity determination of polluting matter emitted and data about observance of fixed emission polluting limit* (in Slovak).
[11] VIRČÍKOVÁ, E.: *Experiences in appraisal of hospital waste incinerators and view of technical possibility of waste processing regarding current interpretation* (in Slovak). Proceedings of the conference "Emission Limits". DT ZSVTS Bratislava, pp. 184–191, 1997.
[12] SABÓ, G.: *MODIM – calculating programme for imission diffusion* (in Slovak). Bulletin of ME of the SR, No. 5, point I.5, 1996.
[13] HORBAJ, P.: *Present state of preparation of biofuels from waste and biomass* (in Slovak). In: European Commission Directorate General Joint Research Centre, Institute for Energy, CLEANWEB Technical Workshop in collaboration with EU Candidate Countries, Recovered fuels from waste and biomass: Methods of syngas / biofuels / biogas production and cleaning; Fuel utilisation for energy production; 9. – 10. 12. 2003, Bergen, Holandsko http://ie.jrc.cec.eu.int/prewin
[14] FRUHAUFOVÁ, I.: *Actualization of environmental regionalization SR – work for ArcView* (in Slovak). Enviromagazín, 4/2003, ISSN 1335-1877.
[15] KUNCA, V., 2003: *Critical loads of selected forest ecosystems in the Poľana Biosphere Reserve* (in Slovak). Scientific essay, 4/2003/A, Technical University in Zvolen, pp. 72
[16] KUNCA, V., 2004: *Soil resistance against anthropogenic acidification in the Protected Landscape Area – Biosphere Reserve Poľana* (in Slovak). Acta Facultatis Ecologiae, 12, Technical University in Zvolen, pp. 17–21.
[17] KUNCA, V., ŠTEFFEK, J., OLAH, B., GAVLAS, V., WIEZIK, M., 2005: *Dynamics of ecosystems in Štiavnické vrchy Mts (Evaluation from point of view of landscape utilization changes, structure of chosen zoocenosis and forest ecosystem stability).* Technical University in Zvolen, pp. 103
[18] KUNCA, V., 2005: *Determination of base cations amount released by weathering in forest soils as the one of main parameters in critical loads calculations* (in Slovak). Acta Faculta tis Ecologiae, 13, Technical University in Zvolen, pp. 61–69.

COMMUNICATIONS – Scientific Letters of the University of Žilina
Writer's Guidelines

1. Submissions for publication must be unpublished and not be a multiple submission.
2. Manuscripts written **in English language** must include abstract also written in English. The submission should not exceed 7 pages (format A4, Times Roman size 12). The **abstract** should not exceed 10 lines.
3. Submissions should be sent: **by e-mail** (as attachment in system Microsoft WORD) to one of the following addresses: *holesa@nic.utc.sk* or *vrablova@nic.utc.sk* or *polednak@fsi.utc.sk* **with a hard copy** (to be assessed by the editorial board) **or on a 3.5″ diskette** with a hard copy to the following address: Zilinska univerzita, OVaV, Univerzitná 1, SK-10 26 Zilina, Slovakia.
4. Abbreviations, which are not common, must be used in full when mentioned for the first time.
5. Figures, graphs and diagrams, if not processed by Microsoft WORD, must be sent in electronic form (as GIF, JPG, TIFF, BMP files) or drawn in contrast on white paper, one copy enclosed. Photographs for publication must be either contrastive or on a slide.
6. References are to be marked either in the text or as footnotes numbered respectively. Numbers must be in square brackets. The list of references should follow the paper (according to **ISO 690**).
7. The author's exact **mailing address of the organisation where the author works, full names, e-mail address or fax or telephone number,** must be enclosed.
8. The editorial board will assess the submission in its following session. In the case that the article is accepted for future volumes, the board submits the manuscript to the editors for review and language correction. After reviewing and incorporating the editor's remarks, the final draft (before printing) will be sent to authors for final review and adjustment.
9. The deadlines for submissions are as follows: September 30, December 31, March 31 and June 30.
10. Topics for the next issues: 3/2006 – Informative and communication tools for decision-making support, 4/2006 – Fatigue and endurance of constructional materials, 1/2007 – Mechatronics in electrotechnical systems.

POKYNY PRE AUTOROV PRÍSPEVKOV DO ČASOPISU
KOMUNIKÁCIE – vedecké listy Žilinskej univerzity

1. Redakcia prijíma iba príspevky doteraz nepublikované alebo inde nezaslané na uverejnenie.
2. Rukopis musí byť **v jazyku anglickom**. Príspevok by nemal prekročiť 7 strán (formát A4, písmo Times Roman 12 bodové). K článku dodá autor **resumé** v rozsahu maximálne 10 riadkov (v anglickom jazyku).
3. Príspevok prosíme poslať: **e-mailom**, ako prílohu spracovanú v aplikácii Microsoft WORD, na adresu: *holesa@nic.utc.sk* alebo *polednak@fsi.utc.sk* príp. *vrablova@nic.utc.sk* (alebo doručiť na diskete 3,5″) **a jeden výtlačok** článku na adresu Žilinská univerzita, OVaV, Univerzitná1, 010 26 Žilina.
4. Skratky, ktoré nie sú bežné, je nutné pri ich prvom použití rozpísať v plnom znení.
5. Obrázky, grafy a schémy, pokiaľ nie sú spracované v Microsoft WORD, je potrebné doručiť buď v digitálnej forme (ako GIF, JPG, TIFF, BMP súbory), prípadne nakresliť kontrastne na bielom papieri a predložiť v jednom exemplári. Pri požiadavke na uverejnenie fotografie priložiť ako podklad kontrastnú fotografiu alebo diapozitív.
6. Odvolania na literatúru sa označujú v texte alebo v poznámkach pod čiarou príslušným poradovým číslom v hranatej zátvorke. **Zoznam použitej literatúry** je uvedený za príspevkom. Citovanie literatúry musí byť **podľa STN 01 0197 (ISO 690)** „Bibliografické odkazy".
7. K rukopisu treba pripojiť **plné meno a priezvisko autora a adresu inštitúcie v ktorej pracuje, e-mail adresu** alebo číslo telefónu event. faxu.
8. Príspevok posúdi redakčná rada na svojom najbližšom zasadnutí a v prípade jeho zaradenia do niektorého z budúcich čísiel podrobí rukopis recenziám a jazykovej korektúre. Pred tlačou bude poslaný autorovi na definitívnu kontrolu.
9. Termíny na dodanie príspevkov do čísiel v roku sú: 30. september, 31. december, 31. marec a 30. jún.
10. Nosné témy ďalších čísiel: 3/2006 – Informatické a komunikačné nástroje na podporu rozhodovania, 4/2006 – Únava a životnosť konštrukčných materiálov, 1/2007 – Mechatronika v elektrotechnických systémoch.

komunikácie
COMMUNICATIONS

VEDECKÉ LISTY ŽILINSKEJ UNIVERZITY
SCIENTIFIC LETTERS OF THE UNIVERSITY OF ŽILINA
7. ROČNÍK – VOLUME 7

Adresa redakcie:
Address of the editorial office:
Žilinská univerzita
Oddelenie pre vedu a výskum
Office for Science and Research
Univerzitná 1, Slovakia
SK 010 26 Žilina
E-mail: komunikacie@nic.utc.sk, polednak@fsi.utc.sk,

Každý článok bol oponovaný dvoma oponentmi.
Each paper was reviewed by two reviewers.

Časopis je excerpovaný v Compendexe
Journal is excerpted in Compendex

Vydáva Žilinská univerzita
v EDIS – vydavateľstve ŽU
J. M. Hurbana 15, 010 26 Žilina
pod registračným číslom 1989/98
ISSN 1335-4205

It is published by the University of Žilina in
EDIS - Publishing Institution of Žilina University
Registered No: 1989/98
ISSN 1335-4205

Objednávky na predplatné prijíma redakcia
Vychádza štvrťročne
Ročné predplatné na rok 2006 je 500,– Sk

Order forms should be returned to the editorial office
Published quarterly
The subscription rate for year 2006 is 500 SKK

Jednotlivé čísla časopisu sú uverejnené tiež na:
http://www.utc.sk/komunikacie
Single issues of the journal can be found on:
http://www.utc.sk/komunikacie